Intracortical mechanisms compensating weakened thalamic input in the hyperexcitable somatosensory cortex of *reeler* mutant mice

Dissertation

for the award of the degree

"Doctor of Philosophy"

Faculty of Biology

of the Georg-August-Universität Göttingen

within the doctoral program *Sensory and Motor Neuroscience*

of the Georg-August University School of Science (GAUSS)

submitted by

Anouk Johanna Maria Meeuwissen

Born in Oosterhout, the Netherlands

Göttingen 2021

Thesis Committee

Prof. Dr. Jochen F. Staiger
Institute for Neuroanatomy, University Medical Center, Göttingen

Prof. Dr. Tim Gollisch
Department of Ophtalmology, University Medical Center, Göttingen

Dr. Camin Dean
German Center for Neurodegenerative Diseases, Berlin

Members of the Examination Board

1st Referee: Prof. Dr. Jochen F. Staiger
Institute for Neuroanatomy, University Medical Center, Göttingen

2nd Referee: Prof. Dr. Tim Gollisch
Department of Ophtalmology, University Medical Center, Göttingen

Further members of the Examination Board

Prof. Dr. Dr. Oliver Schlüter
Department of Psychiatry and Psychotherapy, University Medical Center, Göttingen

Prof. Dr. Thomas Dresbach
Department of Anatomy and Embryology, University Medical Center, Göttingen

Prof. Dr. Ralf Heinrich
Department of Cellular Neurobiology, University of Göttingen, Göttingen.

Date of oral examination: 17 November 2021

Declaration

I, Anouk Johanna Maria Meeuwissen, hereby declare that the present thesis was written independently and with no other sources and aids than those quoted. All results presented here were the outcome of my own labour unless stated otherwise.

……..……

Anouk Johanna Maria Meeuwissen

September 30, 2021

Göttingen, Germany

Table of Contents

List of figures

List of tables

List of Abbreviations

4-AP	4-aminopyridine
AAC	Axo-axonic chandelier cell
AAV5	Adeno-Associated virus serotype 5
ACSF	Artificial cerebrospinal fluid
ANOVA	Analysis of variance
BC	Basket cell
CC	Current clamp
ChR2	Channelrhodopsin-2
Cs	Cesium
Dab1	Disabled1
DAPI	4’,6-diamidino-2-phenylindole
EPSC	Excitatory postsynaptic current
EPSP	Excitatory postsynaptic potential
FS	Fast-spiking
GABA	Gamma-aminobutyric acid
GFP	Green fluorescent protein
GPN	GABAergic projection neuron
HBlock	Blocked HCN1 channels
HCN	Hyperpolarization-activated cyclic nucleotide-gated
IC	Intracellular solution
I_h	Hyperpolarization-activated current
IPSC	Inhibitory postsynaptic current
IPSP	Inhibitory postsynaptic potential
L	Layer
Median	Mdn

Min	Minutes
mRNA	messenger ribonucleic acid
n.s.	Not significant
P	Postnatal day
PuC	Putative contact
PFA	Paraformaldehyde
POm	Posterior nucleus
Prv	Principle trigeminal nucleus
PV	Parvalbumin
R	Reeler
RT	Room temperature
S1	Primary somatosensory cortex
S1BF	Primary somatosensory barrel field cortex
SD	Standard deviation
SEM	Standard error of the mean
SpS	Spiny stellate
Spv	Spinal trigeminal nucleus
Syt2	Synaptotagmin-2
TB	Tris buffer
TBS	Tris-buffered saline
TBST	Tris-buffered saline with Triton-X 100
TC	Thalamocortical
TTX	Tetodoxtoxin
VC	Voltage clamp
VPm	Ventral posteromedial nucleus
Vrest	Resting membrane potential
WM	White matter
WT	Wild-type
YFP	Yellow fluorescent protein
ZAP	Impedance amplitude profile

Introduction

Sensations such as seeing, smelling, hearing, touching and tasting allow us to experience our environment. The processing of all sensory information occurs in the brain, an intriguing organ consisting of billions of interconnected neurons that communicate with each other. Through highly organized connections between neurons, the brain is able to perform a wide variety of functions amongst which the receiving and processing of sensory information in the cerebral neocortex. What are the exact neuronal mechanisms in the brain responsible for the processing of sensory information? This is one of the many questions that have fascinated neuroscientists for a long time. In order to study the processing of sensory information and unravel the inherent neuronal circuits, scientists have used rodent models. Rodents gather tactile information from their surroundings via their whiskers, also called vibrissae. These signals are then processed in the primary somatosensory cortex that due to its distinctive neuron pattern and strikingly organized architecture has formed an important tool in studying the underlying mechanisms of sensory information processing.

The pathways from whiskers to cerebral cortex

Mice gather sensory information about their surroundings via their whiskers. This information then travels to the primary somatosensory cortex (S1) where it is processed. There are multiple pathways known to carry sensory information from the whiskers to the primary somatosensory cortex; the two main pathways with their characteristic projection patterns are demonstrated in **Figure 1**: the paralemniscal and lemniscal pathway (Staiger & Petersen, 2021). In the paralemniscal pathway, sensory information goes from the whisker to the spinal trigeminal nucleus (Spv) of the brainstem. Then, the information travels via the posterior nucleus (POm) of the thalamus to the somatosensory cortex (Lu & Lin, 1993; Wimmer et al., 2010). In the lemniscal pathway, tactile information travels from the whiskers to the barrelettes of the

principal trigeminal nucleus (Prv) of the brainstem (Belford & Killackey, 1979). From there, the signal is carried via the barrelloids in the ventral posteriomedial nucleus (VPm) of the thalamus and finally projected to the somatosensory cortex. Remarkably, the barrelettes of the brainstem and barreloids of the thalamic VPm are each positioned in a pattern isomorphic to the whiskers (Brecht, 2007; Diamond et al., 2008; Feldmeyer et al., 2013; Lübke & Feldmeyer, 2007; Van Der Loos, 1976). From all thalamic projections, the majority of whisker sensory information travels via the lemniscal pathway to the primary somatosensory cortex (Diamond et al., 1992). Each of the two parallel sensory pathways is thought to transmit unique types of whisking information. Whereas the lemniscal pathway is thought to perform spatial sensory processing, the paralemniscal pathway is involved in making sense of temporal aspects of sensory signals (Ahlssar et al., 2000). Both pathways project to the primary somatosensory cortex where each pathway presents its own specific termination pattern (see **Figure 1**).

The barrel cortex

The rodent somatosensory cortex receives and processes sensory information regarding the immediate surroundings that are detected by the whiskers. A particular interesting feature of the primary somatosensory cortex is its highly organized architecture. Within the somatosensory cortex neurons are arranged in layers and columns (see **Figure 1**). The primary somatosensory neocortex, by definition, is structured in six different layers (L1-6). Each layer can be characterized by its composition of various types of neurons and the denseness of these neurons (Staiger, 2015). In the somatosensory cortex, each layer is thought to have its own specific task in the receiving and processing of sensory information. Accordingly, neurons expressing distinctive cellular properties and local microcircuits are probably organized in a layer-specific manner.

The thalamic afferents from the lemniscal and paralemniscals pathway express individual targeting patterns onto the primary somatosensory cortex as shown in **Figure 1** (cf. Lu & Lin, 1993; Wimmer et al., 2010). The sensory information from the thalamic VPm (lemniscal pathway) is received predominantly in L4 and, to a lesser extent, at the border of L5/6 of the primary somatosensory cortex (Bernardo & Woolsey, 1987; Lu & Lin, 1993). Via the paralemniscal pathway, thalamocortical (TC) axons from the thalamic POm project to the

septum (area in between columns), within the columns to L1 and L5a of the somatosensory cortex and to various other cortical areas. (Lu & Lin, 1993; Wimmer et al., 2010). However, the primary source of tactile information goes via the lemniscal sensory pathway and is projected to L4, therefore also known as the main input layer (Agmon & Connors, 1991; Brecht & Sakmann, 2002; Diamond et al., 1992; Oberlaender et al., 2012). In turn, excitatory neurons of L4 forward the received and processed whisker sensory information onto pyramidal neurons of L2/3 (Varani et al., 2021). The axons of L2/3 pyramidal neurons target the L5 pyramidal neurons that then project the whisker information to several subcortical structures (Lefort et al., 2009; Lübke & Feldmeyer, 2007). This canonical microcircuit of excitatory neurons contributes to the processing of sensory information in the primary somatosensory cortex. These excitatory neurons comprise the majority (~80 %) of all neurons found in the primary somatosensory cortex and their activity is well controlled by GABAergic interneurons that represent the remaining ~20 % of neurons (DeFelipe & Fariñas, 1992; Meyer et al., 2011).

Besides a layered organization, neurons in the primary somatosensory cortex are also organized in columns (see **Figure 1**). Each column is marked by an area with an increased neuron density located in L4, termed a barrel due to its shape. On the same line, the rodent primary somatosensory cortex is also known as the barrel cortex, or barrel field (S1BF). Like the barrelettes and barreloids, the cortical barrels are positioned in a pattern isomorphic to the whiskers on the rodent's snout and each barrel receives and processes the information coming from the corresponding contralateral whisker (Woolsey & Van der Loos, 1970).

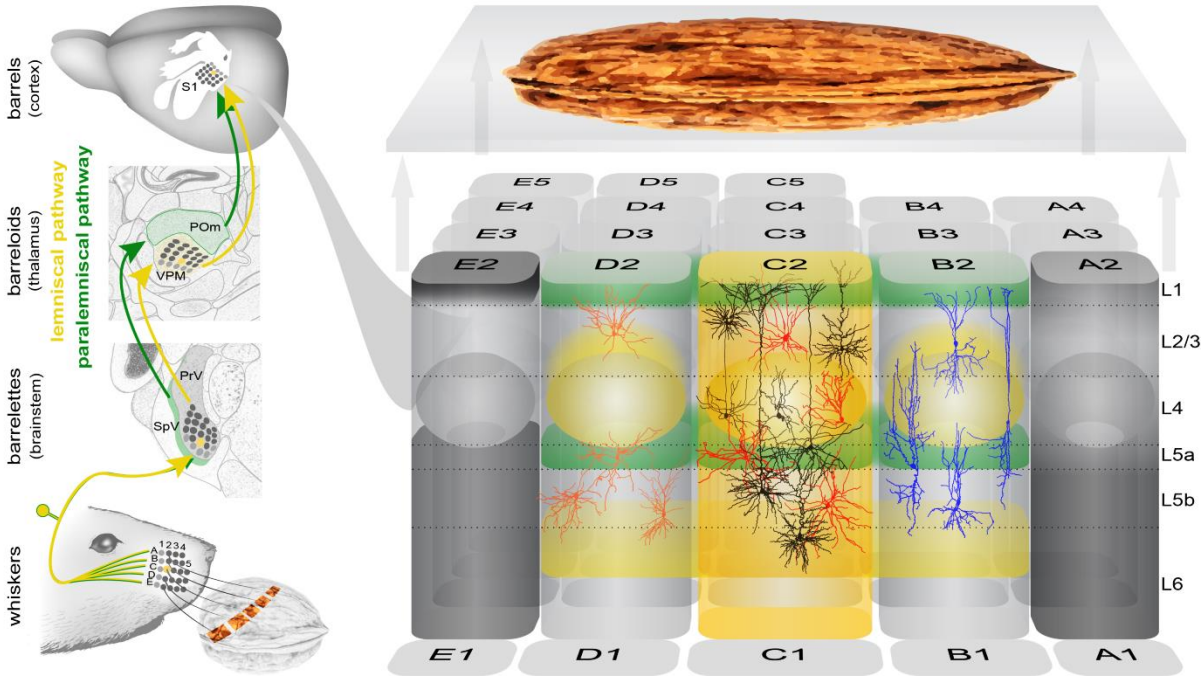

Figure 1: Organization of the primary somatosensory (barrel) cortex.

Sensory information gathered via the whiskers travels via the lemniscal pathway (yellow) or paralemnsical pathway (green) to S1BF. S1BF is a highly organized structure where neurons are arranged in columns (isomorphic to whisker pattern) and six layers. Via the lemniscal pathway, sensory information from the VPm thalamic nucleus is transmitted to mainly L4 and, to a lesser extent, the border of L5/6. Via the paralemniscal pathway, sensory information from the POm thalamic nucleus is projected to L1 and L5a. Within S1BF, sensory information gathered from the whiskers is received and processed. Taken from Staiger & Petersen, 2021 with permission.

Spiny stellate neurons

As previously described, L4 receives the majority of thalamic input in S1BF and is also known to process and redistribute these signals to other layers. One particular type of neurons in L4 are spiny stellate (SpS) neurons. These relatively small excitatory neurons have a key role in fulfilling the tasks of L4 in the barrel cortex. Together with pyramidal neurons and star pyramidal neuron, SpS neurons represent the excitatory neurons found in L4 of the barrel cortex (Schubert et al., 2003; Staiger et al., 2004). Unlike the other L4 excitatory neuron, the dendritic arborisation of SpS neurons is restricted to the individual barrel structure (Lübke et al., 2000; Petersen & Sakmann, 2000; Schubert et al., 2003; Staiger et al., 2004). In addition, TC axons from the VPm are strongly targeting SpS neurons in L4 of S1BF (Benshalom & White, 1986; Petersen, 2002). However, thalamocortical synapses represent only a minority (ca. 8 – 10 %) of all of the excitatory synapses targeting L4 SpS neurons. It has been demonstrated in juvienile animals that SpS neurons are also connected amongst each other with

a connectivity rate of approximately 25% (Feldmeyer, 2005; Feldmeyer et al., 1999; Lefort et al., 2009; Stratford et al., 1996; Tarczy-Hornoch et al., 1999). This recurrent excitation between SpS neurons indicates that these neurons in addition to receiving thalamic VPm input, also amplify and process the incoming sensory information. The majority of axonal branches from SpS neurons target the supragranular layers (L2/3) and a lesser amount of SpS neuron axonal branches target the infragranular layers (L5/6) (Staiger et al., 2004). This axonal morphology and targeting pattern suggest that SpS neurons redistribute sensory information from the VPm to other layers. In summary, SpS neurons play an import role in the receiving, amplifying, and rerouting of sensory information in S1BF.

Fast spiking interneurons

The activity of SpS neurons is predominantly controlled by GABAergic inhibition from parvalbumin-expressing (PV) inhibitory interneurons located in the same barrel (Koelbl et al., 2015). The PV-expressing interneurons form the largest subclass of the highly diverse GABAergic interneurons in S1BF and can be further subdivided in axo-axonic (or: chandelier) cells (AAC) and basket cells (BC) (Ascoli et al., 2008; Staiger & Petersen, 2021). These two types of PV-expressing interneurons can be distinguished by their morphology and synapse-targeting pattern. AAC neurons are known to specifically target axon initial segment of the excitatory postsynaptic neurons only (Freund & Katona, 2007; Vereczki et al., 2016; Veres et al., 2014). Although typically identified by their soma and proximal dendrites targeting pattern, few studies have indicated that BC neurons also innervate more distally on the dendrites of the postsynaptic excitatory neurons (Karube, 2004; Kawaguchi & Kubota, 1993; Kubota et al., 2007; Kubota et al., 2015; Staiger et al., 2009; Tamas et al., 2000). Both subtypes of PV-expressing interneurons demonstrate a characteristically fast action potential waveform, hence they are also called fast-spiking (FS) interneurons. Within S1BF, PV-expressing FS interneurons are spread from L2 to L6, enabling them to provide powerful and precise inhibition the excitatory neurons across all layers of S1BF (Boyle et al., 2011; Wang et al., 2019). Excitation of SpS neurons is thus regulated by PV-expressing FS interneurons that are also located in L4 of S1BF, mostly in the same barrel.

Similarly to SpS neurons in L4, PV-expressing FS interneurons also receive excitatory input from thalamic afferents originating from the thalamic VPm (Cruikshank et al., 2007, 2010;

Staiger, 1996). It has been suggested that there are four different types of PV-expressing FS interneurons in L4 of S1BF, based on their soma location and dendritic arborisation relative to the barrel (Shigematsu et al., 2018). All these subtypes however are known to receive thalamic input from the VPm. The thalamic input onto FS interneurons demonstrated to be faster and stronger compared to VPm input to SpS neurons (Cruikshank et al., 2007; Hull et al., 2009; Porter et al., 2001; Swadlow, 2003). In addition, FS interneurons and SpS neurons within a single barrel are found to be strongly connected, with connectivity rates up to 67 % (Koelbl et al., 2015). By receiving input from both thalamocortical afferents originating from the VPm and from SpS neurons, FS interneurons form both a feedforward and a feedback inhibitory circuit (Bagnall et al., 2011; Cruikshank et al., 2007, 2010; Staiger et al., 2009). The feedforward circuit from VPm thalamic afferents to SpS neurons, via FS interneurons, has been extensively studied as an important mechanism in the processing of sensory information in S1BF (Agmon & Connors, 1992; Swadlow, 1989; Swadlow, 1995).

The *reeler* mouse mutant

As described earlier, each of the six layers in the primary somatosensory cortex is thought to have its own task in sensory information processing. However, is it possible to assign specific functions to each layer? What would happen to these functions in a cortex with absence of proper layering? And what effect would improper cortical layering of the somatosensory cortex have on the neuronal circuitry involved with the processing of sensory information? These questions can be studied in a mutant with absence of proper cortical layering, called the *reeler* mutant mouse.

In 1946, a spontaneous mutation in the reelin gene was first observed at the Institute of Animal Genetics in Edinburgh (Falconer, 1951). The mutation was discovered due to an abnormal phenotype consisting of tremor, ataxia and an impaired motor coordination that were the effect of the autosomal recessive reelin mutation. A deletion in the reelin gene results in lack of expression of the protein. The reelin protein is secreted by Cajal-Retzius cells in the marginal zone where it plays a crucial role in cellular interactions required for cortical developmental (Caviness, 1988). It is the task of reelin to guide migration of neurons to their rightful location in the cerebral cortex (Caviness, 1982; D'Arcangelo et al., 1995; Frotscher, 1998; Lambert de

Rouvroit & Goffinet, 1998). Therefore, an absence of the reelin protein results in a highly disorganized cortex that lacks proper layering. The disturbed layering of the *reeler* S1BF is presented in **Figure 2**, where different layers in cortical brain slices are visualized with *in situ* hybridization for layer-specific markers. Although the neurons are scattered throughout the *reeler* S1BF, the mutation has no effect on the survival of the neurons (Caviness, 1988). Hence, all the types of neurons found in wild-type (WT) are also found in the *reeler* S1BF.

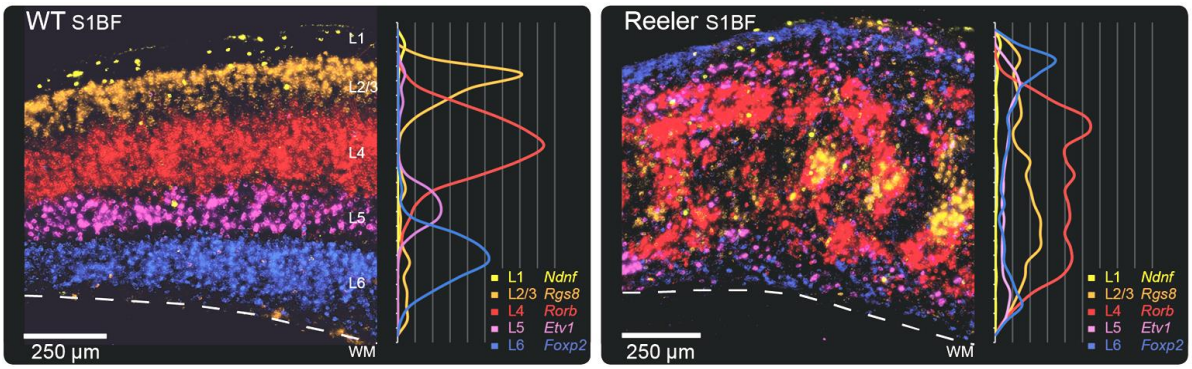

Figure 2: The disorganized *reeler* S1BF.

Layered organization is visualized using in situ hybridization for layer specific mRNA markers in cortical brain slices containing S1BF of a WT mouse (left) and a *reeler* mutant mouse (right). Each layer was labelled in a different cortical slice, the images shown here represent a merge of all stained slices. A layer-specific neuron density plot is shown on the right of each image. Striped white line marks the white matter (WM) border. L1 is labelled with Ndnf, shown in yellow, L2/3 is labelled with Rgs8, shown in orange, L4 is labelled with Rorb, shown in red, L5 is labelled with Etv1, shown in purple, L6 is labelled with Foxp2, shown in blue. Adapted from Mingo-Moreno, 2018 and Wagener et al., 2016.

Distribution of excitatory and inhibitory neurons in the *reeler* S1BF

Reelin deficiency leads to disorganization of both excitatory and inhibitory neurons in the neocortex. As mentioned earlier, the excitatory neurons of the *reeler* S1BF show a severely scattered pattern compared to the organized and layered structures observed in the WT S1BF (see **Figure 2**). Whereas the L4 excitatory neurons in the WT S1BF are organized in barrels, they are distributed in small clusters throughout the depth of the cortex in *reeler* mutant mice. These small clusters of L4 excitatory neurons in the *reeler* S1BF are called barrel-equivalents (Boyle et al., 2011; Caviness, 1976; Cragg, 1975; Wagener et al., 2010; Welt & Steindler, 1977).

In addition to an altered migration and scattered pattern of excitatory neurons in the *reeler* S1BF, the effect of reelin deficiency on the migration and distribution of GABAergic interneurons has been studied. A subgroup of GABAergic interneurons have been found to express the glycoprotein reelin (Miyoshi et al., 2010). In the *reeler* mutant mouse, it has been reported that the migration of GABAergic interneurons to the neocortex is not affected, but that the correct placement of these interneurons within the neocortex fails (Hammond, 2006; Yabut et al., 2007). Various studies have suggested that reelin is not responsible for guiding inhibitory interneurons to their proper locations within the cortex, rather a model is proposed where GABAergic interneurons within the cortex require position-cues from local excitatory neurons (De Marco García et al., 2011; Hammond, 2006; Pla et al., 2006). As of yet, the exact mechanism behind the placement of GABAergic interneurons in the disorganized *reeler* cortex is not fully understood. Few studies have quantified the amount and distribution of GABAergic interneurons in both the WT and *reeler* S1BF (Hevner et al., 2004). In coronal brain slices of adult mice, fluorescent *in situ* hybridization for parvalbumin showed subtle changes in the distribution of PV-expressing interneurons in the *reeler* S1BF compared to WT (Boyle et al., 2011). Whereas the density of PV-expressing interneurons was similar between genotypes, the distribution of interneurons was slightly altered (Boyle et al., 2011; Wagener et al., 2016). In the WT S1BF PV-positive neurons were found predominantly distributed in L3 to L6, while in the *reeler* S1BF, PV-positive neurons were observed to be evenly spread throughout the neocortex. The cortical distribution of other GABAergic interneuron subclasses, such as somatostatin-expressing interneurons and vasoactive intestinal peptide-expressing interneurons, has so far only been studied in young mice (P7) where a mirrored positioning of these neurons was found in the *reeler* S1BF compared to WT. In summary, these studies indicate that reelin deficiency affects the positioning of both excitatory and inhibitory neurons in S1BF. While correct placement of both excitatory neurons and inhibitory interneurons is essential for proper functioning of microcircuits in the cortex, it can be expected that the reception and processing of sensory information is affected in the highly disorganized *reeler* S1BF.

Weakened thalamic input and increased network activity in the *reeler* cortex

Considering the effect of reelin deficiency on the organization of excitatory and inhibitory neurons in S1BF, it is possible that the sensory information processing is also affected in the *reeler* mutant mice. A crucial component of sensory information processing is the proper

thalamic VPm innervation of SpS neurons in L4 of S1BF. Using viral tracing methods, previous results from our lab showed that regardless of the displacement of L4 excitatory neurons, TC fibers from the VPm still manage to target the L4 excitatory neurons in the *reeler* S1BF (Wagener et al., 2010, 2016). In this study, L4 excitatory neurons were Scnn1a-tdTomato marked in a cre-dependent manner. Noticeably, it was found that TC axons were first directed towards the pial surface of the *reeler* S1BF, after which they turned and colocalized with L4-fated neurons. After having found that TC afferents target L4-fated neurons in S1BF of *reeler* mutant mice, the functionality of the synapses was tested. A channelrhodopsin virus injection in the thalamic VPm, allowed for optogenetic stimulation of TC fibers in L4 while performing electrophysiological recordings of SpS neurons (Guy, 2015; Guy et al., 2017). Using this method, it was found that the combination of thalamic and local input in response to TC fiber stimulation was significantly greater in the *reeler* S1BF compared to WT, indicating a hyperexcitable cortical network. Interestingly, when pharmacologically isolating the pure thalamic input in SpS neurons, a weakened thalamic input was found in the *reeler* S1BF as compared to the WT S1BF (Guy, 2015; Guy et al., 2017). In summary, results of the previous work from our lab present a conundrum: *reeler* SpS neurons receive a weakened thalamic input but show a hyperexcitable cortical network in response to optogenetic stimulation of TC fibers.

Aims of the thesis

How does lack of proper layering influence the neuronal circuitry? Which synaptic mechanisms are conserved and which are modified? Previous studies reported a greater local network activity upon thalamic input in the *reeler* S1BF. However, the pure thalamic input onto SpS neurons was found to be weaker, compared to the WT S1BF (Guy et al., 2017). These discoveries point towards the presence of a cellular and/or synaptic mechanism in the *reeler* cortex that is able to compensate for the weakened VPm input. The aim of this thesis is to elucidate this mechanism responsible for counterbalancing the excitation in the *reeler* S1BF. To this end, a simplified neuronal circuit was considered of the thalamic VPm neurons, the SpS neurons, and FS interneurons located in L4 or L4-equivalent (see **Figure 3**). In the WT S1BF, TC fibers reach L4 and excite both the SpS neurons and the FS interneurons. In turn, these two types of neurons are connected with each other. This allows FS interneurons to provide powerful and precisely timed inhibition to SpS neurons. These forms of feedforward and

feedback inhibition onto SpS neurons ensure a controlled local neuronal network and prevent hyperexcitability. In addition, SpS neurons are also found to be connected among themselves, allowing for amplification of the numerically weak thalamic input.

From this circuit, multiple compensatory mechanisms can be hypothesized that could make up for the weakened VPm input to *reeler* SpS neurons. First, the weakened thalamic input onto *reeler* SpS neurons could be compensated for by a stronger connection between SpS neurons to amplify the weakened signal (see **Figure 3A**). Furthermore, this stronger connection between SpS neurons could be featured by a higher connectivity rate and/or a more reliable or stronger connection. The second hypothesized compensatory mechanism involves a weakening of the connection between FS interneurons and SpS neurons in the *reeler* S1BF (see **Figure 3B**). This would result in a weakening of the feedforward and/or feedback inhibition of SpS neurons, leading to more excitation. Last, in addition to a weakened VPm input to SpS neurons, it could be imagined that FS interneurons likewise receive a weakened VPm input which would reduce the inhibition in the L4-equivalent network in the *reeler* S1BF. In the present thesis, the first two hypotheses were investigated (see **Figure 3**):

A Enhanced recurrent excitation between SpS neurons as a compensatory mechanism in the *reeler* cortex, amplifies the weakened VPm input in the *reeler* cortex.

B A reduced and/or weakened connection between FS interneuron and SpS neuron would affect the feedforward and feedback inhibition, leading to more excitation in the *reeler* S1BF.

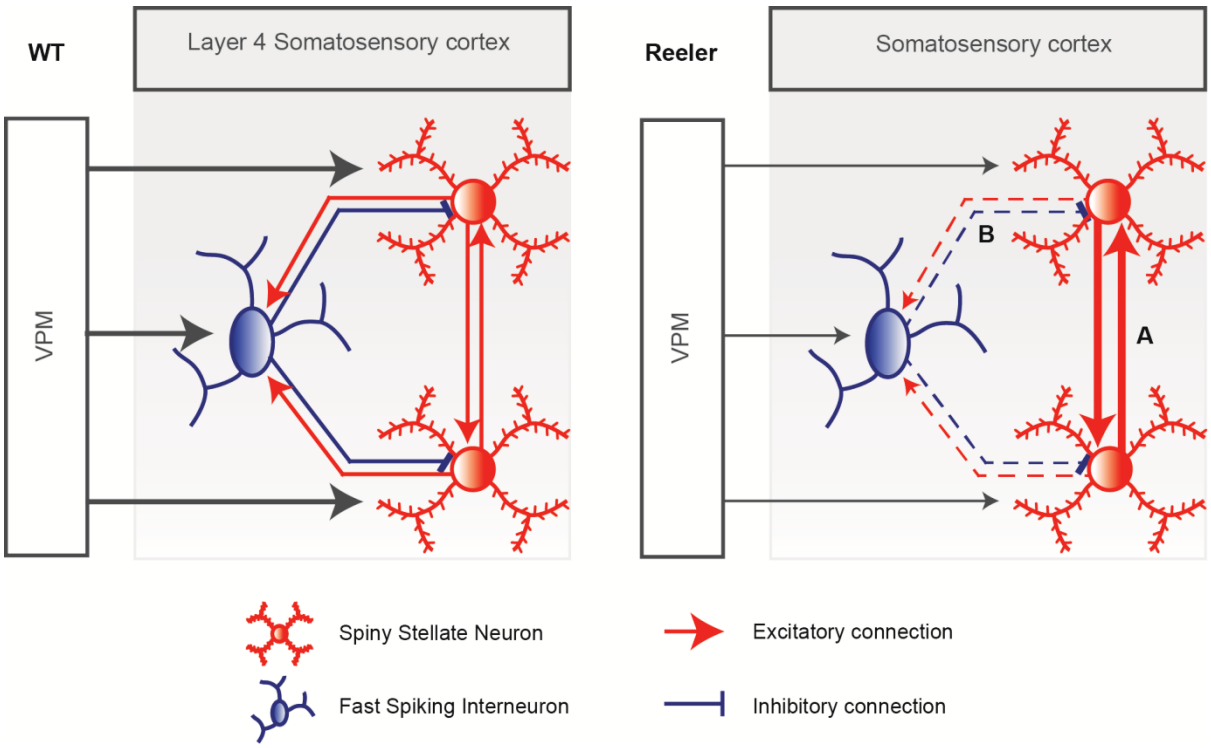

Figure 3: Hypothesized mechanisms that could compensate weakened VPm input in *reeler* S1BF.

Considering the simplified neuronal circuit between the VPm and L4 SpS neurons and FS interneurons in the WT somatosensory cortex (left), where each of the L4 neurons are also connected amongst each other, two hypothesized compensatory mechanisms for the weakened thalamic input in the *reeler* cortex were investigated (A and B in right panel). Hypothesis A: enhanced recurrent excitation between SpS neurons, amplifies the weakened thalamic input in the *reeler* S1BF. Hypothesis B: A weakened or reduced feedforward and/or feedback inhibition mediated by FS interneurons, could lead to more excitation in the *reeler* mutant mouse cortex.

In order to study the connections between SpS neurons and the connections between FS interneurons and SpS neurons in WT and *reeler* mutant mice, paired whole-cell patch clamp recordings were performed. This approach allowed for evaluating the connectivity rate, reliability of the connection and the strength of each connected pair of neurons. In addition, the inhibitory innervation pattern of SpS neurons was examined by using neuronal reconstructions and immunolabeleling of a FS interneuron bouton marker.

Methods

Animals

In the present study Scnn1a^{cre}-tdTomato-*reeler* mice were used. In this mouse line, L4 excitatory neurons express tdTomato in a cre-dependent manner allowing the identification of L4 neurons in the disorganized *reeler* cortex. The breeding scheme of this mouse line was previously described (Guy et al., 2015). Heterozygous Scnn1a^{cre}-tdTomato-*reeler* mice (*reeler* +/-) were excluded from the study. Wild-type mice (*reeler* +/+*)* of the same litters were used as a control group for the *reeler* mutant mice (*reeler* -/-). Mice of both sexes were used. Mice were housed in standard cages at a 12-hour light/dark cycle. All mice had access to food and water *ad libitum*. All animal experiments were performed in accordance with the German laws on animal research.

Stereotactic Injections

In order to optogenetically stimulate thalamocortical fibers in L4 (or L4 equivalent in the *reeler* mutant mouse) originating from the VPm, stereotactic injections were performed to express channelrhodopsin-2 (ChR2) in thalamic VPm neurons. The virus construct used was an adeno-associated-virus (AAV5) with an hSyn.hChR2(H134R)-eYFP vector (#26973P, Addgene; Penn Vector Core, Perelmann School of Medicine, University of Pennsylvania, see **Table 2**). Mice, aged postnatal day (P) 21 - 26, were anesthetized with 5 % isoflurane (see **Table 2**) after which they were transferred to a stereotaxic setup (Kopf Instruments) where anaesthesia was maintained with 0.5 - 1 % isoflurane through a mask. Anaesthesia depth was monitored by observation of breathing rate and breathing intensity. Constant depth of anaesthesia was ensured throughout the surgery by slight adjustment of isoflurane concentration. Body

temperature was maintained at 37 °C using a heating pad regulated with an ATC1000 DC Temperature Controller (World Precision Instruments). Ointment (Bepanthen, Bayer) was applied on the eyes of the anesthetized mouse to prevent eye dehydration. Local analgesia on the scalp was administered by subcutaneous injection of a 2 µg/g mixture of bupivacaine/lidocaine (Astra Zeneca/Bela-pharm). A small incision was made on the scalp and a craniotomy performed over the VPm area on both hemispheres. Injections pipettes were pulled from borosilicate glass capillaries (GB150F-8P, Science Products) using a P-97 puller (Sutter Instruments). The pipette tip was cut to a final diameter of ~20 µm and front-filled with AAV5-hSyn.hChR2(H134R)-eYFP virus construct diluted with phosphate buffer (titer of 1.96 * 10^9 particles/µL). The coordinates used to target the VPm with respect to Bregma (-1.7 mm antero-posterior, +/- 1.75 mm medio-lateral and -3.25 mm dorso-ventral) were chosen based on the Paxinos Atlas (Paxinos & Franklin, 2001). The coordinates were corrected to match the small size of three-week-old WT and *reeler* mutant mice. Correction factor calculation was based on the distance between Bregma and Lambda, which is 4.2 mm in adult mice. For each mouse the distance between Bregma and Lambda was calculated (D), and from there the corrected coordinates were calculated:

$$\text{anterior} - \text{posterior} = -1.7 * \left(\frac{\text{D}}{4.2}\right)$$

$$\text{medio} - \text{lateral} = +/-1.75 * \left(\frac{\text{D}}{4.2}\right)$$

$$\text{dorso} - \text{ventral} = -\left(\frac{2}{3} * \left(1 - \frac{\text{D}}{4.2}\right) + \text{D}\right) * 3.25$$

The filled injection pipettes were brought to the corrected VPm coordinates and approximately 250 nL of virus solution was injected (4 pulses of 200 ms with 12.5 psi) using a PDES-02DX picospritzer (Npi). Before retraction, the pipette was left at the injection location for 5 minutes (min) to reduce potential backflow. The scalp was cleaned with 0.9 % NaCl solution and stitched (Ethilon II USP 6/0, Ethicon) and the mouse was allowed to recover from anaesthesia. Mice received a subcutaneous injection of Carprofen (5 µg/g, Rimadyl, Pfizer) every 24 hours for three days following surgery for additional analgesia. Body weight, wound and overall recovery were closely monitored over the same period. Mice received soft food in their cage consisting of their regular food grinded, oats, glucose, and water. 21 to 24 days later, mice were sacrificed for *in vitro* electrophysiology experiments using optogenetic stimulation.

In vitro electrophysiology

Slice preparation

Scnn1a-tdTomato-reeler mice, age P28-P52 were deeply anesthetized with isoflurane and decapitated. The brain was dissected, and separated hemispheres were kept in ice cold cutting solution (containing in mM: 87 NaCl, 1.25 NaH_2PO_4, 2.5 KCl, 10 glucose, 75 sucrose, 0.5 $CaCl_2$, 7 $MgCl_2$, 26 $NaHCO_3$, infused with 95% O_2 and 5% CO_2; pH 7.4, see **Table 2**). 300 µm thick thalamocortical slices were prepared using a vibratome (VT1200S Leica) according to a protocol previously described by Porter and colleagues (Porter et al., 2001). Slices were incubated in artificial cerebrospinal fluid (ACSF) (containing in mM: 125 NaCl, 1.25 NaH_2PO_4, 2.5 KCl, 25 glucose, 2 $CaCl_2$, 1 $MgCl_2$, 26 $NaHCO_3$ infused with 95% O_2 and 5% CO_2; pH 7.4, see **Table 2**) at room temperature (RT) for 60 min prior to electrophysiological recordings.

Electrophysiological characterization of neurons

Following the incubation period of 60 min, thalamocortical slices were transferred to a recording chamber, kept at a temperature of 32˚C and continuously perfused (2 mL/min) with recording ACSF. Slices were imaged with an upright microscope (Axia Examiner A1, Zeiss, Germany). A low magnification (2.5X / 0.075 objective, Zeiss) was used in order to visualize the barrel cortex under bright-field illumination. SpS neurons were identified by their tdTomato fluorescence using a 40X water immersion objective (40X / 0.80 W, Olympus). FS interneurons were targeted by their lack of tdTomato fluorescence and distinct soma morphology (large, oval shaped somata). For paired whole cell patch clamp recordings, SpS neurons and FS interneurons were chosen to be located within ±50 µm proximity from each other within the same barrel (or *reeler* barrel equivalent). Membrane potentials were recorded with SEC-05XS amplifiers (Npi electronics, Tamm, Germany) in discontinuous current-clamp mode with a switching frequency of 50 kHz, filtered at 3 kHz, and digitized at 10 – 25 kHz using a CED Power1401 (CED limited, Cambridge, UK). Patch pipettes were pulled from borosilicate glass capillaries (GB150F-8P, Science Products) using a pipette puller (P-1000, Sutter Instruments, Novato, USA). For FS interneurons, pipette resistance was 5 – 7 MΩ and for spiny stellate neurons the pipette resistance was 7 – 10 MΩ. Patch pipettes were either filled with a potassium-based intracellular (IC) solution (containing in mM: 135 K-Gluconate, 5 KCl,

10 HEPES, 4 MgATP, 0.3 NaGTP, 10 Na-P-creatin, see **Table 2**) or a cesium-based IC solution (containing in mM: 135 $CsMeSO_4$, 5 CsCl, 0.5 EGTA, 10 HEPES, 4 MgATP, 0.3 NaGTP, 10 Na-P-creatin, see **Table 2**). Both solutions were set at a pH of 7.4 and had an osmolarity of 290 – 310 mOsm (when needed adjusted with sucrose). Prior to recording, 0.3 – 0.5 % biocytin (see **Table 2**) was added to the IC solution. Patch pipettes were navigated through the slice towards the target neurons with micromanipulators (Luigs & Neumann). Membrane potentials were not corrected for a liquid junction potential of approximately 16 mV. Access resistance was monitored and compensated for during the whole recording, recordings where access resistance could not be compensated were discarded. Traces were collected and analyzed with Signal 5 software (CED limited).

After obtaining the whole-cell configuration, passive and active intrinsic properties of each neuron were systematically recorded to obtain a thorough characterization of each neuron. Passive properties such as resting membrane potential (V_{rest}), input resistance, sag index and membrane time constant were calculated. In addition, active properties among which rheobase current, firing threshold, AP width and AP amplitude were measured from action potential firing. During characterization, neurons were recorded in current clamp mode at V_{rest}. Hyperpolarizing, 1 s current pulses of -10 pA and -50 pA were applied with a 1.5 s stimulus interval to evaluate passive properties such as input resistance and membrane time constant. For each current step, ten response repetitions were recorded and averaged for analysis. Next, current-voltage (I-V) curves were recorded by giving various current strength pulses of 1 s ranging from -100 pA to depolarizing currents that elicit series of action potentials, with increments of 10 pA. The rheobase of each neuron was assessed by determining the minimum strength of depolarizing current (1 s pulse) in order to reliably elicit an action potential. Last, the firing pattern of FS interneurons and SpS neurons were recorded with a 1 s depolarizing current pulse exceeding rheobase current.

Paired recordings

Paired recordings between SpS neurons were performed with potassium-based intracellular solution, see **Figure 4**. For each pair, after characterization of individual neuron's passive and active properties, the connection between neurons was tested. For that, the presynaptic SpS neuron was kept in current clamp at -70 mV and was stimulated to fire an action potential using

a 5 ms depolarizing current pulse of 350 – 570 pA. The postsynaptic SpS neuron was kept in voltage clamp at a holding potential of -70 mV. When neurons were synaptically connected, at least 20 iterations were recorded for each connection with a 10 s sweep interval, so that the response average could be used for further analysis. Synaptic connections were tested for in both directions. A pair of neurons was considered connected when at least 10% of presynaptic action potentials led to a time-locked postsynaptic response. Postsynaptic responses were detected when their amplitudes exceeded a threshold of three times the standard deviation of the baseline membrane potential that was measured in the 100 ms before stimulation onset. Experiments were excluded from analysis when recordings showed evidence of impaired recording stability or health of the tissue. Recording stability was determined by monitoring the input resistance changes over time with a small 200 ms hyperpolarizing current pulse preceding each postsynaptic response. If input resistance changed more than 30 % during the recording from starting value, the recording was excluded from analysis.

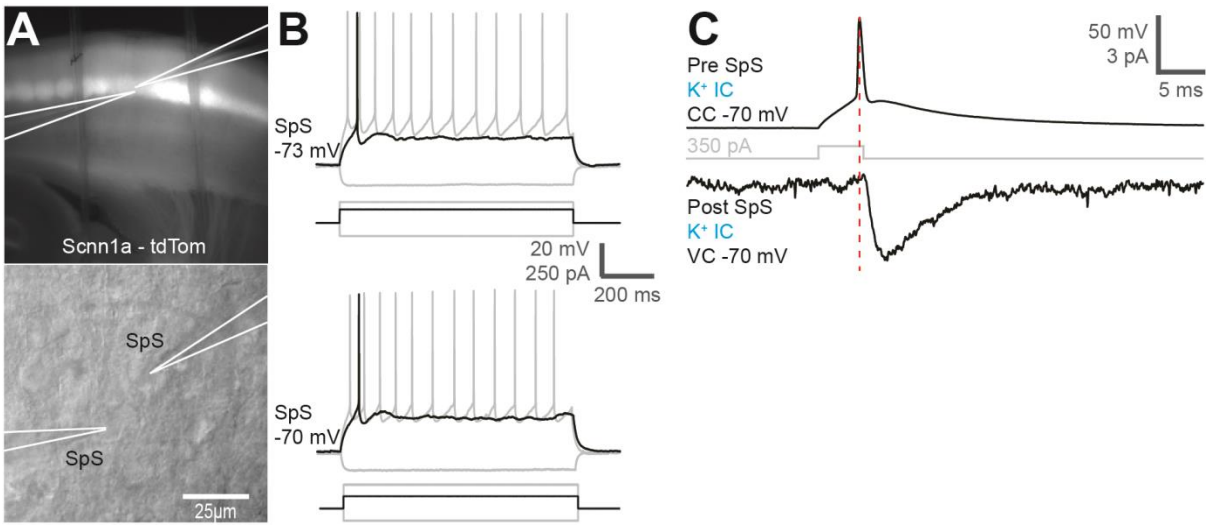

Figure 4: Example paired recording between SpS neurons in WT.

A) Top, microscopic snapshot showing the Scnn1a-tdTomato positive barrels in the somatosensory cortex, patch pipettes targeting two SpS neurons located within a single barrel. Bottom, 40X objective snapshot of patched SpS neuron pair. **B)** Characterization of SpS neurons at V_{rest}. **C)** Representative example of a direct synaptic connection between SpS neurons. Presynaptic SpS neuron AP is followed after a short latency by an EPSC in the postsynaptic SpS neuron.

Paired recordings between FS interneurons and SpS neurons were performed in three different paradigms, see **Figure 5**. First, recordings were performed with potassium-based intracellular

solution in both patch pipettes, see **Figure 5A-C**. In order to test for a connection, a single action potential was triggered in the presynaptic FS interneuron by current injections (3-5 ms current pulse, 250-600 pA) while kept in current clamp at -70 mV. If the neurons were connected, a time locked IPSC could be recorded in the postsynaptic SpS neuron. The membrane potential of the postsynaptic SpS neuron was maintained at -50 mV in voltage clamp to facilitate IPSC detection. In order to test for a reciprocal connection, the FS interneuron was subsequently kept at -70 mV in voltage clamp, and a single action potential was generated in the presynaptic SpS neuron (5 ms current pulse, 300-500 pA) kept in current clamp at a membrane potential of -70 mV. When neurons were found connected, a time locked EPSC was recorded in the postsynaptic FS interneuron, kept in voltage clamp at -70 mV.

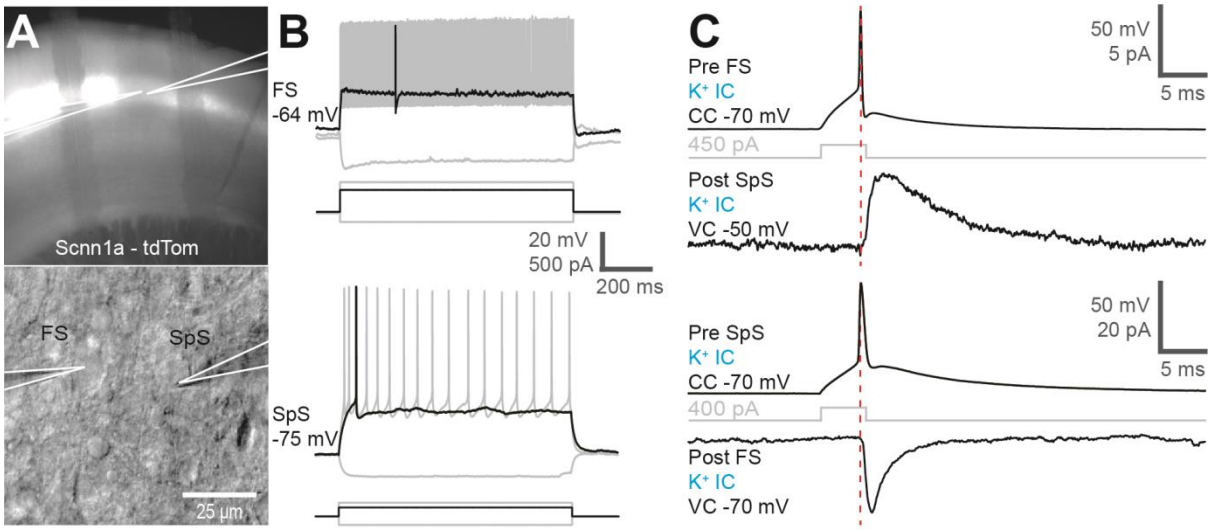

Figure 5: Example paired recording between a FS interneuron and a SpS neuron in WT.

A-C) Initial recordings between FS interneuron and SpS neuron were performed with standard potassium-based intracellular solution. **A)** 2.5X overview image with tdTomato signal and below a higher magnification highlighting the close proximity of the neurons. **B)** Individual neuron characterization. **C)** In this example, a bidirectional connection between FS interneuron and SpS neuron was found. Top: Presynaptic FS interneuron was made to fire an AP, resulting in an IPSC in the postsynaptic SpS neuron. Bottom: Presynaptic SpS neuron firing led to an EPSC response in postsynaptic FS interneuron. Red dotted line shows the time locked onset of postsynaptic response with the presynaptic AP peak.

If recording stability and slice health allowed, train stimulations were recorded in pairs of SpS neurons or between a FS interneuron and SpS neuron. Train stimulation was only performed for reliable connections, in other words, connections that showed a low rate of synaptic failures. Each train stimulation protocol consisted of 5 current pulses (5 ms, varying current strengths)

delivered to the presynaptic neuron at various frequencies (1 Hz, 5 Hz, 20 Hz, 50 Hz or 100 Hz). At least 10 iterations per frequency were recorded with a 10 s interstimulus interval. Averages were used for further analysis.

After each recording, slices were fixed in 4 % paraformaldehyde (PFA) and 15 % picric acid in phosphate buffer (0.1 M, pH 7.4, see **Table 2**) overnight at 4 ˚C.

Optogenetic stimulation

To compare VPm input to SpS neurons in WT versus *reeler* mutant mice, a subset of mice was subjected to stereotaxic injection to express ChR2 specifically in VPm neurons. 21-24 days post injection, mice were sacrificed for *in vitro* electrophysiology combined with optogenetic stimulation. ChR2-expressing TC fibers in L4 (or L4 equivalent) were stimulated optogenetically using laser pulses of 1 ms with intensities ranging from 0.01 – 5 mW in full-field stimulation (250 * 250 µm illuminated area). The 473 nm diode laser (Rapp OptoElectronic) was controlled via SysCon software (version 1.1.2.2., Rapp OptoElectronic) and was integrated in Signal software configurations designed by Dr. Martin Möck (Institute for Neuroanatomy, University Medical Center, Göttingen). Both thalamic and network inputs were recorded upon photostimulation in SpS neurons kept in current clamp at -70 mV. Purely thalamic input, isolated for recurrent excitation, was recorded after washing in recording ACSF containing 0.5 µM tetodoxtoxin (TTX; Tocris) and 0.1 mM 4-aminopyridine (4-AP; Sigma Aldrich) (Cruikshank et al., 2010; Petreanu et al., 2009).

Respectively, TTX and 4-AP (see **Table 2**) ensured blocking of voltage-gated sodium channels and blocking of voltage-gated Kv1 potassium channels. This prevented the neuronal network from generating action potentials, so that only ChR2-expressing TC fibers that are in contact with the recorded SpS neuron would contribute to the optogenetically evoked response. Upon laser stimulation, depolarization of thalamic presynaptic terminals was sufficient to activate high threshold calcium channels which induced neurotransmitter release through vesicle fusion. In this way, mono-synaptic direct thalamic input could be recorded in SpS neurons while blocking network activity. Excitatory postsynaptic potentials (EPSPs) were recorded

before and after bath application of TTX and 4-AP using a range of different laser intensities. For each laser intensity, three iterations were recorded with a 10 s interstimulus interval and the average of the three iterations was used for further analysis.

Analysis of electrophysiological recordings

All patch clamp recordings were analyzed with Signal 5 software, with custom scripts written by Dr. Martin Möck (Institute for Neuroanatomy, University Medical Center, Göttingen).

Analysis of SpS neuron and FS interneuron characterization

Right after obtaining whole-cell patch clamp configuration, the V_{rest} of each neuron was noted. Input resistance, membrane time constant and sag index were calculated from the average of the 1 s hyperpolarizing -50 pA traces. The input resistance provides an indication of the proportion of opened channels on the membrane and is calculated by the change in membrane potential from V_{rest} to steady state of the hyperpolarizing response with Ohm's law (resistance is voltage divided by current). The membrane time constant (τ) is calculated in milliseconds from the stimulation onset to the 63 % voltage change from its final value, calculated with an exponential fit applied from the stimulation onset to the highest voltage deflection. Therefore, the membrane time constant represents the speed with which the membrane responds to current inputs. The sag index is an assessment of the slow membrane potential rectification that has been assigned to the hyperpolarization-activated cation current, called I_h. The sag index is the measured as a percentage of the ratio between the steady state membrane potential and the highest voltage deflection (Karagiannis et al., 2009). Action potentials elicited during the rheobase protocol were used to analyze action potential waveform parameters such as: firing threshold (mV), width (ms) and amplitude (mV). The firing threshold is defined by the membrane potential from which an action potential is triggered and is identified by slope of 10 % at the onset of the AP rising phase. The duration of the AP at the halfway point of the peak amplitude was measured as the AP width. The AP amplitude was calculated as the voltage difference between the peak amplitude and firing threshold.

Analysis of paired recordings, EPSCs and IPSCs

From the total amount of connections tested per dataset, the connection probability was calculated as the percentage of unconnected, unidirectionally connected and bidirectionally connected pairs. Per connection, the synaptic failure rate was calculated as the percentage of presynaptic action potential elicited for which no time-locked response was observed in the postsynaptic neuron. From averaged single EPSCs and IPSCs, the following parameters were analyzed: latency (ms), time-to-peak (ms), amplitude (pA) and decay (ms). From paired train recordings, the amplitude for each response was calculated. In case of overlapping postsynaptic responses at higher frequencies, an exponential fit was placed on the decay of the preceding response until the membrane potential baseline was reached. Amplitude of the subsequent response was then measured from response peak till the fit, thus excluding the previous response.

Perfusion and brain slicing

Mice were deeply anesthetized by intraperitoneal injection of a ketamine/xylazine mixture (300 mg/kg ketamine, 30 mg/kg Xylazine, see **Table 2**). When deeply anesthetized, mice were transcardially perfused with NaCl 0.9%, followed by 4 % paraformaldehyde (PFA) solution containing 15 % picric acid in 0.1 M phosphate buffer for approximately 20 min. After perfusion, the brain was dissected and post fixed in PFA with picric acid overnight at 4 °C. The fixated brains were cut in 50 µm coronal slices containing the barrel cortex, using a vibratome (VT1200S, Leica). Coronal brain slices were used for immunohistochemistry.

Immunohistochemistry

Fixed 300-µm-thick thalamocortical brain slices from *in vitro* electrophysiology experiments were stained for biocytin with Alexa 633 conjugated streptavidin to visualize neuron morphology and with DAPI to label cell nuclei. In addition, the YFP fluorescence of the viral construct was enhanced by immunolabeling YFP with anti-GFP antibodies in order to confirm the location of the injection site and the projection pattern of VPm neurons onto the barrel cortex. The 50-µm-thick coronal brain slices obtained from perfused animals were subject to immunolabeling for synaptotamin-2. All antibodies and chemicals used are listed in **Tables 1 and 2**, respectively.

All fixed brain slices were first washed with phosphate buffer (five times 15 min) to remove PFA and picric acid solution. The phosphate buffer (0.1 M, pH 7.4) was made freshly by diluting 14.42 g of Na_2HPO_4 and 2.62 g NaH_2PO_4 in water. All washing steps were carried out at RT. Slices were then washed in TRIS buffer (TB, 0.05M, pH 7.6) and TRIS buffer saline (TBS), each for 15 min. Next slices were washed twice with TRIS buffer saline containing 0.5 % Triton-X 100 (TBST), for 15 min each. Then, slices were incubated for 90 min in blocking solution containing TBST, 0.25 % Albumin Fraction V (Roth) and 10 % normal serum (donkey or goat, Jackson Laboratories). After washing out the blocking solution with TBST, slices were incubated for 48 – 72 hours at 4 °C with goat polyclonal anti-GFP (1:2000, Abcam) and/or streptavidin conjugated to Alexa 633 (1:300, Invitrogen) and/or synaptotagmin-2 conjugated to Alexa 488 (1:200, University of Oregon) in TBST. This incubation period was followed by three 15 min-long washing steps in TBST and one washing step in TBS. Afterwards, DAPI (1:5000, 5 min incubation, Invitrogen) staining was performed to visualize all cell nuclei. Finally, brain slices were washed with TBS and TB (15 min each) before being mounted on a glass slide using Aqua-polymount (Polysciences) and covered with a coverslip (24 x 50 mm, 0.08 – 0.12 mm thick, Menzel). All histochemistry procedures were carried out by Patricia Sprysch (Institute for Neuroanatomy, University Medical Center, Göttingen).

Table 1: Antibodies used in this study.

Antibody	Company	Cat. No.	Dilution
Anti GFP	Abcam	Ab5450	1:2000
DAPI	Invitrogen	P1306	1:5000
Streptavidin	Invitrogen	S21375	1:300
Synaptotagmin-2	University of Oregon	Gifted (from Zebrafish International Resource center)	1:200

Imaging and reconstructing

Overview images of brain sections were scanned with an upright epifluorescence microscope (Axio Observer, Zeiss) with a 10X objective controlled by ZEN software (Zeiss). The barrel cortex area with biocytin-filled neuron pairs was scanned in tiles with an inverted confocal microscope (LSM 880, Zeiss) with a 63X objective. Potential putative contact sites between neurons detected in reconstructions (see next paragraph) were scanned using the Airy Scan mode of the LSM 880 with the 63X objective. Airy Scan mode was also used for high-resolution images of the synaptotamin-2 staining. Images were stitched using the ZEN software, and maximum intensity projections of stacks were made for neuron morphology overview images. Brightness contrast levels of images were adjusted in Fiji software for representation purposes.

Neuron reconstructions

Pairs of neurons that showed sufficient biocytin filling were used for morphological reconstruction with Neurolucida software. Barrels and their equivalents in *reeler* mutant mice were reconstructed from the Scnn1a-tdTomato signal. Layer borders were reconstructed from DAPI signal. The dendritic arborizations of neurons was studied with Neurolucida Explorer software to analyse the total dendritic length, average length per dendrite and the amount of branching points. For visualisation purposes of all morphological reconstructions in this work, the thickness of axonal and dendritic branches was enhanced with Adobe Illustrator CS6. For pairs of reconstructed neurons, potential sites of contact detected in reconstructions were additionally scanned in high resolution, Airy Scan mode. Based on high resolution images (voxel size: 0.04 * 0.04 * 0.18 µm), putative contacts were assigned when processes crossed within the same Z-plane. Student assistants Johanna Rieke, Nicolas Zdun, and Sabrina Hübner helped with the reconstructions.

Puncta detection

Quantification of synaptotagmin-2-positive puncta in contact with SpS neurons in WT and *reeler* mutant mice was performed on single tile, high resolution image stacks scanned in Airy Scan mode. Soma and proximal dendrites of biocytin-filled SpS neurons were manually reconstructed with Neurolucida software. The stack image Bleaching Correction function in Fiji was used on the synaptotagmin-2 channel to adjust staining intensity level and decrease the staining decay as a function of depth throughout the stacks. Synaptotagmin-2 positive puncta, adjacent to the reconstructed SpS neuron, were detected using Puncta Detection in Neurolucida 360 software. Neurolucida parameters for puncta detection were set as: detector diameter of 2 µm, detector sensitivity of 120 %, minimum size of 75 voxels (equivalent to $\geq$21.6 nm^3) and proximal distance of puncta middle to reconstruction contour of 0.5 µm. Spines were not reconstructed and were excluded from the analysis. Using a custom Python 3 script, written by Alexander P. Wegner (G3-7 Information Technology, UMC Göttingen), markers were placed on the exact location of detected puncta, allowing for further analysis with Neurolucida Explorer. Besides measuring soma volume and dendritic tree length and complexity, branch structure analysis of Neurolucida Explorer allowed for measuring marker distance from the soma, along the reconstructed dendritic branch.

Statistics

Time histograms showing the mean membrane potential variation around optical stimulation were made by a custom Matlab (R2021a, Mathworks) script written by Dr. Julien Guy (Institute for Neuroanatomy, University Medical Center, Göttingen). Statistical analysis on these graphs was performed using two-way ANOVA with a Holm-Sidak post-hoc comparison test. For statistical comparison of the mean of two groups, datasets were first tested for equal variance and normal distribution with the Shapiro-Wilk test. When both were confirmed, means were compared with the two-tailed student t-test. When the equal variance and/or normality test failed, Mann-Whitney rank sum test was performed to compare means of two groups. To compare percentages of neuronal connectivity and connection reliability in WT versus *reeler* mutant mice, Chi square or Fisher exact test was calculated. The peak amplitudes of optogenetically evoked EPSP trains, used to compare the effect of hyperpolarization-activated

current on temporal summation in WT versus *reeler* mutant mice, were tested with a three-way ANOVA (shown in **Figure 28G-I**). Values are presented as mean ± standard deviation (sd) for normally distributed datasets; when this was not the case the median (Mdn) was reported, unless stated otherwise. The threshold for statistical significance (*) was set at $p < 0.05$. Datasets on graphs lacking an asterisk, were not significantly different. Besides the peristimulus time histograms, all graphs were made in Graphpad Prism (version 8.4.3, Graphpad). All statistical tests were done in SigmaPlot (Version 13.0, Systat Software).

Chemicals, reagents, and viruses

Table 2: Chemicals, reagents and viruses used in this study.

Reagent	Company	Cat. No.
0.9 % NaCl	Braun	3570160
4-AP	Sigma-Aldrich	275875
AAV5-hSyn.hChR2(H134R)-eYFP	Addgene	26973P
Albumin Fraktion V	Roth	8076.1
Aqua-polymount	Polysciences	18606-5
Biocytin	Sigma-Aldrich	B4261
Bupivacain	AstraZeneca	
$CaCl_2$	Sigma-Aldrich	223506
Carprofen (Rimadyl®)	Zoetis	
CsCl	Sigma-Aldrich	C3032
$CsMeSO_4$	Sigma-Aldrich	C1426
EGTA	Sigma-Aldrich	E4378
FK506	Sigma-Aldrich	F4679
Glucose	Millipore	14431-43-7
Gt anti Ms IgG2A-Alexa488	Molecular Probes	A21131
HEPES	Sigma-Aldrich	H3375
Isoflurane	Cp-pharma	1214
KCl	Merck	1.04936
Ketamin	Serumwerk	Ursotamin
K-Gluconate	Sigma-Aldrich	G4500
Lidocainhydrochlorid 2 %	Bela-pharm	1650
MgATP	Sigma-Aldrich	A9187
$MgCl_2$	Sigma-Aldrich	M2670
NaCl	Honeywell	S9888
NaGTP	Sigma-Aldrich	G8877
Na_2HPO_4	Roth	4984.1
NaH_2PO_4	Merck	1.06346
$NaHCO_3$	Merck	1.06329
Na-P-Creatin	Abcr	Ab264373
Normal donkey serum	Jackson Laboratories	146288
Normal goat serum	Jackson Laboratories	152469
Paraformaldehyde	PanReac AppliChem	8B012144
Picric acid	Sigma-Aldrich	6744-1G4
Sucrose	Sigma-Aldrich	S9378
TRIS HCl	Sigma-Aldrich	T3253
TRIS base	Sigma-Aldrich	T1503
Triton-X-100	Merck	1.08603
TTX	Tocris	1078
Xylazin	Ecuphar	Xylariem
ZD7288	Tocris	1000

Results I

Previous studies from our lab reported hyperexcitability in L4-equivalent neurons in the *reeler* mutant mouse compared to WT mice, by combining optogenetic and *in vitro* electrophysiological experiments. This hyperexcitability demonstrated itself as an enhanced responsiveness to stimulation of TC fibers, originating from the VPm, in SpS neurons, even though the TC input itself was found to be slightly weaker (Guy, 2015; Guy et al., 2017). This raised the possibility that recurrent excitatory excitation may be stronger in the *reeler* mutant mouse, or that inhibition was weakened compared to WT mice. Both could be understood as a compensatory mechanism in S1BF of *reeler* mutant mice, which rescales synaptic weights so as to rescue a weakened sensory input from the VPm. Based on these observations, two hypotheses were defined that are investigated in the present work. The first hypothesis proposes that enhanced recurrent excitation between SpS neurons in the *reeler* cortex compensates for the weakened VPm input. The second hypothesis postulates a weakened feedforward/feedback inhibition between FS interneuron and SpS neuron resulting in reduced inhibition as a compensatory mechanism for weakened VPm input in *reeler* mutant mice. Before testing these hypotheses, it was first attempted to replicate our previous observations, namely the stronger cortical network activity and the weakened VPm input in SpS neurons of the *reeler* mutant mouse that formed the foundational observations leading to this project. Furthermore, electrophysiological characteristics of SpS neurons and FS interneurons in WT and *reeler* mutant mice were investigated, as possible alterations could interfere with the interpretation of neuronal connection properties between the two genotypes.

Weakened thalamic input in the hyperexcitable *reeler* cortex

This study's first objective was to replicate previous findings showing that thalamic input onto the *reeler* S1BF resulted in an overall greater net excitation and a weakened direct monosynaptic VPm input onto *reeler* SpS neurons, compared to the WT S1BF. These findings provided the impetus of this entire project, hence the importance of replication. Similar to the previous experiments, this study used optogenetic stimulation of varying laser intensities to control thalamocortical fibers in L4 of S1BF and record VPm input onto SpS neurons in both WT and *reeler* mutant mice (Guy, 2015; Guy et al., 2017). The ChR2 expressing VPm neurons and their projection pattern in S1BF of WT and *reeler* mutant mice, are shown in **Figure 6**. In WT mice, thalamic afferents terminated mainly in L4 and the border of L5-6 (see **Figure 6A**). In the disorganized *reeler* S1BF, VPm input was densest in barrel equivalents, which were defined as clusters of tdTomato expressing neurons (see **Figure 6B**).

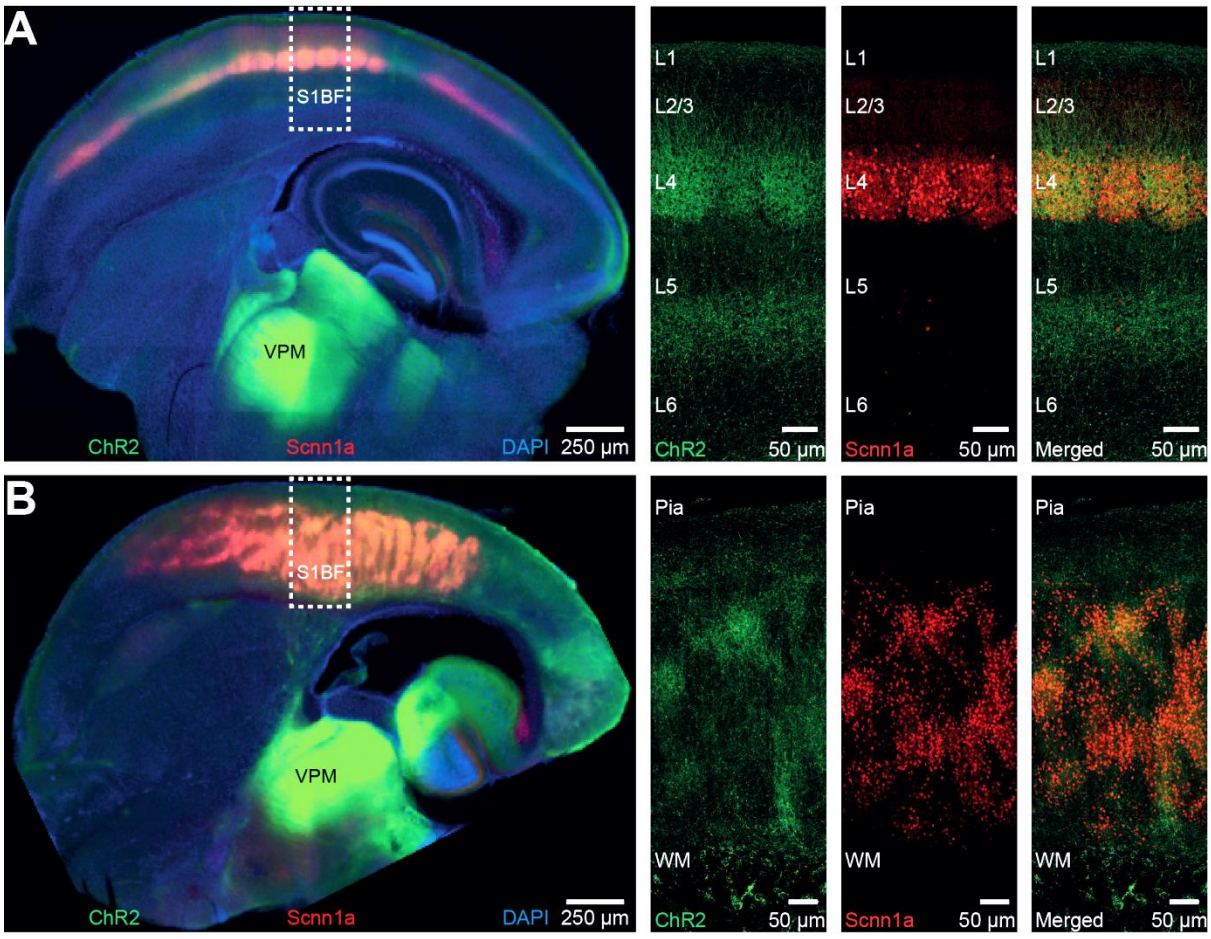

Figure 6: Projection pattern of VPm neurons onto the WT and *reeler* S1BF.

A) The left panel shows 300-µm-thick thalamocortical brain slice after ChR2 injection targeted at the VPm (green) and characteristic projection pattern onto L4 and border L5-6 of the somatosensory cortex (white box) in WT mice. On the right, a higher magnification can be seen of S1BF area in the white box. First panel shows ChR2 expression pattern in green, second panel shows Scnn1a-tdTomato fluorescent neurons and third panel shows merge image. Pia indicates pial surface, WM is white matter. **B)** Same for *reeler* mutant mice. ChR2-expressing thalamocortical fibers in the *reeler* cortex mainly colocalize with the barrel equivalents seen in the Scnn1a-tdTomato channel.

Photostimulation (1 ms pulses) reliably triggered excitatory postsynaptic responses in SpS neurons, including AP firing when stimulation intensity exceeded a threshold (see **Figure 7A-B**). Optogenetically evoked AP firing is shown for 10 WT SpS neurons (black) and 9 *reeler* SpS neurons (green) in **Figure 7A**, with the grand average per genotype indicated in red. The optical threshold was defined as the laser intensity required to elicit action potentials (APs) in SpS neurons kept in current clamp at -70 mV and did not significantly differ between WT (1.46 mW ± 0.82) and *reeler* mutant mice (1.58 mW ± 1.04; two-tailed T-test, t (17) = -0.282, p = 0.781, power = 0.058). In the 50 ms following AP firing, SpS neurons of the *reeler* mutant mice remained significantly more depolarized compared to WT mice as shown in the peristimulus time histogram in **Figure 7C** (two-way ANOVA, F (99, 1700) = 3.624, p = < 0.001). This graph demonstrates the mean change in membrane potential variation after optogenetic stimulation for WT SpS neurons (black), *reeler* SpS neurons (green) and the average difference between them (red). These results suggest a greater network activity upon TC fiber stimulation in SpS neurons of *reeler* mutant mice compared to SpS neurons of WT mice. Subthreshold responses evoked by a 1 ms optical stimulation pulse with a laser intensity set at 0.4 mW, allowed for comparison of multicomponent depolarizing responses in SpS neurons of WT mice (n = 10) and *reeler* mutant mice (n = 10; **Figure 7D**, dark coloured traces). On average, SpS neurons of *reeler* mutant mice showed a greater net depolarization following VPm stimulation than SpS neurons of WT mice (two-way ANOVA, F (99, 1900) = 0.917, p = <0.001, see **Figure 7E**). In summary, the prolonged depolarization following AP firing and the increased network activity observed in subthreshold multicomponent traces are indicative of a hyperexcitable network in the *reeler* cortex.

In order to isolate direct monosynaptic thalamic input, 0.5 µM TTX and 0.1 mM 4-AP were added to the recording ACSF (see Methods). The excitatory postsynaptic potentials (EPSPs) were recorded in SpS neurons, kept in current clamp at a holding potential of -70 mV, and were

compared between WT and *reeler* mutant mice by fixing the laser intensity at 1 mW (**Figure 7D**). Isolated direct thalamic input responses were recorded in 10 WT SpS neurons and 10 *reeler* SpS neurons as shown in **Figure 7D**. The amplitude of direct thalamic input responses recorded in SpS neurons of *reeler* mutant mice (Mdn 0.94 mV) was found significantly lower compared to WT mice (Mdn 2.34 mV) (Mann-Whitney rank sum test U = 21.00, p = 0.031, see **Figure 7F**). Moreover, the EPSP width was similar in WT (15.322 ms ± 4.99) and *reeler* mutant mice (19.181 ms ± 4.618) as shown in **Figure 7G**. This difference in EPSP width between genotypes was not significant (two-tailed t-test, t (18) = -1.794, p = 0.090, power = 0.397). Overall, the direct thalamic input responses onto *reeler* SpS neurons was found significantly smaller compared to EPSPs recorded in WT SpS neurons.

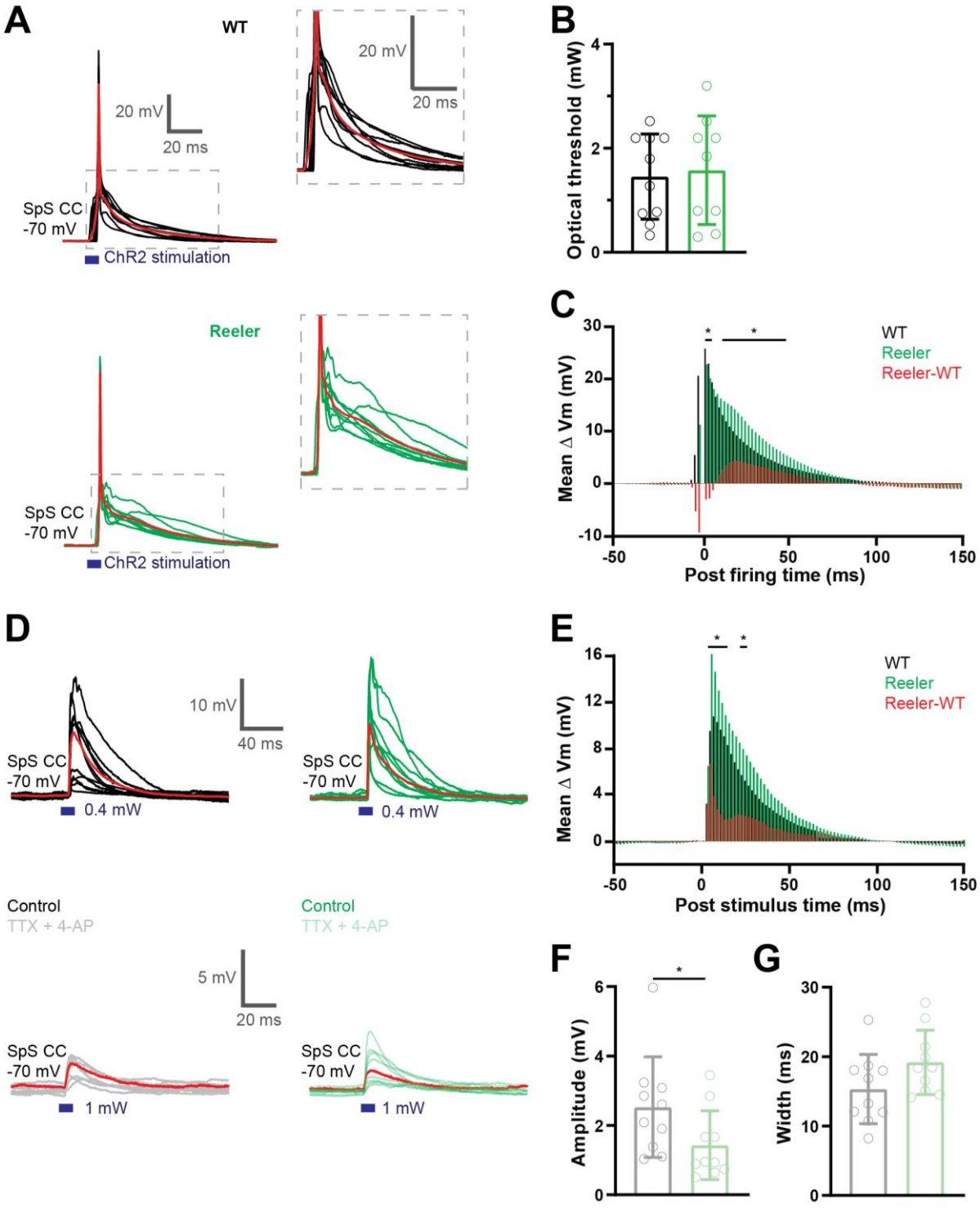

Figure 7: Optogenetic stimulation of thalamocortical fibers recorded in SpS neurons.

A) Photostimulation of thalamocortical fibers generated action potentials in SpS neurons (WT black n = 10, reeler green n = 9). Red traces represent grand average per genotype. Grey dotted box shows higher magnification of post spike depolarization. Blue bars represent 1 ms laser stimulation pulse. Scale bars in WT apply to reeler as well. B) Laser intensity required to reliably elicit an AP was not significantly different between genotypes (two-tailed T-test, t (17) = -0.282, p = 0.781, power = 0.058)). **C)** Average change in membrane potential in the 50 ms post AP firing was significantly more depolarized in reeler compared to WT (two-way ANOVA, F (99, 1700) = 3.624, p = < 0.001; 2 ms bin

size). Red bars represent the average difference between genotypes. **D)** Control condition showed subthreshold multicomponent postsynaptic potentials for each SpS neuron in response to TC fiber stimulation with 0.4 mW laser power (dark coloured traces; WT n = 10, reeler n = 10). Washing in recording ACSF with TTX and 4-AP allowed for isolating direct monosynaptic thalamic responses (light coloured traces). Isolated thalamic responses evoked with 1 mW laser strength were compared between WT (n = 10) and reeler (n = 10). Here, EPSPs recorded for each SpS neurons are overlaid and the red traces represent grand average per genotype. **E)** Average membrane potential variation of the subthreshold control condition responses post stimulus in 2 ms bins for WT mice, reeler mutant mice and the average difference between the genotypes. Optogenetically stimulated TC fibers (0.4 mW) led to significantly stronger net depolarization in reeler as compared to WT (two-way ANOVA, F (99, 1900) = 0.917, p = <0.001). **F)** Bar graph comparing amplitude (pA) of monosynaptic direct thalamic responses (TTX + 4-AP) evoked by 1 mW laser intensity in WT versus reeler. EPSP amplitude was significantly reduced in reeler mutant mice as compared to WT mice (Mann-Whitney rank sum test U = 21.00, p = 0.031). **G)** EPSP width (ms) did not significantly differ between WT and reeler mutant mice (two-tailed t-test, t (18) = -1.794, p = 0.090, power = 0.397).

Identical to previous findings, SpS neurons in the *reeler* mutant mouse showed a greater overall excitation in response to thalamic input. This was observed by a stronger, prolonged depolarization following APs and a greater depolarization seen in subthreshold multicomponent responses (**Figure 7A-E**). Upon blocking network activity, monosynaptic thalamic input was found to be weakened in SpS neurons of *reeler* mutant mice compared to WT mice (**Figure 7D, F and G**). Overall, the present results are a validation of earlier findings.

Electrophysiological and morphological characterisation of neurons in *reeler* vs WT

Having replicated previous findings, paired recordings were performed to test the main hypotheses. To that end, whole-cell patch clamp recordings were made of tdTomato expressing SpS neurons and FS interneurons in WT and *reeler* mutant mice (see Methods). Each recording typically started with a thorough characterization of the electrophysiological properties of the recorded neurons (see Methods). This did not only help with confirming the type of neuron, but also allowed me to investigate whether passive or active neuronal properties of SpS neurons and FS interneurons were altered due to a lack of the *reelin* protein. In order to correctly interpret connection differences between WT and *reeler* mutant mice, it is essential to first establish whether there are differences in neuronal properties (electrophysiological and morphological) between these genotypes. Passive properties such as resting membrane

potential, input resistance, sag index and membrane time constant were calculated from an averaged response to a 1 s hyperpolarizing current pulse of -50 pA, while neurons were kept in current clamp at their resting membrane potential. Action potential waveform parameters such as firing threshold, AP width and AP amplitude were analysed from spikes elicited during rheobase recordings. In addition to characterizing various electrophysiological parameters, morphological parameters of dendritic arborizations were studied. Biocytin-filling of recorded neurons allowed for post-hoc microscopic visualization followed by morphological reconstruction of the neurons (see Methods). Due to the fainter biocytin signal in distal axonal branches, morphological characterisation was restricted to the dendritic arborisation. Dendrite morphology parameters such as the number of dendrites, total dendritic length, average length per dendrite and amount of branching points per neuron were analysed. Subsequently, it was studied whether these electrophysiological and morphological properties in SpS neurons and FS interneurons were altered due to a mutation in the *reelin* gene.

Spiny stellate neurons

Spiny stellate neurons were selected by their expression of Scnn1a-tdTomato, their tendency to occur in small clusters of densely packed somata and their small diamond shaped soma. A hyperpolarized resting membrane potential and a regular spiking firing pattern further confirmed the cell type. For analysis of basic neuron characteristics, exclusively cells patched with standard potassium-based intracellular solution were used (WT $n = 114$, *reeler* $n = 52$). A subset of these SpS neurons with sufficient biocytin filling were imaged and reconstructed (WT $n = 3$, *reeler* $n = 6$) for examination of the dendritic morphology.

Representative morphologies of SpS neurons in respectively a WT mouse and a *reeler* mutant mouse are presented in **Figure 8A and B**. Dendritic arborisation of both WT and reeler SpS neurons was restricted to the home barrel or barrel equivalent, as the outlines of which are represented in black dotted lines. In both genotypes, SpS neurons had a similar amount of dendritic main branches (WT Mdn 4.00; *reeler* Mdn 4.00; Mann-Whitney rank sum test, $U = 7.500$, $p = 0.714$, see **Figure 8C**). Similarly, the total dendritic length measured in WT SpS neurons (1834.27 µm ± 134.21) did not significantly differ from *reeler* SpS neurons (2127.07 µm ± 354.63) (two-tailed T-test; $t(7) = -1.344$, $p = 0.221$, power = 0.214, see **Figure 8D**). The average length per dendrite was also not affected in *reeler* SpS neurons (559.72 µm ± 103.127)

compared to WT SpS neurons (505.93 µm ± 57.30) (two-tailed T-test; t (7) = -0.823, p = 0.437, power = 0.110, see **Figure 8E**). Last, the complexity of dendritic arborisation was evaluated by the amount of branching points per SpS neuron. The number of branching points did not differ between WT SpS neurons (Mdn 20.00) and *reeler* SpS neurons (Mdn 24.00) (Mann-Whitney rank sum test, U = 4.000, p = 0.262, see **Figure 8F**). Summarizing, the absence of reelin protein does not cause a significant change in the dendritic morphology of SpS neurons.

Characteristic voltage responses following various current pulses are depicted for SpS neurons recorded in WT mice (**Figure 9A**) and SpS neurons recorded in *reeler* mutant mice (**Figure 9B**). These voltage responses were then analysed to compare passive and active properties of FS interneurons between both genotypes. Various passive properties of SpS neurons were compared between the two genotypes: resting membrane potential (mV), input resistance (MΩ), sag index (%) and tau (ms). The resting membrane potential was found to be similar in WT SpS neurons (-72.27 mV ± 3.27) and *reeler* SpS neurons (-72.70 mV ± 3.89) (two-tailed T-test; t (164) = 0.737, p = 0.462, power = 0.113), see **Figure 9C**. Likewise, the input resistance measured in WT SpS neurons (Mdn 128.20 MΩ) and *reeler* SpS neurons (Mdn 129.46 MΩ) did not change (Mann-Whitney rank sum test, U = 2741.00, p = 0.439, see **Figure 9D**). The absence of reelin also did not influence the sag index of *reeler* SpS neurons (Mdn 2.93 %), compared to WT SpS neurons (Mdn 3.15 %) (Mann-Whitney rank sum test, U = 2779.00, p = 0.521, see **Figure 9E**). Last, the membrane time constant (τ) of WT SpS neurons (Mdn 8.38 ms) was comparable to *reeler* SpS neurons (Mdn 7.16 ms) (Mann-Whitney rank sum test, U = 2632.00, p = 0.248, see **Figure 9F**). In summary, the lack of reelin protein did not affect passive properties of SpS neurons.

Next, the active properties of SpS neurons were analysed, namely: rheobase (pA), firing threshold (mV), AP width (ms) and AP amplitude (mV). First, the rheobase of SpS neurons was not affected by the reelin mutation (WT Mdn 150.52 pA; *reeler* Mdn 139.97 pA; Mann-Whitney rank sum test, U = 2021.00, p = 0.060, see **Figure 9G**). Subsequently, SpS neurons in the *reeler* mutant mouse displayed a median firing threshold value of -31.94 mV compared to a median value of -31.80 mV in WT SpS neurons (Mann-Whitney rank sum test, U = 2490.50, p = 0.984, see **Figure 9H**). Also no difference was found in the AP width of *reeler* SpS neurons (Mdn 0.65 ms) versus WT SpS neurons (Mdn 0.66 ms) (Mann-Whitney rank sum

test, U = 2088.50, p = 0.107, see **Figure 9I**). Last, *reeler* SpS neurons showed a similar median AP amplitude of 62.83 mV comparable to that of WT SpS neurons (Mdn 64.71 mV) (Mann-Whitney rank sum test, U = 2278.50, p = 0.390, see **Figure 9J**). These results showed that active properties of SpS neurons are also not affected in the *reeler* mutant mouse.

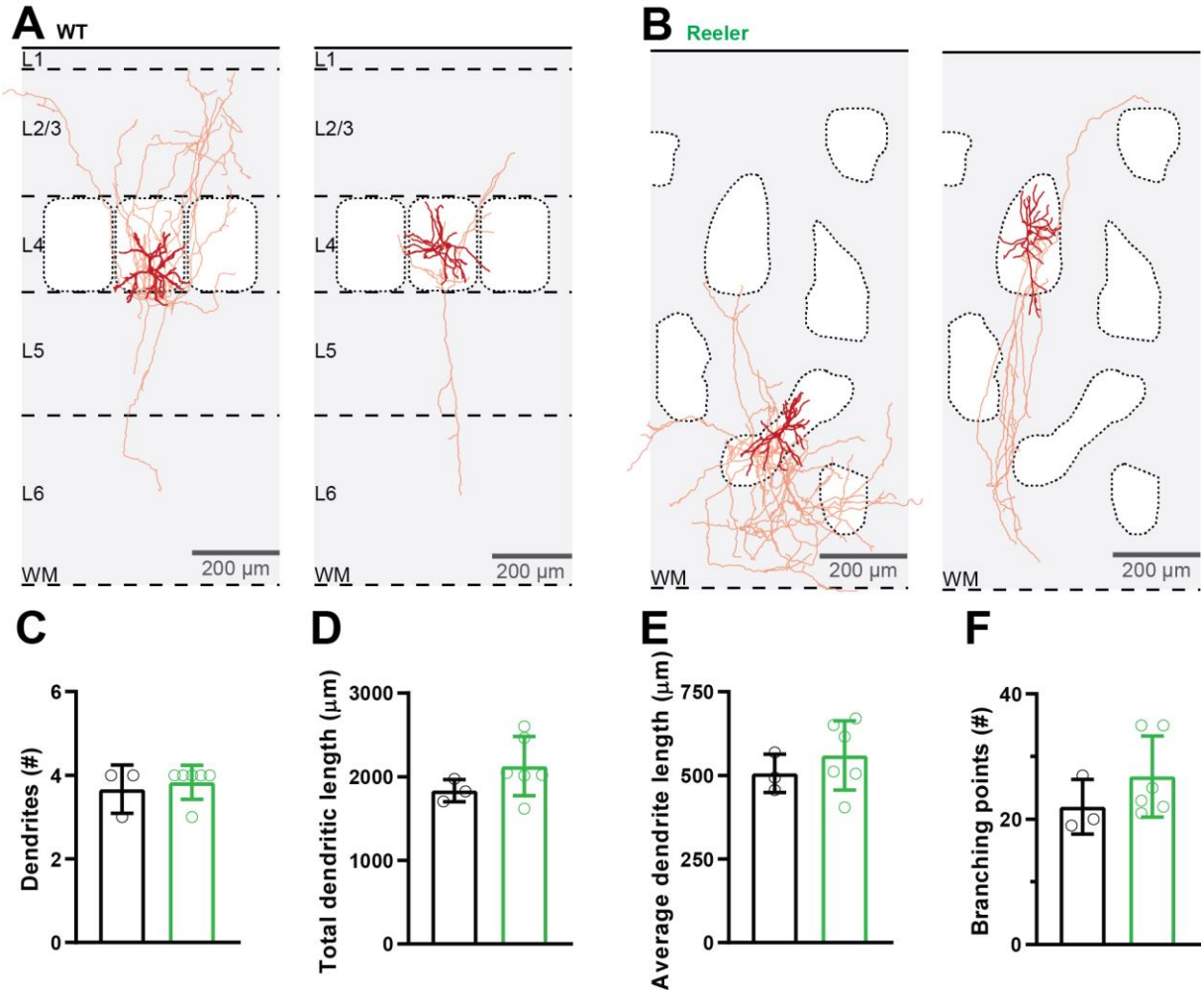

Figure 8: Dendritic morphology of SpS neurons.

A) Example reconstructions of SpS neuron morphology in the WT S1BF. Striped lines represent layer (L) and white matter (WM) borders and dotted lines represent barrel contours. Somatodendritic arbor shown in dark colour, axon shown in light colour. **B)** Example reconstructions of *reeler* SpS neuron morphology. Dotted contours represent an exemplar of barrel equivalents spread over S1BF. **C-F)** Dendritic morphology parameters such as number of dendrites per SpS neuron, total dendritic length, average dendrite length per SpS neuron, and number of dendritic branching points where not significantly different between genotypes.

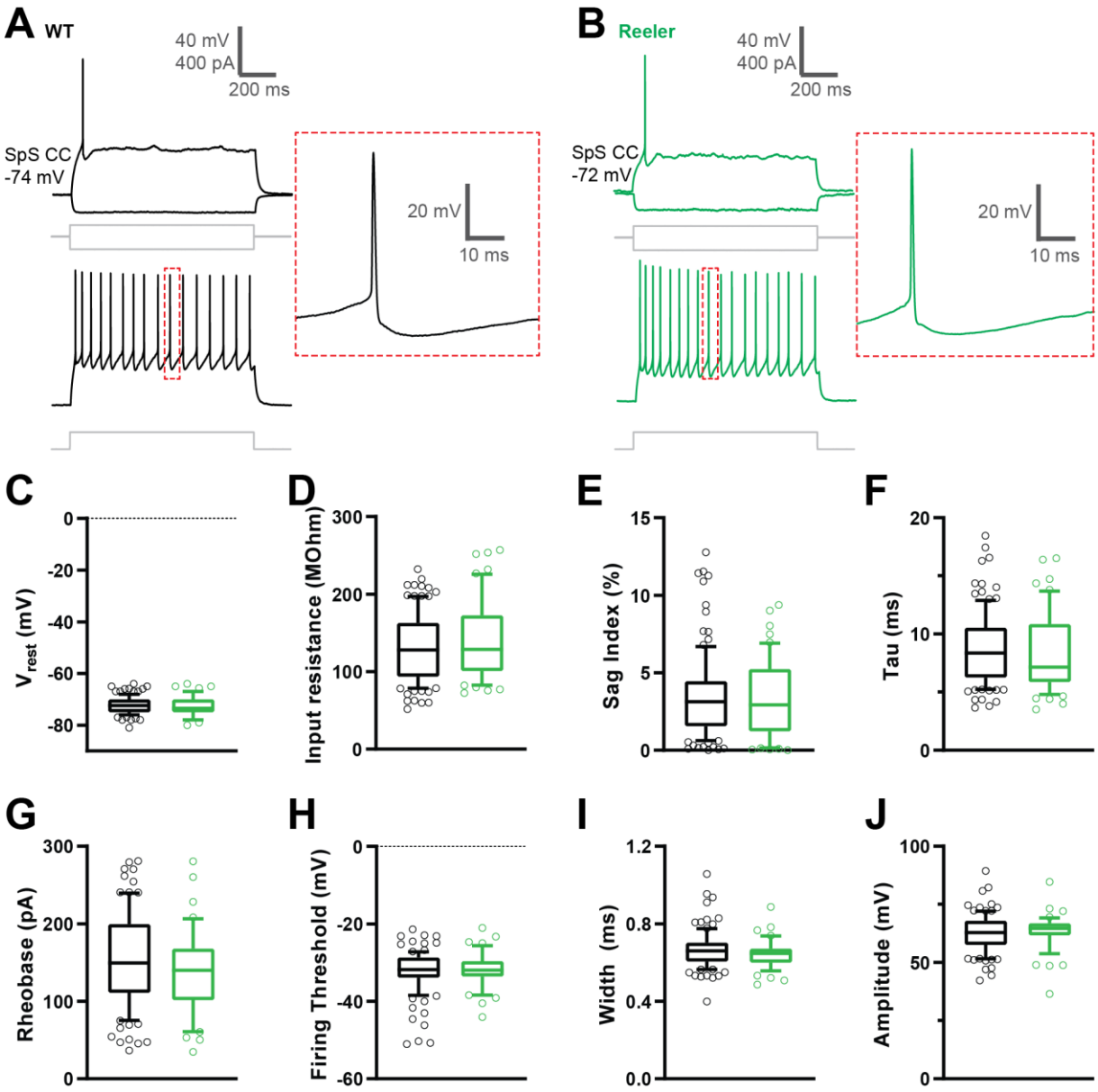

Figure 9: Electrophysiological properties of SpS neurons.

A) Typical firing pattern of WT SpS neurons (left) and high magnification (red dotted box) of a single AP waveform (right). **B)** Representative firing pattern (left) and high magnification (red dotted box) of a single AP waveform (right) of a *reeler* SpS neuron. **C-F)** Passive properties of SpS neurons in response to -50 pA current pulses, recorded at resting membrane potential, did not significantly differ. **G-J)** Spiking properties of SpS neurons in response to depolarizing current pulses, recorded at resting membrane potential, did also not significantly vary.

Fast spiking interneurons

FS interneurons were identified based on their morphology. Their typically large and oval shaped soma, as well as the lack of Scnn1a-tdTomato expression, aided the targeting and morphological identification of FS interneurons. Furthermore, a fast-spiking AP pattern, steep

afterhyperpolarizations, small AP amplitudes and high frequency firing supported their identification. In total, 23 WT and 21 *reeler* FS interneurons were analysed for electrophysiological properties. From a subset of these FS interneurons with successful biocytin filling, post-hoc confocal imaging followed by reconstructing allowed for morphological analysis (WT $n = 3$, *reeler* $n = 6$).

Example morphological reconstructions are shown in **Figure 10A and B** for respectively WT FS interneurons and *reeler* FS interneurons. From these reconstructed FS interneurons, various parameters were analysed to evaluate the dendritic morphology. The number of dendritic branches in *reeler* FS interneurons (5.17 ± 1.72) was similar compared to WT FS interneurons (5.00 ± 1.00) (two-tailed T-test, t (7) = -0.152, $p = 0.883$, power = 0.052, see **Figure 10C**). The total length of the dendritic arborisation was also not affected by a lack of reelin protein (WT 2881.60 µm ± 864.72; *reeler* 3263.03 µm ± 899.16; two-tailed T-test, t (7) = -0.606, $p = 0.563$, power = 0.082, see **Figure 10D**). In addition, the average length per FS interneuron dendrite was comparable in WT and *reeler* mice (WT 602.27 µm ± 270.02; *reeler* 657.35 µm ± 157.29; two-tailed T-test, t (7) = -0.397, $p = 0.703$, power = 0.064, see **Figure 10E**). Last, the number of branching points in the dendritic arborisation of WT FS interneurons (Mdn 31.00) did not significantly differ from those quantified in *reeler* FS interneurons (Mdn 31.00) (Mann-Whitney rank sum test, U = 8.500, $p = 0.905$, see **Figure 10F**). In brief, dendritic morphology of FS interneurons was unaffected in the *reeler* mutant mouse.

Regarding the elctrophysiological properties, representative firing patterns and AP waveforms of FS interneurons recorded in WT and *reeler* mutant mice can be seen in **Figure 11A and B**. Subsequently, these traces were analysed to compare passive and active properties of FS interneurons between WT and *reeler* mutant mice. Several passive properties of FS interneurons were analysed and compared between WT and *reeler* mutant mice: resting membrane potential (mV), input resistance (MΩ), sag index (%) and τ (ms). First, the resting membrane potential of *reeler* FS interneurons (-65.07 mV ± 3.19) and WT FS interneurons (-63.86 mV ± 3.65) did not significantly differ (two-tailed T-test, t (42) = 1.169, $p = 0.249$, power = 0.208, see **Figure 11C**). On average, the input resistance measured in *reeler* FS interneurons (92.69 MΩ ± 35.00) was comparable to the input resistance found in WT FS interneurons (106.74 MΩ ± 36.83) (two-tailed T-test, t (40) = -1.267, $p = 0.213$, power = 0.235, see **Figure**

11D). Furthermore, *reeler* FS interneurons displayed a similar sag index (Mdn 3.95 %) compared to WT FS interneurons (Mdn 5.51%) (Mann-Whitney rank sum test, U = 180.00, p = 0.314, see **Figure 11E**). Last, the τ was also not significantly different between *reeler* FS interneurons (Mdn 5.30 ms) and WT FS interneurons (Mdn 4.53 ms) (Mann-Whitney rank sum test, U = 173.00, p = 0.237, see **Figure 11F**). In brief, the passive properties of FS interneurons are not affected in the *reeler* mutant mouse.

Then, the active properties of WT and *reeler* FS interneurons were analysed, more specifically: rheobase (pA), firing threshold (mV), AP width (ms) and AP amplitude (mV). The rheobase of *reeler* FS interneurons (270.66 pA ± 124.35) showed to be similar to that of WT FS interneurons (306.77 pA ± 141.35) (two-tailed T-test, t (33) = 0.787, p = 0.437, power = 0.119, see **Figure 11G**). In addition, *reeler* FS interneurons had an AP firing threshold (-34.19 mV ± 6.62) comparable to that of WT FS interneurons (-35.74 mV ± 9.18) (two-tailed T-test, t (33) = -0.553, p = 0.584, power = 0.084, see **Figure 11H**). The median value for AP width in *reeler* FS interneurons was 0.269 ms, which was not significantly different from the median AP width value in WT FS interneurons (Mdn 0.247 ms) (Mann-Whitney rank sum test, U = 118.00, p = 0.294, see **Figure 11I**). Finally, the median values of AP amplitude in *reeler* FS interneurons (38.72 mV ± 10.52) and WT FS interneurons (37.38 mV ± 10.87) did also not significantly differ (two-tailed T-test, t (33) = -0.367, p = 0.716, power = 0.065, see **Figure 11J**). These results demonstrated that active properties of FS interneurons are not affected by an absence of the reelin protein.

In conclusion, various biophysical and morphological dendrite properties were assessed in order to determine whether SpS neurons and FS interneurons are comparable between genotypes. The results confirmed that basic electrophysiological parameters (both passive and active) and the dendritic arborizations do not vary significantly as a result of a loss of reelin. Therefore, differences in network properties and evoked response amplitudes cannot be explained by changes in biophysical properties or changes in dendritic morphology caused by the absence of reelin. Instead, observed differences between genotypes, are most likely the result of changes in synaptic properties.

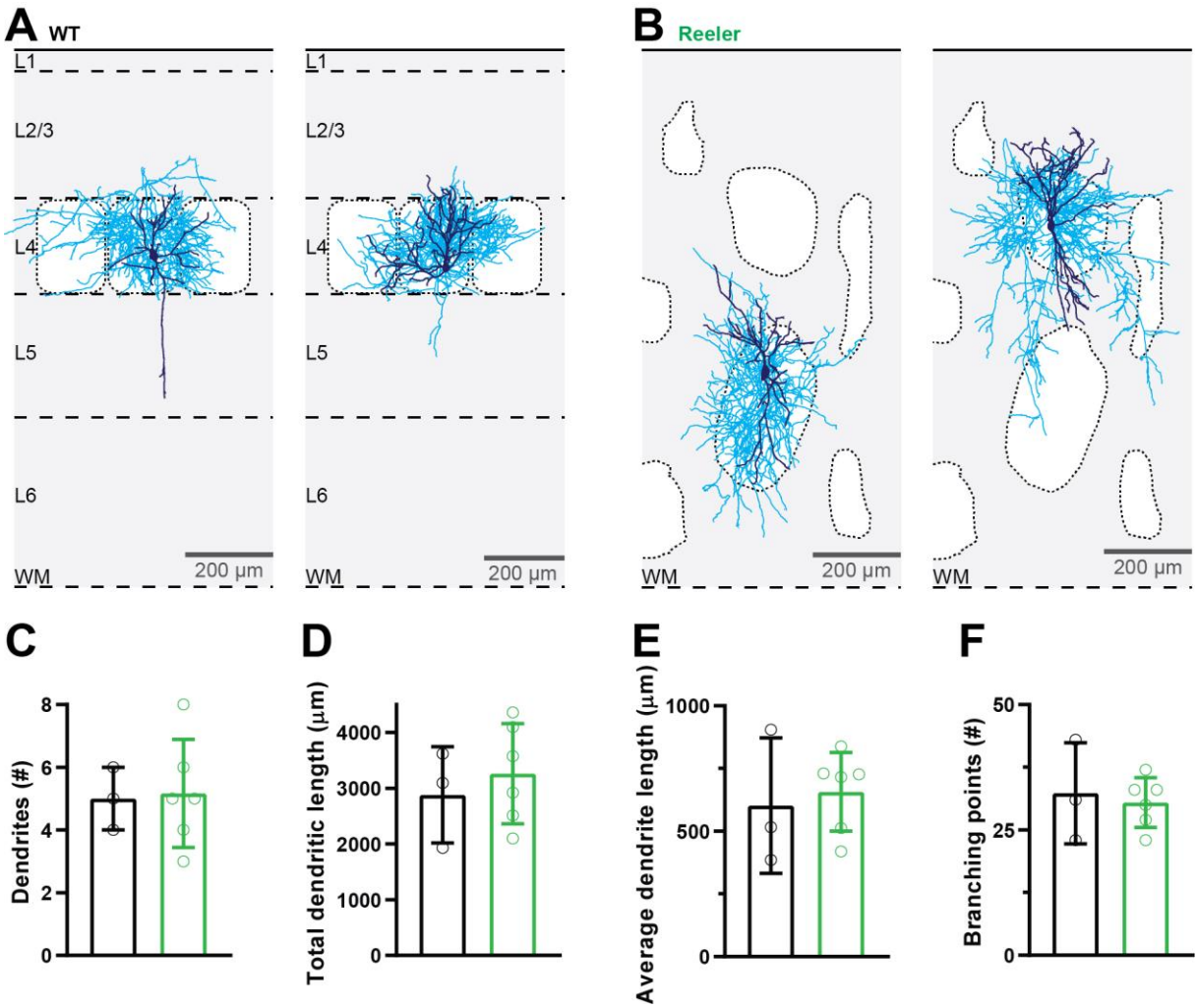

Figure 10: Dendritic morphology of FS interneurons.

A) Example reconstructions of FS interneuron morphology in the WT S1BF. Striped lines represent layer (L) and white matter (WM) borders and dotted lines represent barrel contours. Somatodendritic arbor shown in dark colour, axon shown in light colour. **B)** Example reconstructions of *reeler* FS interneuron morphology. Dotted contours represent an exemplar of barrel equivalents spread over S1BF. **C-F)** Dendritic morphology parameters such as number of dendrites per FS interneuron, total dendritic length, average dendrite length per FS interneuron, and number of dendritic branching points where not significantly different between genotypes.

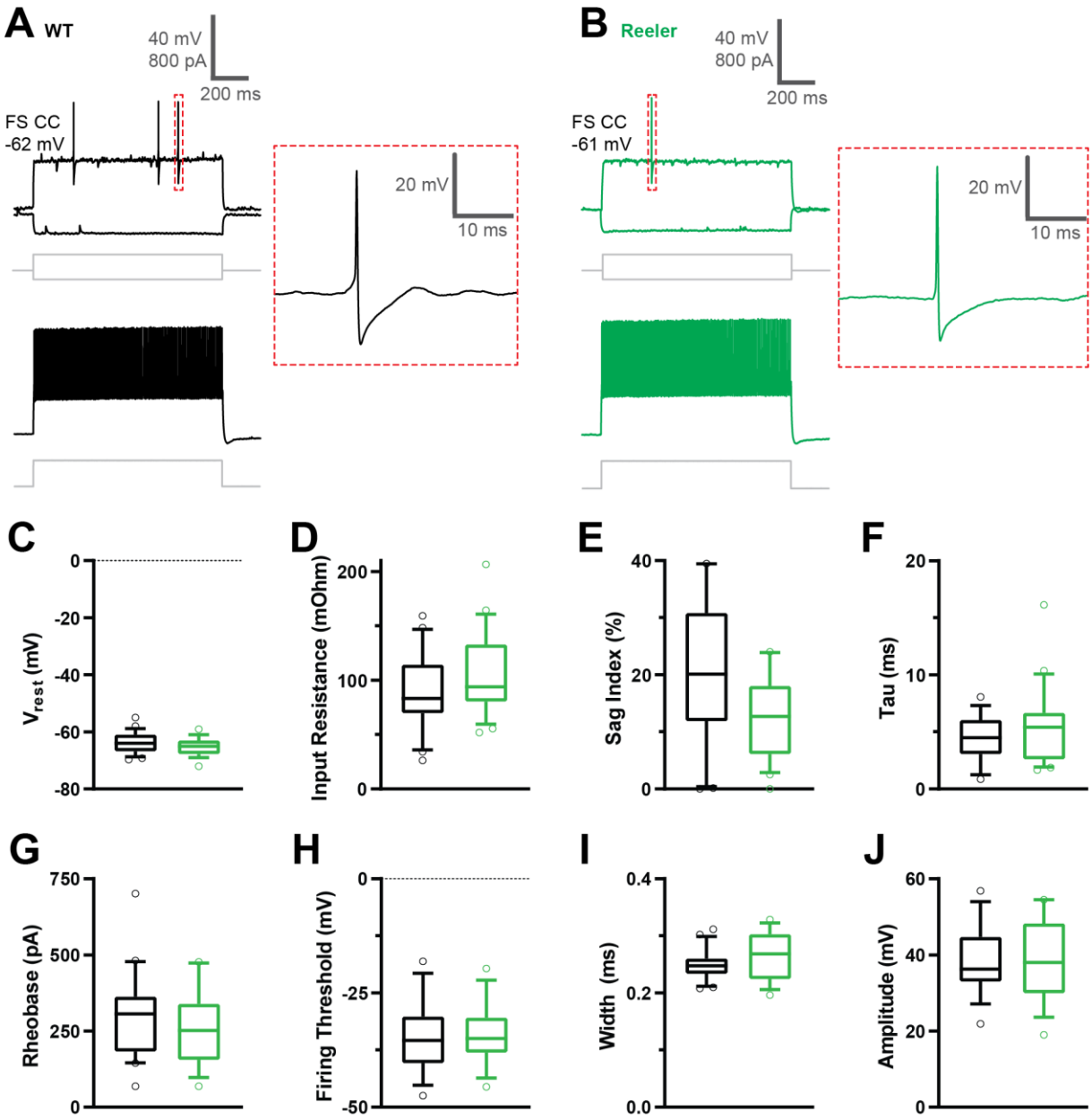

Figure 11: Electrophysiological properties of FS interneurons.

A) Typical firing pattern of WT FS interneurons (left) and high magnification (red dotted box) of a single AP waveform (right). **B)** Representative firing pattern (left) and high magnification (red dotted box) of a single AP waveform (right) of a *reeler* FS interneuron. **C-F)** Passive properties of FS interneurons in response to -50 pA current pulses, recorded at resting membrane potential, did not significantly differ between genotypes. **G-J)** Spiking properties of FS interneurons in response to depolarizing current pulses, recorded at resting membrane potential, did also not significantly vary.

Connectivity between SpS neurons is unaffected in the *reeler* S1BF

Having established that elementary neuronal properties are comparable across genotypes, I set out to explore possible differences in unitary connectivity among SpS neurons themselves and with FS interneurons. The first hypothesized cortical mechanism to compensate for the weakened thalamic input in *reeler* mutant mice is an increase in recurrent excitation between SpS neurons. Greater recurrent excitation between SpS neurons could be caused by a higher rate of connections between excitatory neurons, more reliable connections (less synaptic failures) and/or larger excitatory postsynaptic current (EPSC) responses. These parameters were studied using paired whole-cell patch clamp recordings between SpS neurons in WT and *reeler* mutant mice (see Methods).

Out of 49 pairs of SpS neurons patched in WT mice, 9 pairs were connected (18.4 %; see **Figure 12**). Connections were either bidirectional (2 out of 49, 4.1 %) or unidirectional (7 out of 49, 14.3 %). Similarly, connection probability between SpS neurons in *reeler* mutant mice was 17.7 % (3 out of 17). From the recorded connections, 1 out of 17 (5.9 %) was bidirectionally connected and 2 out of 17 pairs (11.8 %) were found unidirectionally connected. In summary, the connection probability between SpS neurons was not obviously elevated in *reeler* mutant mice compared to WT mice (Chi-square, X^2 (2) = 0.150, p = 0.928, power = 0.061).

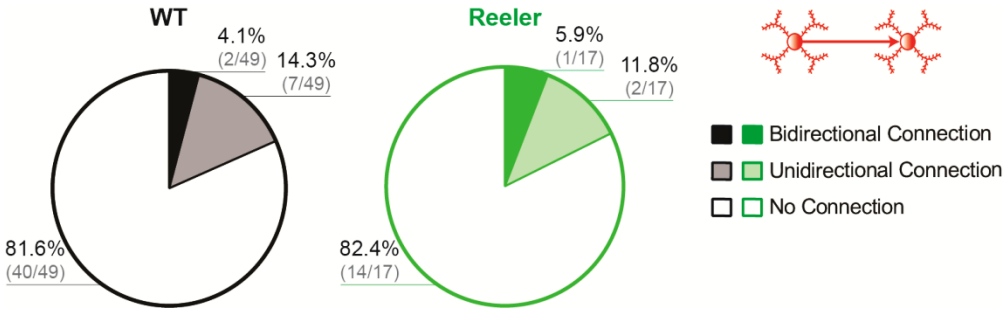

Figure 12: Connection probability between SpS neurons.

Connection probability between SpS neurons in WT (black) and in *reeler* mutant mice (green), was found similar. In these pie charts, dark colour indicates bidirectional connection probability, light colour indicates percentage of unidirectionally connected pairs and white indicates percentage of unconnected pairs.

The averaged EPSCs (WT black n = 5, *reeler* n = 4 green) and a grand average per genotype (in red) are shown in **Figure 13A**. The reliability of the connection was measured as the synaptic failure rate, defined as the percentage of presynaptic APs failing to trigger a

postsynaptic response exceeding three times the standard deviation of the baseline membrane potential. In both WT and *reeler* mutant mice, a highly variable synaptic failure rate was observed (WT 35.21 % ± 35.20 n = 9, *reeler* 47.09 % ± 33.75 n = 4, Fisher exact test, p = 1.000, see **Figure 13B**). The EPSC latency was calculated as the time from the presynaptic action potential (red dotted line in **Figure 13A**) until the onset of the EPSC response, defined as the time point at which the EPSC exceeds a threshold set as the baseline current measured in a 100 ms window preceding stimulus onset plus three times its standard deviation. From recorded pairs of neurons (WT n = 5, *reeler* n = 4), no change in EPSC latency was observed between SpS neurons of WT (1.10 ms ± 0.29) and *reeler* mutant mice (0.95 ms ± 0.21), neither did the time-to-peak (WT Mdn 1.96 ms, *reeler* Mdn 2.19 ms) and amplitude (WT Mdn 4.66 pA, *reeler* Mdn 6.73 pA, see **Figure 13C-E**). Interestingly, the EPSC decay was found to be significantly shorter in *reeler* SpS neurons compared to WT (two-tailed T-test t (7) = 2.613, p = 0.035, power = 0.613, see **Figure 13F**). Due to the low number of neuronal connections analysed it is not possible to exclude a modest increase in EPSC amplitude between SpS neurons in the *reeler* mouse mutant, as an indication of enhanced recurrent excitation.

To investigate the short-term plasticity between SpS neurons, trains of APs were generated in the presynaptic SpS neuron. Train stimulation was only performed in connected SpS pairs showing a low synaptic failure rate. In addition, trains were recorded following the connection test, when there were no signs of recording instability observed by input resistance. Trains of 5 presynaptic APs were elicited with 5 ms current pulses at different frequencies: 1, 5, 20 and 50 Hz (WT n = 1, *reeler* n = 1; see **Figure 14**). At least 10 iterations per frequency were recorded with an interstimulus interval of 10 s. From each EPSC response in the train, the peak amplitude was calculated. These peak amplitudes were then normalized to the first EPSC response amplitude as can be seen on the graphs in **Figure 14**. In both genotypes a short-term depression of EPSC amplitude was observed (see **Figure 14**). The stronger short-term depression observed in the normalized EPSC amplitudes in *reeler* mutant mice could be explained by the larger EPSC amplitude found. Taken together, these proof-of-principle results show no evidence of altered short-term plasticity between SpS neurons in WT and *reeler* mutant mice.

In conclusion, SpS neurons in the *reeler* mutant mouse did not show a higher connectivity that would suggest an enhanced recurrent excitation between these neurons. Moreover, the reliability of the SpS neuron to SpS neuron connection was also similar between the two genotypes. Single EPSCs recorded between SpS neurons did not differ greatly between *reeler* and WT mice. In other words, neither the connection probability nor the connection strength between excitatory neurons were increased in the *reeler* mutant. It is therefore concluded that an increase in recurrent excitation is not a likely explanation for the hyperexcitability of *reeler* SpS neurons reported above.

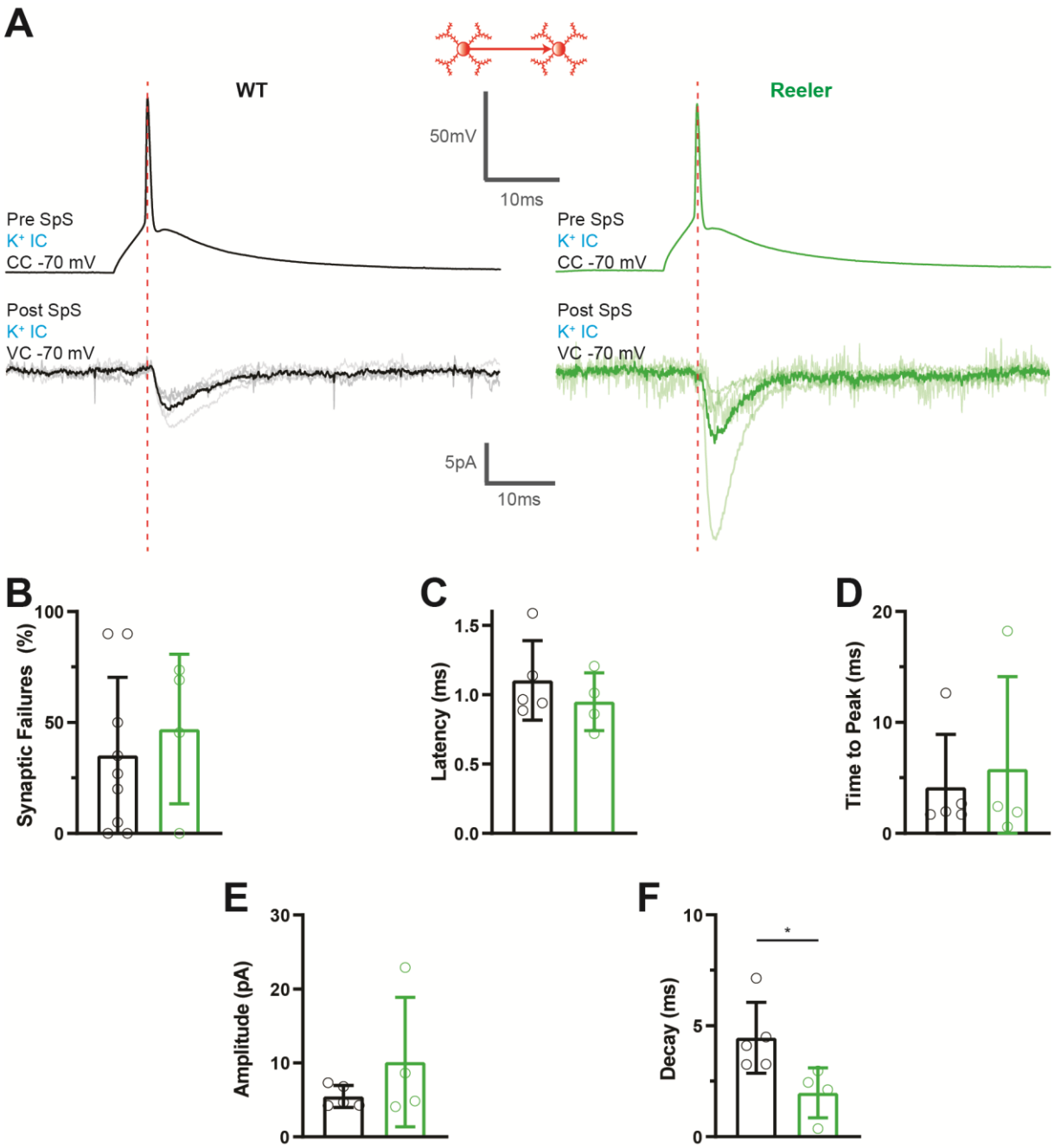

Figure 13: EPSCs recorded between SpS neurons.

A) Averaged EPSCs per connection (light colour; WT black $n = 5$, *reeler* green $n = 4$) and grand average per genotype in darker traces. Red dotted line indicates the time-point of the presynaptic AP peak. SpS neurons were patched with a potassium-based IC solution. **B)** Synaptic failure rate (WT 35.21 % ± 35.20 $n = 9$, *reeler* 47.09 % ± 33.75 $n = 4$, Fisher exact test, $p = 1.000$) did not differ in WT versus *reeler*. **C)** EPSC latency between two genotypes was similar (WT 1.10 ms ± 0.29 $n = 5$, *reeler* 0.95 ms ± 0.21 $n = 4$). **D)** Time-to-peak of EPSCs in both genotypes were comparable (WT Mdn 1.96 ms, *reeler* Mdn 2.19 ms) **E)** No difference was found in EPSC amplitude between WT and *reeler* mutant mice (WT Mdn 4.66 pA, *reeler* Mdn 6.73 pA). **F)** Decay time of EPSCs recorded between SpS neurons in *reeler* mutant mice were significantly shorter compared to WT (two-tailed T-test $t(7) = 2.613$, $p = 0.035$, power = 0.613).

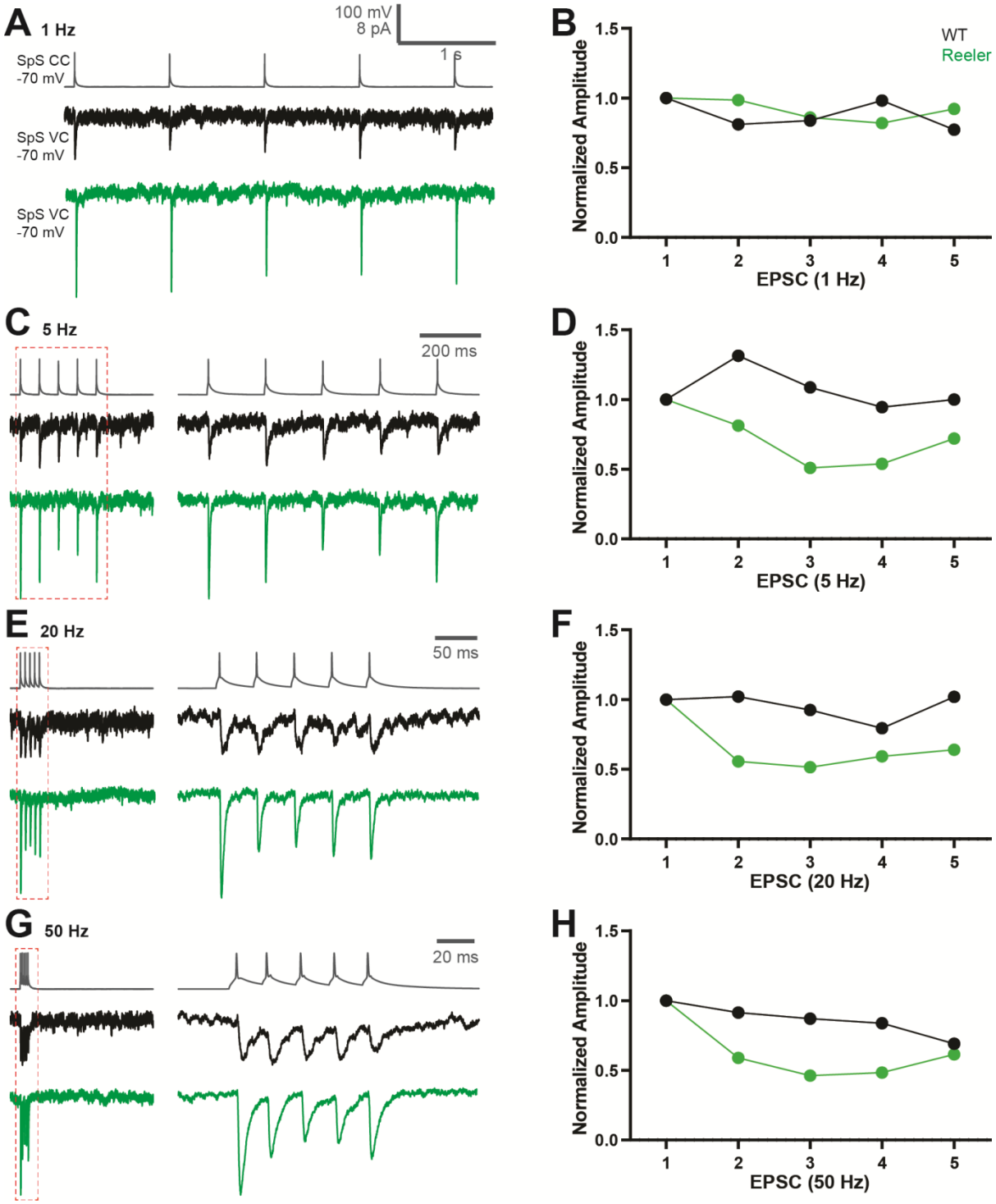

Figure 14: Short-term plasticity between SpS neurons.

A) EPSCs recorded from 1 Hz train stimulation (WT black *n* = 1, *reeler* green *n* = 1). **B)** EPSC amplitudes of the 1 Hz train normalized to the amplitude of the first EPSC response. **C)** 5 Hz train stimulation. Scaling of the traces on the left matches the scaling of the traces in A. Traces in the red dotted box are shown over an elongated timescale on the right. **D)** Normalized amplitude of EPSCs from the 5 Hz train stimulation. **E)** 20 Hz stimulation traces, with the analysed normalized amplitude of EPSCs in **F**. **G)** 50 Hz train stimulation traces, with the normalized EPSC amplitude shown in **H**.

Significantly reduced connectivity between FS interneurons and SpS neurons in the *reeler* S1BF

Having concluded that the hypothesis of an increased recurrent excitation between SpS neurons in the *reeler* mutant mouse is unlikely to be true, the following hypothesis tested for the possibility that GABAergic inhibition may be weakened instead. This hypothesis proposes a weakening of feedforward and/or feedback inhibition of SpS neurons as a compensatory mechanism for weakened thalamic input in the *reeler* S1BF. To examine a crucial component of GABAergic inhibition in the L4 (equivalent) of S1BF, the connection probability, reliability, and strength between FS interneurons and SpS neurons were measured. These parameters were investigated using paired whole-cell patch clamp recordings between SpS neurons and FS interneurons in S1BF of WT and *reeler* mutant mice (see Methods).

To calculate the connection probability, paired recordings of FS interneurons and SpS neurons were categorized in bidirectionally connected, unidirectionally connected (considering both directions) and unconnected pairs (see **Figure 15**). Out of 17 pairs patched in WT mice, 8 showed an inhibitory connection (47.1 %, combined bidirectional connection and unidirectional connection FS interneuron to SpS neuron). In contrast, only one out of 27 pairs patched in *reeler* mutant mice showed an inhibitory connection (3.7 %). These results demonstrate a drastic decrease in inhibitory connectivity from FS interneuron onto SpS neurons in *reeler* mutant mice compared to WT mice (Chi-square, X^2 (3) = 14.431, p = 0.002, power = 0.904). In agreement with the hypothesis and based on this data set, the inhibitory connection probability from FS interneurons to SpS neurons was indeed reduced in *reeler* mutant mice.

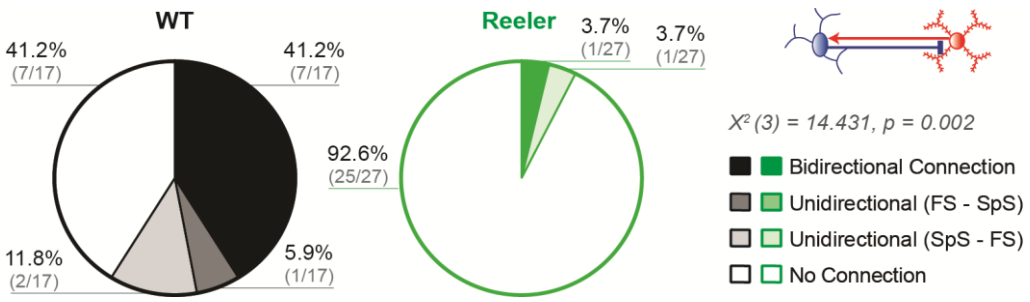

Figure 15: Connectivity between FS interneurons and SpS neurons.

Connection probability between FS interneurons SpS neurons in *reeler* mutant mice (green) was significantly lower compared to WT mice (black; X^2 (3) = 14.431, p = 0.002, power = 0.904). In these pie charts, paired recordings were put in to four categories: bidirectionally connected, unidirectionally connected from FS interneuron to SpS neuron, unidirectionally connected from SpS neuron to FS interneuron and unconnected.

Then, the inhibitory connection reliability and strength from FS interneuron to SpS neuron in WT and *reeler* mutant mice were analysed. The IPSCs recorded are shown in **Figure 16A** (WT n = 3, *reeler* n = 1) with the grand average per genotype shown in dark colour. A high synaptic failure rate was found in the single inhibitory connection recorded in the *reeler* mutant mouse (n = 1, 66.67 %), whereas inhibitory connections recorded in WT mice were strongly reliable (n = 5, synaptic failure rate of 0.00 %, see **Figure 16B**). Subsequently the various IPSC waveform parameters were examined. The latency of IPSCs recorded in WT mice (0.54 ms ± 0.20, n = 3) was similar to that recorded in the *reeler* mutant mouse (0.70 ms, see **Figure 16C**). The single IPSC recorded in a *reeler* mutant mouse was found to be smaller and shorter compared to the IPSCs recorded in WT mice (time-to-peak: WT 2.50 ms ± 1.01, *reeler* 0.55 ms; amplitude: WT 6.76 pA ± 1.42, *reeler* 4.16 pA; decay: WT 5.99 ms ± 2.29, *reeler* 2.99, see **Figure 16D-F**). Taken together, the single inhibitory connection from FS interneuron to SpS neuron found in the *reeler* mutant mouse was less reliable and weaker compared to the inhibitory connections found in WT mice. These results supported the hypothesis that a reduced feedforward and/or feedback inhibition acts as a possible intracortical compensatory mechanisms for the weakened thalamic input in the *reeler* S1BF.

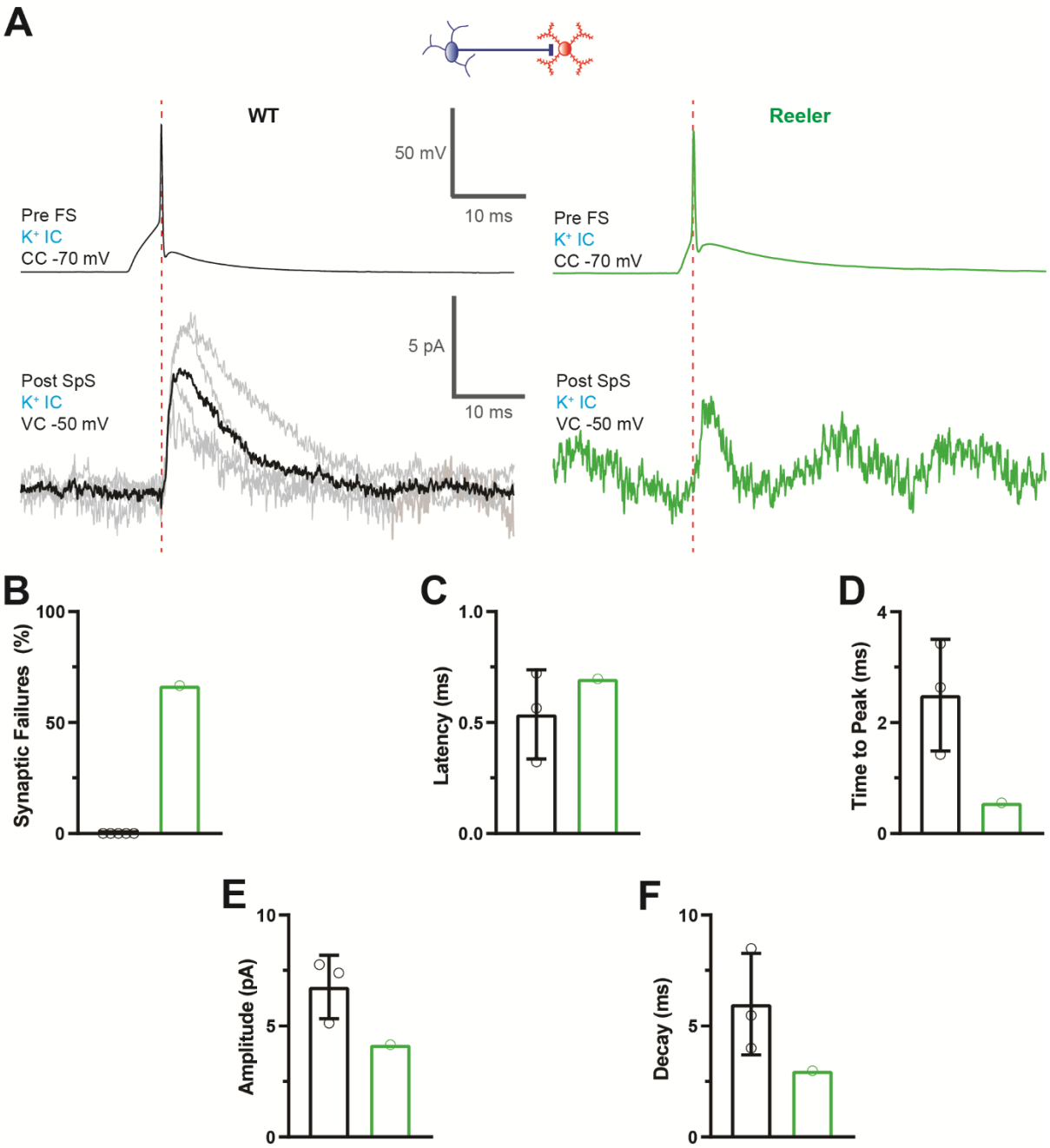

Figure 16: IPSCs recorded between FS interneurons and SpS neurons

A) Averaged IPSCs per connection (light colour; WT black *n* = 3, *reeler* green *n* = 1) and grand average per genotype in darker traces. Red dotted line indicates the time-point of the presynaptic FS interneuron AP peak. Both neurons were patched with potassium-based IC solution. The postsynaptic SpS neurons was kept in voltage clamp (VC) at a holding potential of -50 mV. **B)** Synaptic failure rate was higher in the single inhibitory connection recorded in the *reeler* mutant mouse (WT 0.00 % ± 0.00 *n* = 5, *reeler* 66.67 % *n* = 1). **C)** IPSC latency was similar between the two genotypes (WT 0.54 ms ± 0.20 *n* = 3, *reeler* 0.70 ms *n* = 1). **D)** IPSC time-to-peak was shorter in *reeler* (WT 2.50 ms ± 1.01, *reeler* 0.55 ms). **E)** IPSC amplitude was smaller in *reeler* compared to WT (WT 6.76 pA ± 1.42, *reeler* 4.16 pA). **F)** IPSC decay was shorter in *reeler* mutant mice compared to WT mice (WT 5.99 ms ± 2.29, *reeler* 2.99 ms).

Similarly, the excitatory connection probability from SpS neuron to FS interneuron was studied. Out of 17 pairs patched in WT mice, an excitatory connection was found in 9 (53 %, combined bidirectional connection and unidirectional connection from SpS neuron to FS interneuron, see **Figure 15**). In the *reeler* mutant mouse, only 2 out of 27 pairs exhibited an excitatory connection (7.4 %, see **Figure 15**). These results show a significantly weakened excitatory connection from SpS neurons to FS interneurons in the *reeler* S1BF, compared to the WT S1BF (Chi-square, X^2 (3) = 14.431, p = 0.002, power= 0.904). A weakened excitatory connection from SpS neuron to FS interneuron in the *reeler* mutant mouse points towards an affected feedback inhibition circuitry in absence of reelin.

The averaged EPSCs recorded in WT (black, n = 4) and *reeler* mouse mutants (green, n = 2) are shown in **Figure 17A**, with the darker traces representing the grand average per genotype. The reliability of the excitatory connection from SpS neuron to FS interneuron was reduced in *reeler* mutant mice (Mdn 70.75 % synaptic failure rate, n = 2), compared to WT mice (Mdn 10.00 %, n = 7), see **Figure 17B**. Due to the low connection probability, only few EPSCs per genotype were recorded and used for further analysis. The onset of EPSC response, relative to the presynaptic AP peak, was comparable in WT (latency 0.49 ms ± 0.29, n = 4) and *reeler* mutant mice (0.56 ms ± 0.58, n = 2, see **Figure 17C**). From the low number of EPSCs recorded per genotype, only a trend could be seen towards a longer time-to-peak of EPSC responses recorded in *reeler* mutant mice (2.54 ms ± 0.79) versus WT mice (0.89 ms ± 0.01; see **Figure 17D**). The EPSC response amplitude (WT 7.00 pA ± 3.73, *reeler* 7.73 pA ± 4.57, see **Figure 17E**) and the decay time (WT 1.26 ms ± 0.09, *reeler* 1.69 ms ± 0.58, see **Figure 17F**) were comparable in both genotypes. As a consequence of the low number of EPSCs recorded, it is not possible to exclude modest alterations in EPSC waveform in the *reeler* mutant mouse.

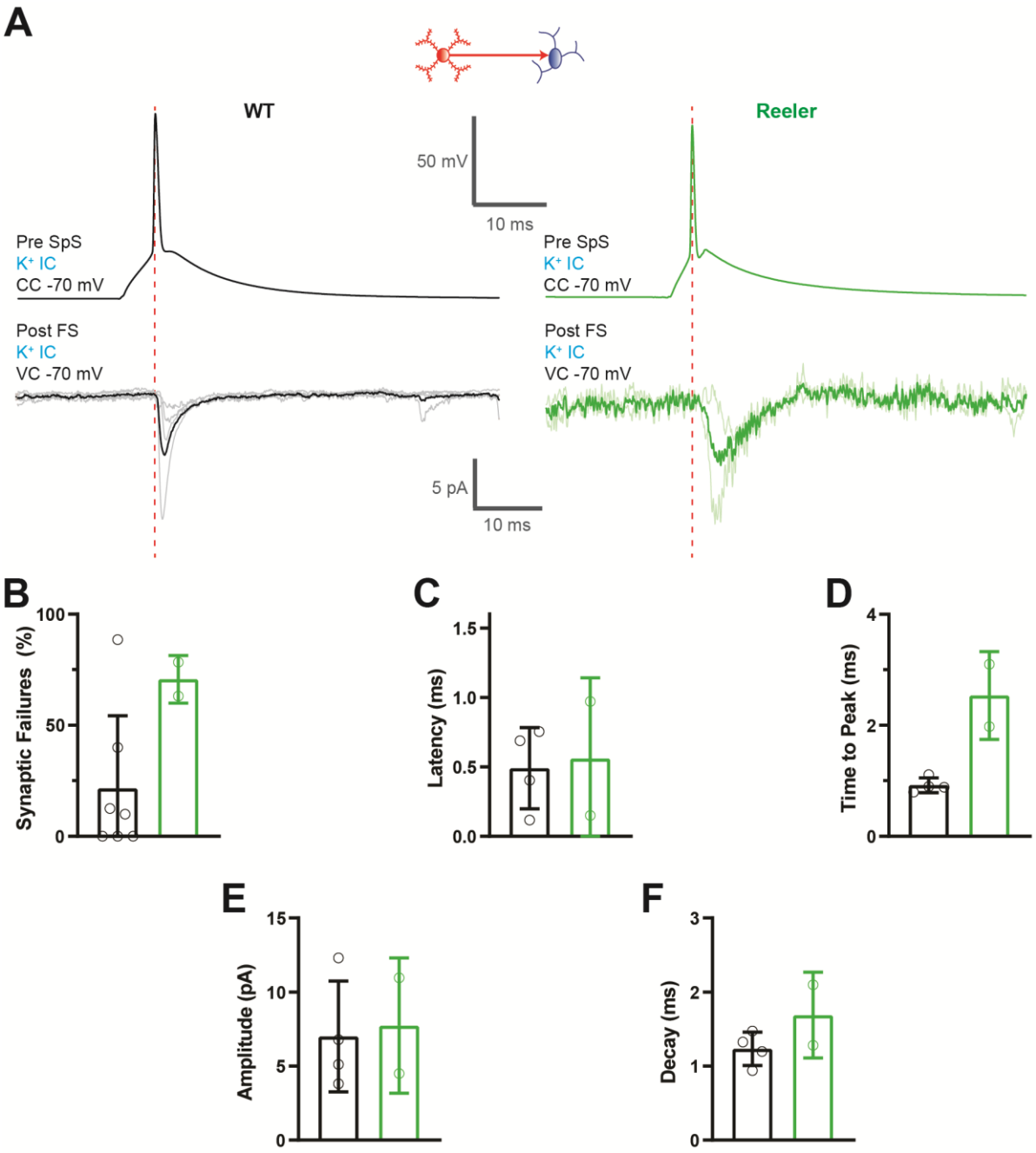

Figure 17: EPSCs recorded between FS interneurons and SpS neurons.

A) Averaged EPSCs per connection (light colour; WT black *n* = 4, *reeler* green *n* = 2) and grand average per genotype in darker traces. Red dotted line indicates the time-point of the presynaptic SpS neuron AP peak. Both neurons were patched with a potassium-based IC solution. The postsynaptic FS interneuron was kept in vc at -70 mV. **B)** On average, the synaptic failure rate was higher in *reeler* mutant mice (Mdn 70.75 %, *n* = 2) compared to WT mice (Mdn 10.00 %, *n* = 7). **C)** EPSC latency was similar in both genotypes (WT 0.49 ms ± 0.29 *n* = 4; *reeler* 0.56 ms ± 0.58, *n* = 2). **D)** EPSC time-to-peak was found longer in *reeler* EPSCs (2.54 ms ± 0.79) compared to WT EPSCs (0.89 ms ± 0.01). **E)** Bar graphs showing EPSC amplitude (WT 7.00 pA ± 3.73, *reeler* 7.73 pA ± 4.57) and EPSC decay time (**F**) (WT 1.26 ms ± 0.09, *reeler* 1.69 ms ± 0.58) were comparable in both genotypes.

In summary, connectivity between FS interneurons and SpS neurons in *reeler* mutant mice was drastically reduced. In addition, the few connections found in either direction showed a higher synaptic failure rate in *reeler* mutant mice, compared to WT mice. Due to the low connection probability in *reeler* mutant mice, few IPSCs and EPSCs were recorded. The single IPSC recorded in *reeler* mutant mice was found to be smaller compared to the average IPSC found in WT mice. The few EPSCs recorded in both genotypes had a similar waveform. Thus, GABAergic inhibition of SpS neurons is drastically reduced in *reeler* S1BF, in agreement with the hypothesis.

Controlling the distal dendritic membrane potential reveals hidden inhibitory inputs onto *reeler* SpS neurons

The paired recordings between FS interneurons and SpS neurons demonstrated a surprisingly large reduction in inhibitory inputs onto SpS neurons in *reeler* mutant mice. However, there were two observations that led to the expectation that the established connection probability underestimated the actual connectivity rate between FS interneurons and SpS neurons in the *reeler* S1BF. First, the drastically reduced connectivity observed might be caused by an overall decrease or change in distribution of FS interneurons in the *reeler* S1BF compared to the WT S1BF. Up to the present, the number and distribution of FS interneurons in the WT and *reeler* S1BF have never been extensively studied. Few studies, however, hinted that the number and density of parvalbumin-expressing FS interneurons in the *reeler* S1BF likely does not differ compared to the WT S1BF (Boyle et al., 2011,Wagener et al., 2016). Therefore, the potentially similar number of FS interneurons in the *reeler* S1BF contradicts the low inhibitory connection probability found. Second, when recording ChR2-evoked APs and multicomponent responses in *reeler* SpS neurons, I occasionally observed small but rapid membrane potential repolarizations that imply the presence of inhibitory inputs (see **Figure 7A and D**). This prompted me to suspect that inhibitory input onto *reeler* SpS neurons may in fact be more frequent and effective than suggested by the results of the paired recordings described above. One possible explanation for this discrepancy is that weaker and more distal inhibitory inputs are harder to detect at the somatic recording site. In order to test this hypothesis, paired recordings between FS interneurons and SpS neurons were repeated, but with a cesium-based IC solution in the postsynaptic SpS neuron. Cesium (Cs^+) is known to block potassium channels, resulting in an improved space clamp and a depolarization of the membrane potential. The cesium-based IC solution allowed for depolarization of the postsynaptic SpS neuron and

holding it in voltage clamp at 10 mV, creating a larger driving force for inhibitory inputs (see Methods). Similar to the parameters measured during previous paired recordings, the connectivity rate, connection reliability and connection strength were studied.

Using a cesium-based IC solution in the postsynaptic SpS neuron, the inhibitory connection probability from FS interneuron to SpS neuron was compared between WT and *reeler* mutant mice. Out of the 35 pairs tested in WT mice, 16 showed an inhibitory connection (47.5 %). In *reeler* mutant mice, an inhibitory connection was found in 15 out of 35 pairs tested (42.9 %). Remarkably, the increase in GABAergic driving force by using a cesium-based IC solution revealed a WT-level connectivity between FS interneurons and SpS neurons in the *reeler* S1BF (Chi-square, X^2 (1) = 0.000, p = 1.000, see **Figure 18**).

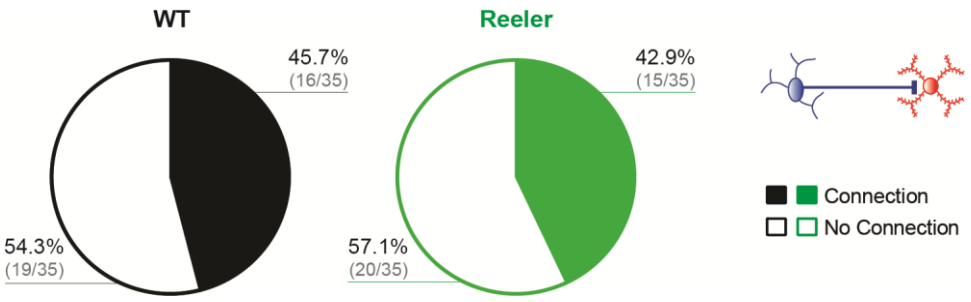

Figure 18: Connectivity between FS interneurons to SpS neurons in presence of Cs^+.

The use of cesium-based IC solution allowed for depolarization of the postsynaptic SpS neuron to 10 mV, thereby increasing the driving force for inhibitory inputs. With this method, a similar connectivity from FS interneurons to SpS neurons was found in *reeler* mutant mice (42.9 %, green) compared to WT mice (45.7 %, black).

Using a cesium-based IC solution, an equal inhibitory connection probability in WT and *reeler* mutant mice was observed. The averaged IPSCs recorded and the grand average per genotype are presented in **Figure 19A** (WT black n = 13, *reeler* green n = 9). Subsequently, the connection reliability from FS interneuron to SpS neuron was analysed by calculating the synaptic failure rate per connection. The synaptic failure rate of the inhibitory connections tested in *reeler* mutant mice (Mdn 0.00 %) was comparable to WT mice (Mdn 0.00 %) (Fishers exact test, p = 1.000, see **Figure 19B**). IPSC latency in the *reeler* mutant mice (Mdn 0.39 ms) was similar to that of WT mice (Mdn 0.41 ms) (Mann-Whitney rank sum test, U = 55.00, p = 0.841, see **Figure 19C**). The time-to-peak of IPSCs recorded in WT mice (Mdn 2.09 ms) did

not significantly differ from IPSCs recorded in *reeler* mutant mice (Mdn 2.65 ms) (Mann-Whitney rank sum test, U = 49.00, p = 0.548, see **Figure 19D**). In *reeler* mutant mice the median IPSC amplitude was 83.15 pA, which was similar to the IPSC amplitude in WT mice (Mdn 60.09 pA) (Mann-Whitney rank sum test, U = 54.00, p =0.789, see **Figure 19E**). Last, the decay time was compared between IPSCs recorded in *reeler* mutant mice (8.53 ms ± 4.34) and WT mice (8.02 ms ± 2.88), see **Figure 19F**. Also, the IPSC decay time showed no significant difference between genotypes (two-tailed T-test, t (20) = -0.328, p = 0.747, power = 0.061). Taken together, the connection reliability and response waveform were similar in WT and *reeler* mutant mice.

In addition to single IPSC responses, train stimulation was performed at various frequencies to investigate whether there are differences in short-term plasticity of inhibitory connections found in WT versus *reeler* mutant mice (**Figure 20**). Train stimulation was done after recording single IPSCs only when there were no signs of recording instability observed by input resistance. Presynaptic FS APs were elicited at various frequencies, namely: 1, 5, 20, 50 and 100 Hz. The averaged IPSC train responses per frequency and per connection are shown in light coloured traces, with overlaid the grand average per frequency and per genotype in the dark coloured trace (see **Figure 20A, C, E, G and I**). The IPSC amplitudes for each response in the train was measured, and response amplitudes were normalized to the first IPSC response in the train stimulation. The average of normalized IPSC amplitudes per frequency and per genotype are shown in **Figure 20B, D, F, H and J**. In both WT and *reeler* mutant mice a short-term depression was found in the inhibitory connection from FS interneuron to SpS neuron. In summary, no difference was found in short-term plasticity of the inhibitory connection between FS interneuron and SpS neurons in WT and *reeler* mutant mice.

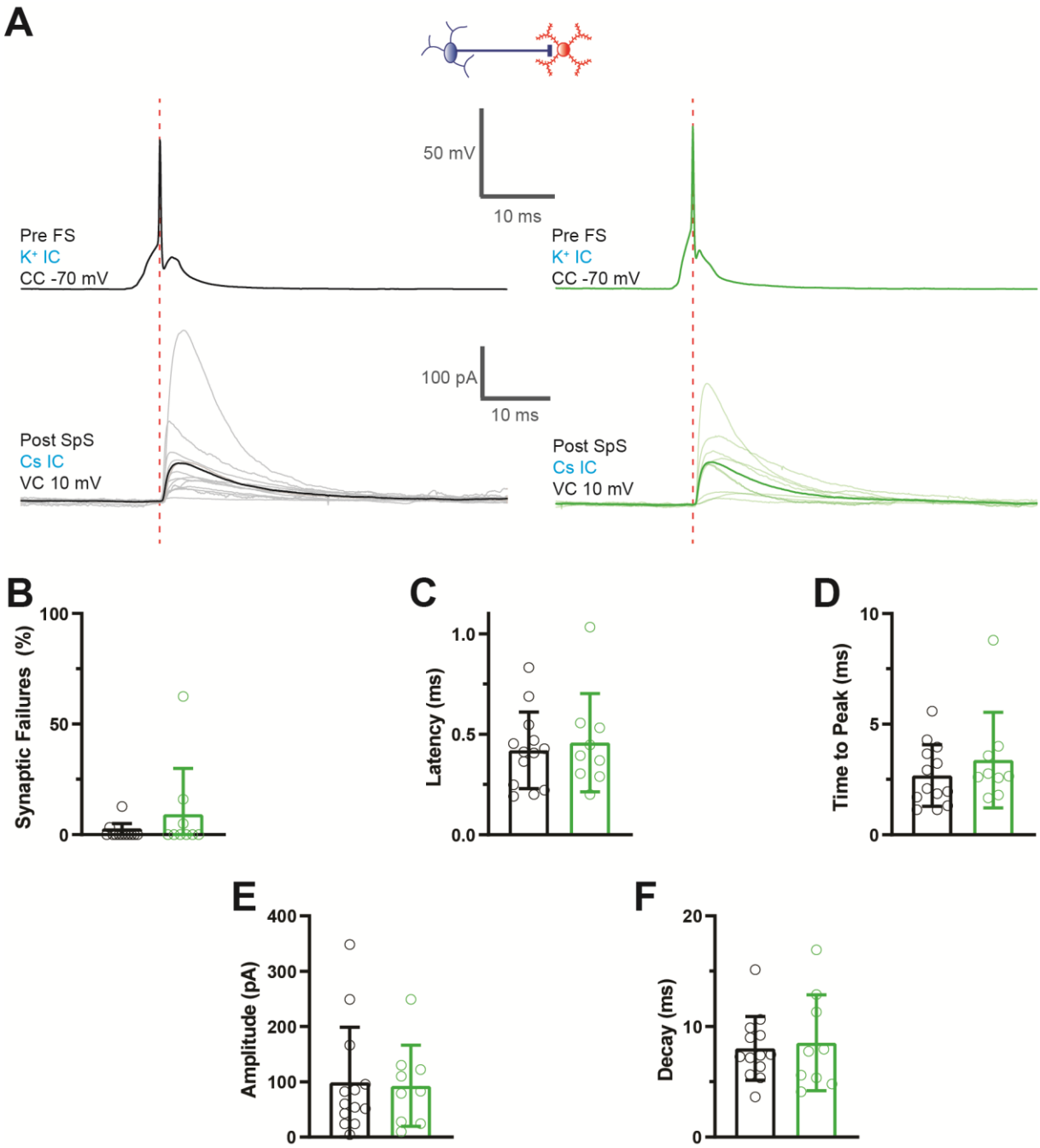

Figure 19: IPSCs recorded between FS interneuron and SpS neuron in presence of Cs^+.

A) Averaged IPSC response per connection (light colour; WT black *n* = 13, *reeler* green *n* = 9) and grand average per genotype in darker traces. Red dotted line indicates the time-point of the presynaptic FS interneuron AP peak. Postsynaptic SpS neurons were patched with cesium-based IC solution and kept in vc at 10 mV. **B)** Synaptic failure rate was similar in WT (Mdn 0.00 %) and *reeler* mutant mice (Mdn 0.00 %). **C)** Bargraph showing equal IPSC latency between genotypes (WT Mdn 0.41 ms, *reeler* Mdn 0.39 ms, n.s.). **D)** IPSC time-to-peak was equal in WT (Mdn 2.09 ms) and *reeler* mutant mice (Mdn 2.65 ms). **E)** IPSC amplitude was also found similar between genotypes (WT Mdn 60.09 pA, *reeler* Mdn 83.15 pA). **F)** IPSC decay was also comparable between WT (8.02 ms ± 2.88), and *reeler* mice (8.53 ms ± 4.34).

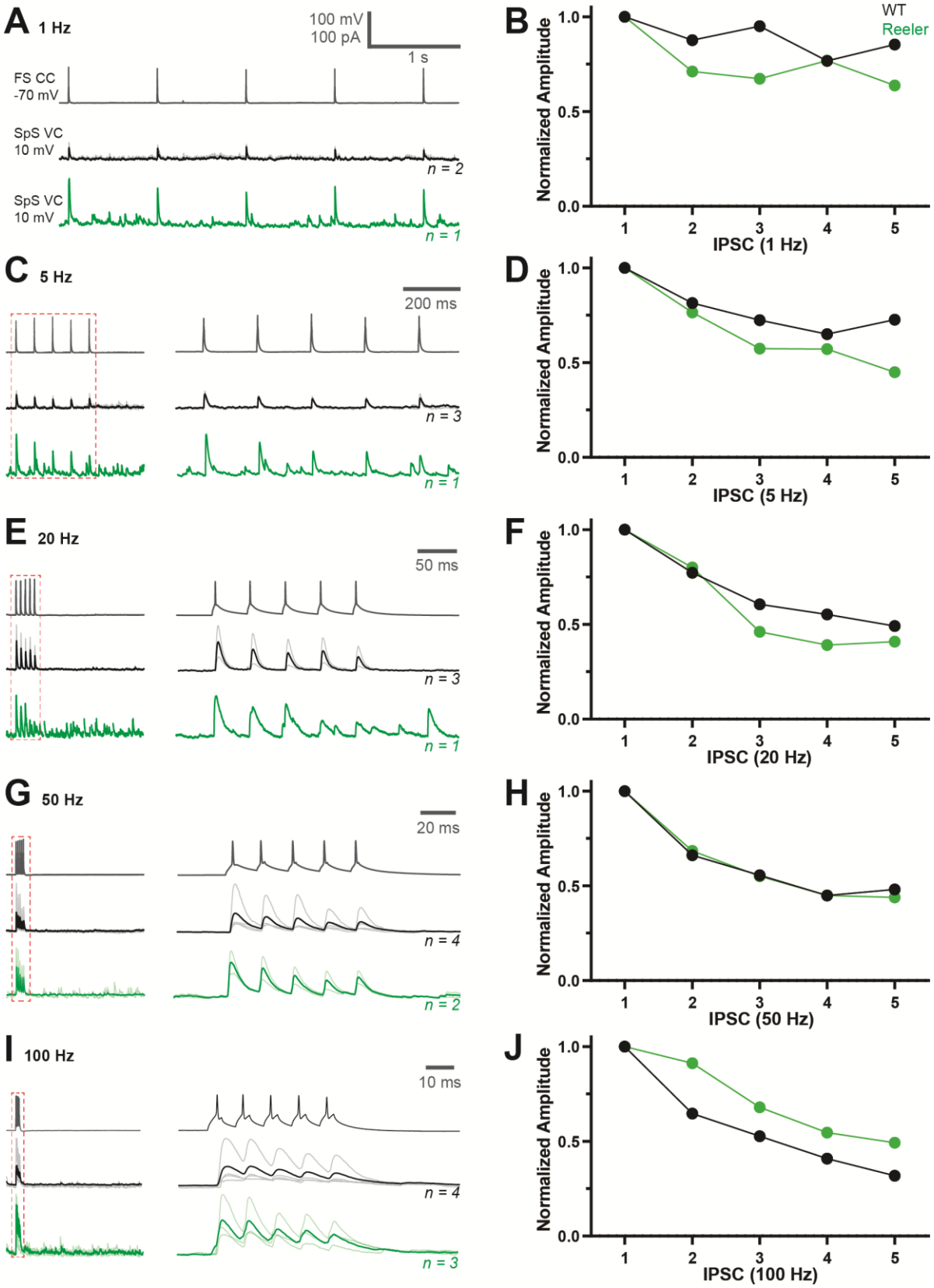

Figure 20: Short-term depression from FS interneuron to SpS neuron.

A) IPSCs recorded from 1 Hz train stimulation (WT black, *reeler* green). The number of connections per frequency is indicated below the trace. Light colour traces represent averages per connection, darker trace represents grand average per genotype. Number of connections tested per frequency is written

below the traces (*n*). **B)** IPSC amplitudes of the 1 Hz train normalized to the amplitude of the first EPSC response. **C)** 5 Hz train stimulation. Scaling of the traces on the left matches the scaling of the traces in A. Traces in the red dotted box are shown over an elongated timescale on the right. **D)** Normalized amplitude of IPSCs from the 5 Hz train stimulation. **E)** 20 Hz stimulation traces, with the analysed normalized amplitude of IPSCs in **F**. **G)** 50 Hz train stimulation traces, with the normalized IPSC amplitude shown in **H**. **I)** 100 Hz train stimulation with normalized IPSC amplitude shown in **J**.

In summary, the connection probability from FS interneuron to SpS neuron was found similar in WT and *reeler* mutant mice. Furthermore, the reliability and strength of the connection were also comparable between the two genotypes. These results showed that a cesium-based IC solution was able to reveal inhibitory inputs in *reeler* SpS neurons that have remained undetected in the paired recordings using potassium-based IC solution.

Putative contacts between FS interneurons and SpS neurons

The paired recordings using a cesium-based IC solution revealed inhibitory connections to *reeler* SpS neurons with a similar connection reliability and strength compared to WT mice. Because a cesium-based intracellular solution ensured a large driving force for inhibitory inputs by depolarizing the membrane potential, more control was also gained over the membrane potential at the distal dendrites of SpS neurons. This allowed for the detection of distal inhibitory inputs, that otherwise would have gone unnoticed when recording at the soma. The results so far obtained from paired recordings using potassium and cesium-based IC solution could point towards a more distal targeting pattern of FS interneuron synapses onto SpS neurons in the *reeler* mutant mouse compared to WT mice. Whereas it is described in the literature that FS interneurons preferentially target excitatory neurons perisomatically in WT mice, the FS interneuron synapse targeting pattern has not been studied in *reeler* mutant mice (Buhl et al., 1994). Next, various approaches were completed to gain insight in the amount and distribution of putative contacts (PuCs) between FS interneurons and SpS neurons in WT and *reeler* mutant mice.

Morphological reconstruction

For the first approach, the morphology of recovered biocytin filled neurons from the paired recordings between FS interneurons and SpS neurons was closely studied. A sufficient biocytin

filling allowed for morphological reconstruction of the soma, dendrites, and axonal tree of the pair of neurons (see **Figure 21A** and **Figure 22A**). From these neuronal reconstructions, PuCs were identified between FS interneurons and SpS neurons, allowing the investigation of the amount and distribution of PuCs in WT and *reeler* mutant mice. In total, 3 pairs of neurons were reconstructed from WT mice and 5 pairs of neurons were reconstructed from *reeler* mutant mice. Examples of such reconstructions from a WT mouse and a *reeler* mutant mouse are presented in **Figure 21B** and **Figure 22B**, respectively. Potential PuC sites detected from these reconstructions (as marked in **Figure 21C** and **Figure 22C**) were additionally scanned at high resolution (0.043 µm * 0.043 µm * 0.18 µm), using Airy Scan mode (see **Figure 21D** and **Figure 22D**). A PuC was defined by the crossing of the axonal bouton of one neuron with the soma or dendrite of another neuron in the same z-plane. It should be pointed out that this approach could potentially result in false negative and false positive PuCs due to a fainter biocytin signal in the distal axon branches. The faded biocytin filling in the distal axon branches could have resulted in incomplete reconstructed axonal trees, thus the total amount of detected PuCs might present an underestimated value. However, it should be noted that the dendritic and axonal arborisations of FS interneurons were usually well-filled. The biocytin-filling of SpS neurons, although showing a weak axonal labelling, presented a well-filled dendritic arbor suggestive of being complete.

In all reconstructed pairs of neurons (WT $n = 3$, *reeler* $n = 5$) an inhibitory connection was confirmed by paired whole-cell patch clamp recordings. In both WT and *reeler* mutant mice the average number of detected inhibitory PuCs from FS interneurons onto SpS neurons per pair was comparable (WT 6.00 ± 2.00, *reeler* 4.80 ± 1.79, see **Figure 23A**). Next, the distribution of inhibitory PuCs across reconstructed SpS neurons was analysed. To this end, the distance from the SpS neuron soma to each detected inhibitory PuC was calculated and measured along the reconstructed dendritic branch. These values of all inhibitory PuCs found per genotype were combined and were plotted as a function of distance from the soma (0 to 160 µm) in 20 µm bins (WT total inhibitory PuCs $n = 18$ from 3 pairs; *reeler* total inhibitory PuCs $n = 24$ from 5 pairs, see **Figure 23B**). In this graph, 0 µm indicates an inhibitory PuC targeting the soma. Analyzing the distribution of inhibitory inputs onto WT and *reeler* SpS neurons, no significant difference was found (two-way ANOVA, $F(1, 7) = 1.842$, $p = 0.217$, see **Figure 23B**). In summary, inhibitory PuCs, in both genotypes, were found both on the soma and on the proximal and distal dendrites of SpS neurons.

In addition to inhibitory PuCs, excitatory PuCs between SpS neurons and FS interneurons were identified from morphological reconstructions as well (see **Figure 21 and 22**). Out of the total amount of reconstructed pairs of neurons, an excitatory connection was confirmed in a subset of pairs using electrophysiological recordings (WT $n = 2$, *reeler* $n = 2$). In a similar fashion, the amount and distribution of detected excitatory PuCs from SpS neurons onto FS interneurons was measured. On average, a comparable number of excitatory PuCs was found in pairs of WT (1.00 ± 0.00) and *reeler* mutant mice (1.33 ± 0.58, see **Figure 23C**). Subsequently, the location of excitatory PuCs on FS interneurons was analysed by measuring the distance of each identified PuC to the soma of the FS interneuron along the reconstructed dendritic branch. The distribution of all detected PuCs per genotype (WT $n = 2$ from 2 pairs of neurons, *reeler* $n = 3$ from 2 pairs of neurons) is presented in **Figure 23D**. Here, the number of excitatory PuCs is plotted against distance from the FS interneuron soma, in 20 µm bins. In total, two excitatory PuCs on FS interneurons in WT mice were identified, which were located in close proximity to the soma compared to the three more distally located excitatory PuCs detected on FS interneurons of *reeler* mutant mice.

In summary, a comparable number of excitatory and inhibitory PuCs was found for each pair in WT and *reeler* mutant mice. Moreover, inhibitory PuCs in both genotypes were found on the soma and on the proximal and distal dendrites. The number of reconstructed neuronal pairs with a confirmed excitatory connection was not sufficient to conclude differences in innervation pattern between WT and *reeler* mice. Overall, these results did not indicate a strongly altered innervation pattern of SpS neurons in *reeler* mutant mice.

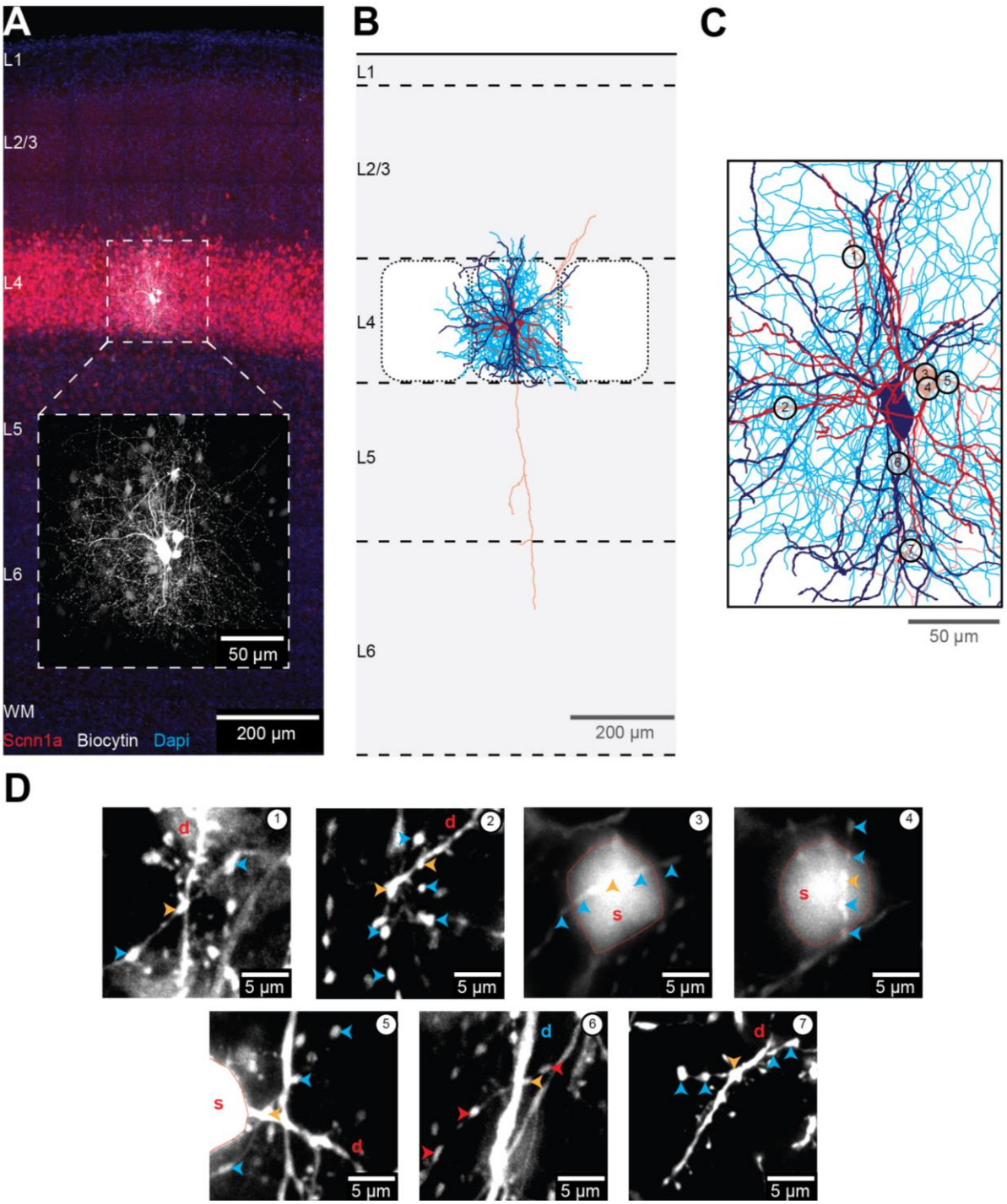

Figure 21: Reconstruction of connected FS interneuron and SpS neuron pair in WT.

A) Maximum intensity projection of a confocal image stack showing recovered morphology of biocytin-filled and bidirectionally connected pair of neurons, FS interneuron and SpS neuron. WM = white matter, L = layer. The white dotted box represents a higher magnification image of the biocytin channel, highlighting the recovered neurons. **B)** Reconstruction of recovered neurons. FS interneuron in blue, SpS neuron in red. Darker colour shows the soma and dendrites, lighter colour represents the axon. **C)** Magnified view showing somatodendritic region with PuC locations numbered (1-7). **D)** Airy Scan mode images showing the PuCs (1-7). Red 'd' marks SpS neuron dendrites, red contour and 's' mark SpS neuron soma, red arrowheads mark SpS neuron axon, blue 'd' marks FS interneuron dendrite, blue arrowheads mark FS interneuron axon, yellow arrowhead marks putative contact sites.

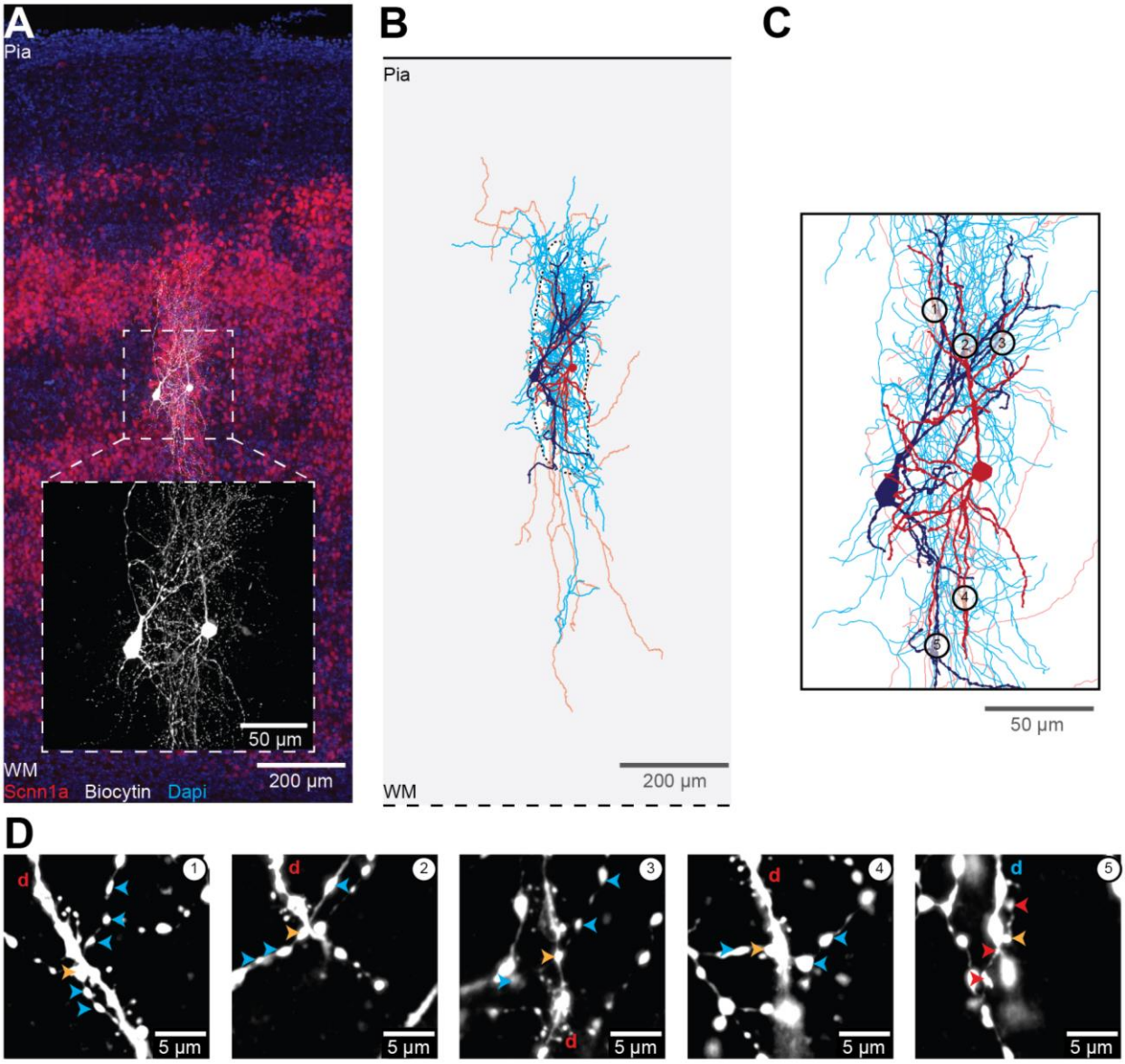

Figure 22: Reconstruction of connected FS interneuron and SpS neuron pair in *reeler*.

A) Maximum intensity projection of confocal image showing recovered morphology of biocytin-filled and bidirectionally connected pair of neurons, FS interneuron and SpS neuron. WM = white matter. The white dotted box presents a higher magnification image of the biocytin channel, highlighting the recovered neurons. **B)** Reconstruction of recovered neurons. FS interneuron in blue, SpS neuron in red. Darker colour shows soma and dendrites, lighter colour represents axon. Dotted black line represents the contour of the barrel-equivalent. **C)** Magnified image of the somatodendritic region with PuC locations numbered (1-5). **D)** Airy Scan mode images showing the putative contacts (1-5). Red 'd' marks SpS neuron dendrites, red contour and 's' mark SpS neuron soma, red arrowheads mark SpS neuron axon, blue 'd' marks FS interneuron dendrites, blue arrowheads mark FS interneuron axon, yellow arrowhead marks putative contact sites.

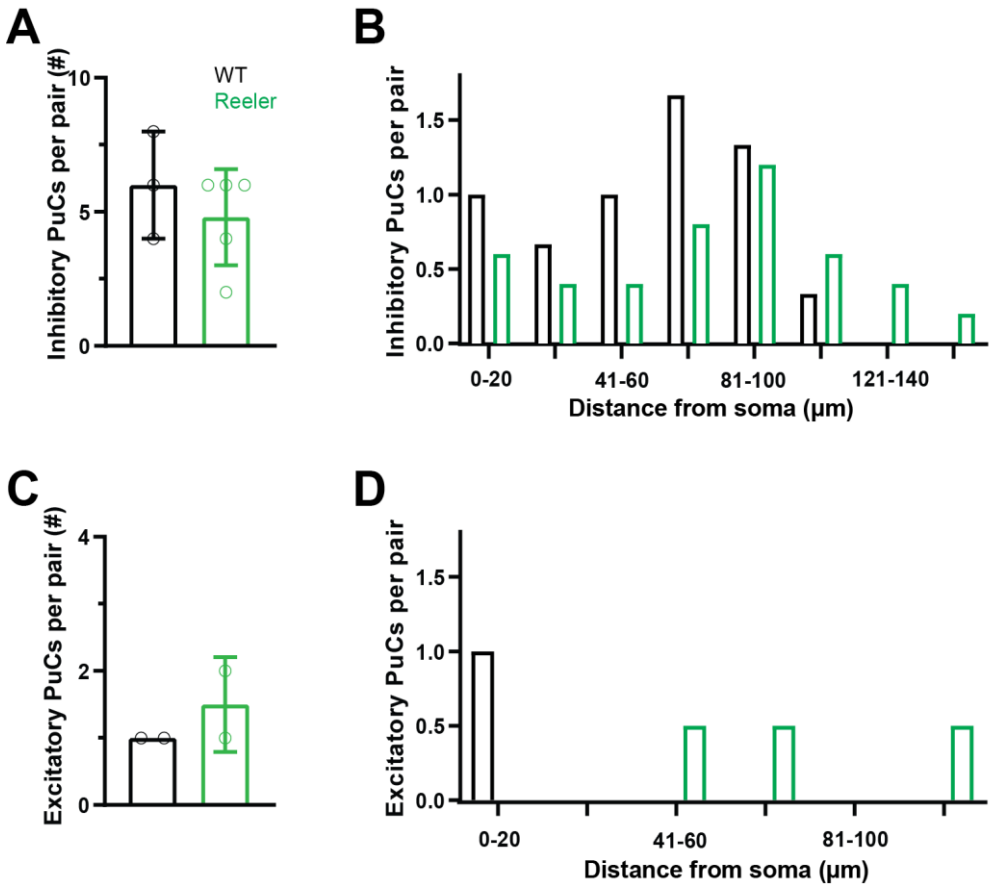

Figure 23: Quantification and distribution of putative contacts.

A) Number of inhibitory PuCs found targeting SpS neurons per reconstructed pair of neurons in WT (black, *n* = 3, 6.00 ± 2.00) and *reeler* mice (green, *n* = 5, 4.80 ± 1.79). **B)** Distribution of total amount of inhibitory PuCs found in WT and *reeler* mutant mice, from soma to distal dendrites, along the reconstructed branch, in 20 µm bins (WT total inhibitory PuCs *n* = 18 from 3 pairs; *reeler* total inhibitory PuCs *n* = *24* from 5 pairs), ns. **C)** Excitatory PuCs were analysed for 2 pairs in WT and 2 pairs in *reeler*. Number of excitatory PuCs detected on FS interneurons in WT and *reeler* mutant mice was comparable (WT 1.00 ± 0.00, *reeler* 1.33 ± 0.58). **D)** Distance of total amount of excitatory PuCs to the FS interneuron soma in 20 µm bins measured along the reconstructed dendritic branch (WT *n* = *2* from 2 pairs of neurons, *reeler n* = 3 from 2 pairs of neurons).

Immunolabeling of parvalbumin-expressing inhibitory presynaptic terminals

In a separate attempt to investigate the inhibitory innervation pattern of L4 excitatory neurons, 50 µm coronal brain slices were immunolabelled for synaptotagmin-2 (Syt-2) to identifity and compare FS interneuron boutons in WT and *reeler* mutant mice. Previous studies have shown that Syt-2 is a reliable marker for presynaptic terminals of FS, parvalbumin-expressing interneurons (Sommeijer & Levelt, 2012). Immunohistochemical staining showed Syt-2 positive boutons targeting somata of L4 excitatory neurons expressing Scnn1a-tdTomato in

both WT and *reeler* mutant mice (see **Figure 24**). These results indicate a similar inhibitory innervation pattern of L4 excitatory neurons between the two genotypes examined.

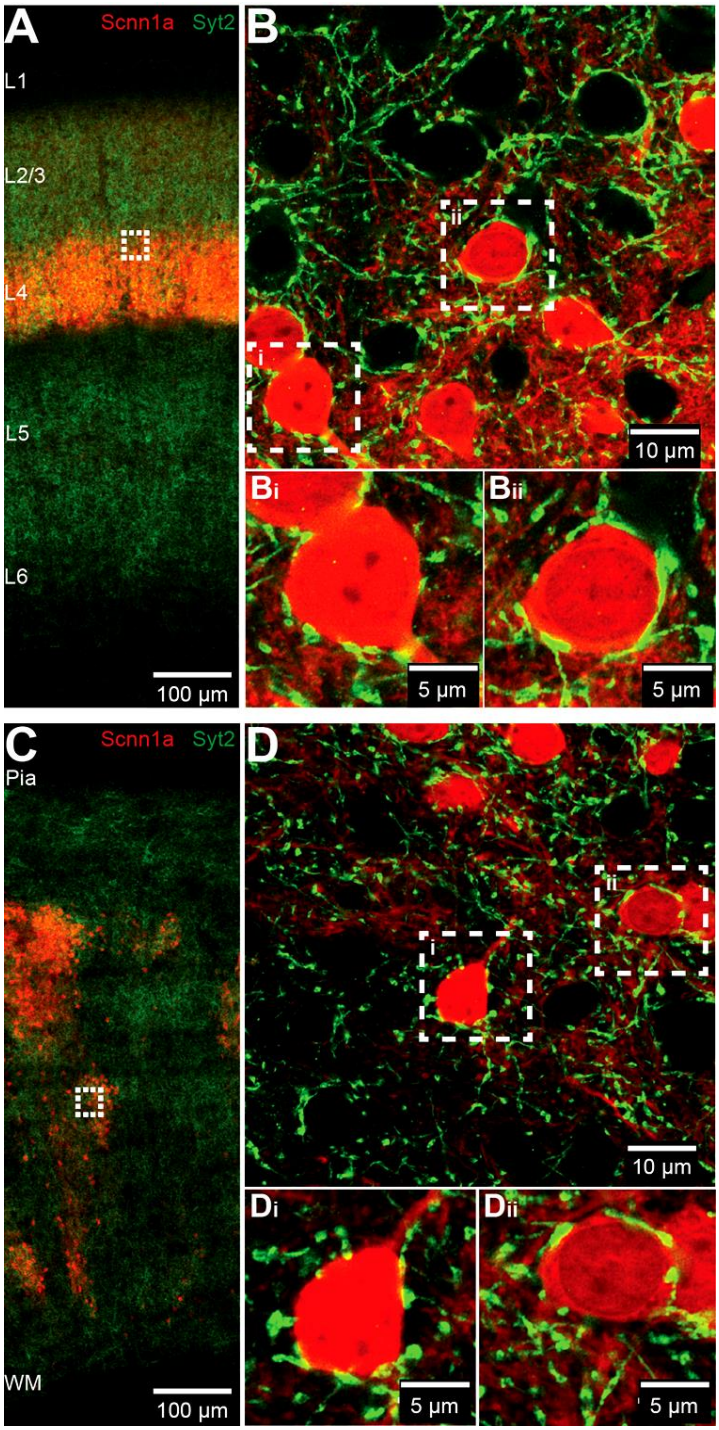

Figure 24: Synaptotagmin-2 expressing boutons targeting somata of excitatory L4 neurons.

A) Barrel cortex overview of a WT mouse. Scnn1a-tdTomato expressed in L4 excitatory neurons is indicated in red and Syt-2 immunolabelling in green. White box area is shown in higher magnification in **B**. **B)** Magnified region of a barrel with two more magnifications (**Bi and Bii**) shown below. **C)** S1BF of a *reeler* mouse. Pia = pial surface. WM = white matter. White box outlines the areas shown at a higher magnification in D. **D)** Magnification of area in barrel-equivalent with two more magnifications (**Di and Dii**).

Quantification of Syt-2 positive boutons on SpS neurons

Last, the inhibitory innervation pattern of electrophysiologically and morphologically identified SpS neurons was investigated. Immunolabeling of Syt-2 was performed on 300-µm-thick thalamocortical slices with biocytin-filled SpS neurons (see **Figure 25A and C**). Using the Neurolucida software, SpS soma and dendrite morphology was reconstructed from the biocytin-filled SpS neurons (see **Figure 25B and D**). Subsequently, Syt-2 expressing boutons that were in close proximity (< 0.5 µm) to the reconstructed neuron were detected using the puncta detection function of Neurolucida software (**Figure 25B and D**, see Methods). This function provided an approximation of the distribution and number of Syt-2 positive puncta in close proximity to the reconstructed SpS neurons of WT and *reeler* mutant mice. The puncta detection was performed on 3 reconstructed WT SpS neurons and 3 reconstructed *reeler* SpS neurons. First, the Syt-2 positive puncta targeting the soma were analysed. On average, no difference was found in the number of somatic puncta in WT SpS neurons (39.33 ± 6.66) versus *reeler* SpS neurons (42.00 ±.4.00, see **Figure 25E**). Taking into account differences in somatic volume between multiple SpS neurons, I calculated the number of Syt-2 positive puncta per 20 μm^2 somatic surface area. No difference was found between the number of somatic Syt-2 puncta on WT SpS neurons (3.00 ± 0.26) and *reeler* SpS neurons (3.40 ± 0.60) per 20 μm^2 somatic surface area (see **Figure 25F**). This data indicates that the amount of inhibitory putative synapses targeting the soma does not differ between WT SpS neurons versus *reeler* SpS neurons. Second, the number and distribution of Syt-2 positive puncta targeting SpS neuron dendrites was analysed. For the puncta detection on dendrites, two random dendrites per reconstructed SpS neuron were analysed. To account for differences in dendritic length, only the proximal 100 µm of each dendrite was used for analysis. The total number of Syt-2 positive puncta detected on SpS neuron dendrites did not differ between WT SpS neurons (52.83 ± 46.88) and *reeler* SpS neurons (63.00 ± 28.71, see **Figure 25G**). Last, the distribution of detected puncta along the reconstructed dendrites was analysed. The number of Syt-2 positive puncta targeting the dendrite was plotted as a function of distance from the soma in 5 µm bins, measured along the reconstructed dendritic branch (see **Figure 25H**). Summarizing, the number and distribution of inhibitory putative synapses targeting SpS neuron dendrites was found comparable between WT and *reeler* mutant mice.

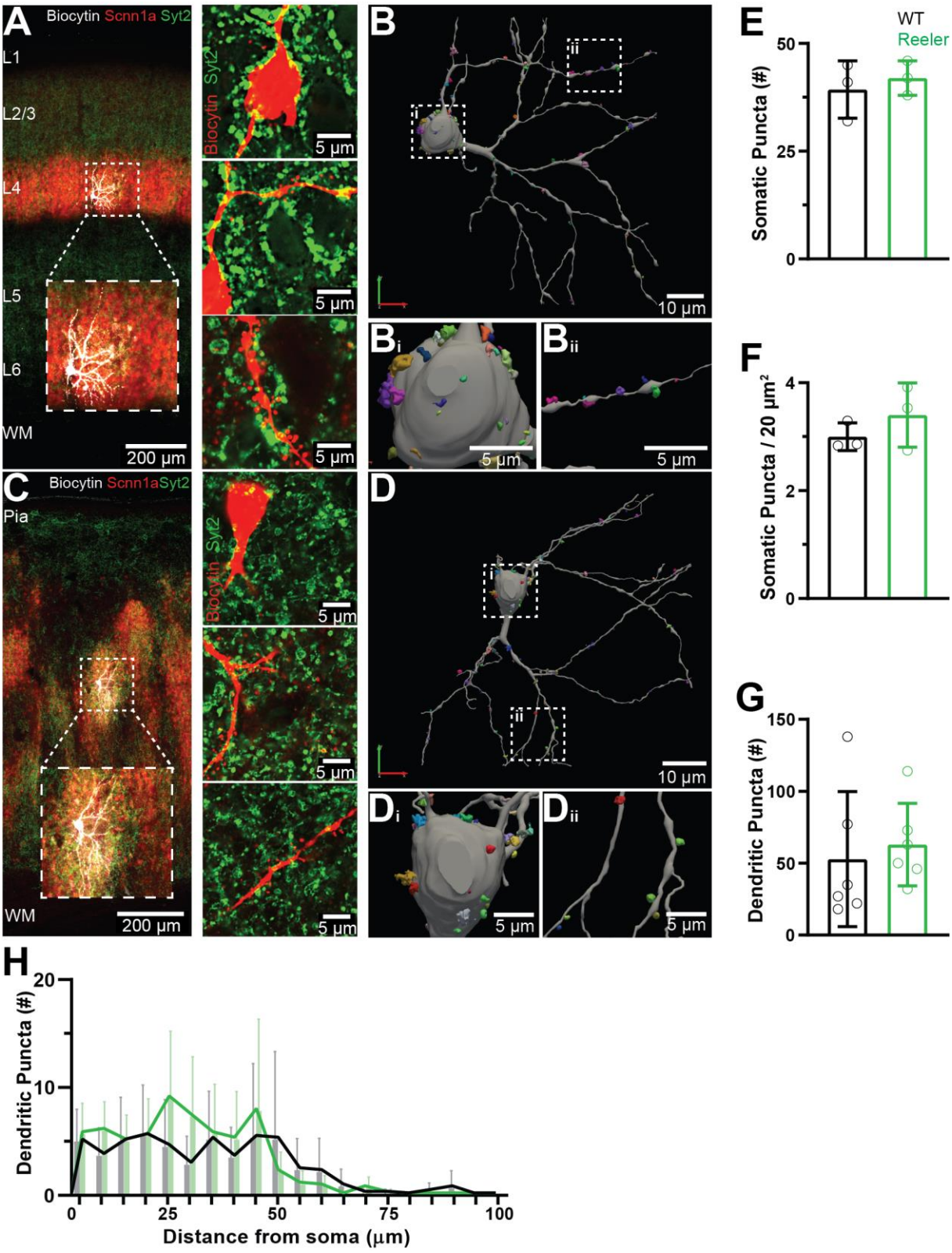

Figure 25: Quantification of Syt-2 expressing boutons targeting SpS neurons.

A) Maximum intensity projection of confocal image showing biocytin-filled SpS neuron, Syt-2 immunolabelling and the Scnn1a-tdtomato signal in the barrel cortex of a WT mouse. White box shows a higher magnification image of the SpS neuron, highlighting its morphology. On the right, three Airy Scan mode images are shown, displaying parts of the biocytin-filled SpS and Syt-2 staining. **B)** Reconstructed SpS neuron (seen in A) shown in grey. Detected Syt-2 puncta are shown in random

colours. A magnification of the soma and a part of the dendritic tree are shown in the lower panels. **C)** Similarly, an example of a biocytin-filled SpS neuron in the *reeler* S1BF is illustrated. **D)** Puncta detection on a reconstructed *reeler* SpS neuron (seen in C). **E)** Number of detected Syt-2 puncta targeting the soma, per reconstructed neuron did not differ between genotypes (WT black 39.33 ± 6.66 n = 3, *reeler* green 42.00 ±.4.00 n = 3). **F)** Amount of Syt-2 puncta per 20 µm^2 of soma surface area per reconstructed SpS neuron was comparable as well between the two genotypes (WT 3.00 ± 0.26, *reeler* 3.40 ± 0.60). **G)** Total number of "dendritic puncta" detected per reconstructed SpS neuron. Two dendrites per SpS neuron were analysed (WT n = 6, *reeler* n = 6). No difference was found in the number of Syt-2 positive puncta targeting the proximal 100 µm of SpS neuron dendrites in WT SpS neurons (52.83 ± 46.88) and *reeler* SpS neurons (63.00 ± 28.71). **H)** Combining all Syt-2 positive puncta targeting dendrites (WT n = 6, *reeler* n = 6), the distribution of detected puncta along the dendrites was represented by plotting the number of "dendritic puncta" as a function of the distance from the soma (in 5 µm bins). Bars represent average with standard deviation. The lines indicate the average of puncta found over the dendritic length for each genotype.

In conclusion, the results from the paired recordings between FS interneurons and SpS neurons in the *reeler* S1BF using potassium and cesium-based IC solution, pointed to the possibility that the inhibitory innervation of *reeler* SpS neurons is shifted distally compared to WT SpS neurons. However, the three independent experimental approaches described above revealed a similar inhibitory innervation pattern of SpS neuron in WT and *reeler* mutant mice. These results imply that the previously described electrophysiological findings cannot be explained by a reduced number or altered distribution of PuCs in the *reeler* mutant mouse. Still, the sensitivity of the performed methods might have been insufficient to exclude minor but functionally relevant changes in the number of putative inhibitory Syt-2 positive synapses or a slight distal shift in the targeting pattern along the dendrite. In contrast to the hypothesis, all three approaches demonstrated that putative inhibitory synapses are found on the soma, proximal dendrites and distal dendrites of WT SpS neurons and *reeler* SpS neurons. These findings have largely ruled out a reduction and a more distal shift of inhibitory inputs targeting *reeler* SpS neurons.

Results II

In the first part of the results it was demonstrated that the electrophysiological and morphological properties of SpS neurons and FS interneurons of the somatosensory cortex are not affected in the *reeler* mutant mouse. In addition, the previous results from our lab were replicated (Guy, 2015; Guy et al., 2017). Accordingly, an enhanced responsiveness of *reeler* SpS neurons to stimulation of TC fibers, originating from the VPm, was detected. This, even though the TC input itself was found to be weaker in SpS neurons of the *reeler* S1BF. In an attempt to clarify this apparent discrepancy, two potential compensatory mechanisms for the weakened thalamic input in the *reeler* S1BF were investigated. The first hypothesis suggested a stronger recurrent excitatory excitation between SpS neurons to overcome the weakened thalamic input in the *reeler* S1BF. Using paired recordings between SpS neurons, a similar connection probability, connection reliability and connection strength was found in WT and *reeler* mice, thereby disproving the hypothesis. The second hypothesis proposed a weakened feedforward/feedback inhibition between FS interneurons and SpS neurons as a compensatory mechanism for weakened VPm input in *reeler* mutant mice. This hypothesis was examined by performing paired recordings between FS interneurons and SpS neurons in the WT and *reeler* S1BF. The paired recordings using a cesium-based IC solution revealed inhibitory connections between FS interneuron and SpS neuron in the *reeler* S1BF, that were undetected during the recordings with a standard potassium-based IC solution. The similar connection probability, connection reliability and connection strength discovered with the cesium-based IC solution recordings between FS interneurons and SpS neurons refuted the hypothesis of a weakened inhibition in the *reeler* S1BF. The contrast in potassium-based IC and cesium-based IC recordings is likely not caused by a more distal inhibitory innervation pattern of *reeler* SpS neuron, as demonstrated by the morphological reconstructions and Syt-2 immunolabeling. So far, the data suggests that inhibitory synapse location and functioning is not affected in the *reeler* mutant mouse. Therefore, it was asked whether the dendritic integration of inhibitory

inputs could be affected in *reeler* SpS neurons, thereby explaining the discrepancy observed in the paired recording data.

Reduced hyperpolarization-activated current (I_h) dampens inhibition and promotes hyperexcitability in the *reeler* cortex

One particular mechanism involved in dendritic integration of postsynaptic potentials in excitatory neurons is hyperpolarization-activated cation current (I_h), a depolarizing current mediated by hyperpolarization-activated cyclic nucleotide-gated (HCN) channels (for reviews see: Combe & Gasparini, 2021; Robinson & Siegelbaum, 2003). In total, four different HCN channel subunits are known, of which HCN1 and, to a lesser extent, HCN2 subunits are expressed in the somatosensory cortex (Moosmang et al., 1999; Notomi & Shigemoto, 2004). In the rodent somatosensory cortex, HCN channels have been shown to be mainly expressed on distal dendrites of L5 pyramidal neurons (Kupferman et al., 2014; Lörincz et al., 2002). The reelin signalling pathway is involved in the enrichment of HCN channels in the distal dendrites of these neurons. In the Disabled-1 (Dab1) knockdown mouse model, an adaptor protein downstream of reelin required for proper signalling, Kupferman and colleagues found reduced HCN expression in the somatosensory cortex (Kupferman et al., 2014). In addition, they reported a hyperpolarized resting membrane potential of pyramidal neurons, which is indicative of a reduced I_h in pyramidal neurons in the Dab1 knockdown mouse model. Since Dab1 is involved in the reelin signalling cascade, a similar condition could be predicted in the *reeler* mutant mouse.

I_h is a mixed cation current consisting of mainly potassium ions and to a lesser extent, sodium ions, resulting in a reversal potential value of approximately -30 mV. Upon membrane potential hyperpolarization, HCN channels open, leading to a depolarization of the membrane through ion influx. This depolarization contributes to the driving force underlying GABA-A receptor mediated currents (Atherton et al., 2010; Pavlov et al., 2011; Williams & Stuart, 2003). Pavlov and colleagues have investigated the effect of I_h on dendritic integration of inhibitory postsynaptic potentials (IPSPs) and EPSPs in hippocampal CA1 pyramidal neurons (Pavlov et al., 2011). Upon pharmacological blockade of HCN channels, or using a HCN knockout mouse

line, they found that IPSPs were abolished and EPSPs were broadened in hippocampal CA1 pyramidal neurons in response to electrical stimulation of Schaffer collaterals. These observations led to the next hypothesis: SpS neuron dendrites in *reeler* mutant mice have a reduced I_h resulting in a compromised driving force for incoming inhibitory inputs (see **Figure 26**). This may explain why a fraction of existing inhibitory connections in *reeler* mutant mice were missed in the paired recordings, as a reduced driving force would have decreased or nullified the amplitude of evoked IPSCs, thereby preventing me from reliably detecting them at somatic sites.

In S1BF, HCN channels are known to be mainly expressed on distal dendrites of L5 pyramidal neurons and only scarcely in other cortical layers (Kupferman et al., 2014; Lörincz et al., 2002). In the present study, it was hypothesized that few HCN channels are also present on the dendrites of SpS neurons in WT mice and that this HCN channel expression is reduced in *reeler* mutant mice. Decreased I_h in *reeler* SpS neuron dendrites would lead to a reduced driving force for IPSPs, explaining the low connection probability and undetected IPSCs in the paired recordings using standard potassium-based IC solution. To study I_h in WT and *reeler* SpS neurons, two different approaches were perfromed. First, the effect of I_h on temporal summation of EPSPs in SpS neurons of WT versus *reeler* mutant mice was investigated by performing optogenetic train stimulation of thalamic fibers and pharmacologically blocking HCN channels. Second, the paired recordings between FS interneurons and SpS neurons with standard potassium-based IC solution were repeated, but this time while pharmacologically increasing I_h, in order to investigate if this restores connection probability and strength.

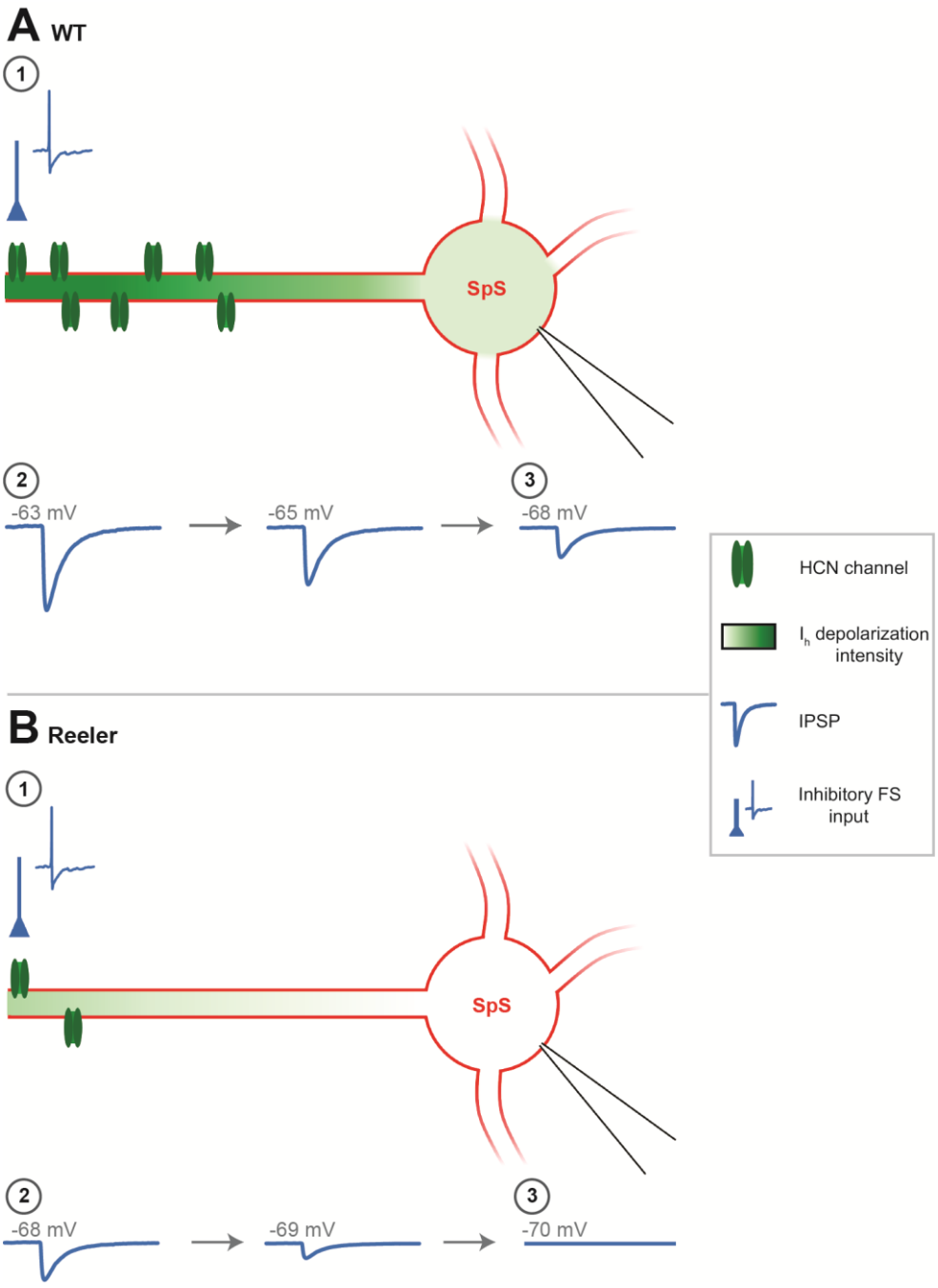

Figure 26: Reduced I_h in the *reeler* SpS neurons leads to a reduced driving force for IPSPs.

A) Schematic representation of a WT SpS neuron (red) receiving inhibitory input from a FS interneuron (1). Due to active HCN channels located at the distal dendrite of the SpS neuron, the membrane potential is depolarized (green gradient) creating a driving force for IPSPs (2). After propagation, the IPSPs can be recorded at the soma (3). **B)** Proposed model of the affected IPSP propagation in *reeler* mutant mice. Inhibitory input from FS interneurons (1) targeting the SpS neuron dendrite results in a smaller IPSP (2) due to less I_h mediated depolarization, and thus less driving force for inhibitory inputs. As a result, the IPSP fails to reach the soma and is therefore not detected at the recording site (3).

The influence of I_h on temporal summation of EPSPs

The effect of I_h on temporal summation of EPSPs has previously been studied using dual recordings of the distal dendrites of hippocampal CA1 pyramidal neurons (Magee, 1998, 1999). In brief, HCN channels are partially active at resting membrane potential prior to depolarization and thereby contribute to membrane potential depolarization as an EPSP is triggered by glutamatergic input upon a dendrite. As the membrane potential depolarizes, HCN channels become deactivated, which progressively abolishes I_h, a process taking up tens to hundreds of ms depending on HCN channel subunit composition (Biel et al., 2009; Shah, 2014). If a synaptic input is repeatedly activated over a short period of time, the deactivation of I_h effectively removes an inward (depolarizing) current from contributing to EPSPs occurring later in the train. This translates into an apparent decrease in temporal summation of EPSPs, or in a decrease in amplitude of EPSPs occurring late in a train. Magee studied the effect of HCN channels on temporal summation by recording the EPSP trains before and after bath application of ZD7288, a specific blocker of HCN channels (Magee, 1999, 2000). The results showed that blocking HCN channels resulted in a stronger temporal summation of EPSPs, verifying that deactivation of HCN channels and removing its depolarizing conductance usually leads to a decrease in temporal summation.

Here it was hypothesized that HCN channels are also expressed on dendrites of WT SpS neurons and, to a lesser extent, in *reeler* SpS neurons. The effect of I_h on temporal summation of excitatory inputs onto dendrites of SpS neurons was measured by recording EPSP trains before and after blocking HCN channels by washing in ZD7288, see **Figure 27**. Reliable excitation of SpS neurons was achieved by optogenetic stimulation of TC fibers targeting the SpS neuron. It was anticipated that pharmacological blockage of HCN channels would result in an increased temporal summation. In addition, it was expected that a decreased HCN channel expression in *reeler* SpS neurons, if true, would result in a smaller effect of HCN channel blockade on temporal summation of EPSPs, compared to WT SpS neurons (see **Figure 27**).

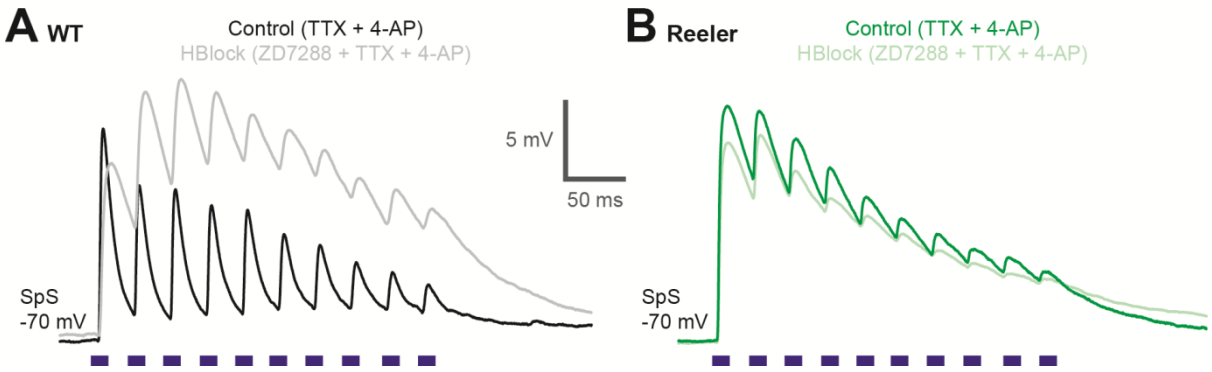

Figure 27: Anticipated effect of I_h on temporal summation of EPSPs.

Recorded example traces, from dataset shown in **Figure 28**, showing optogenetic train stimulation (40 Hz, 10 pulses of 1 ms, indicated by blue stripes) of TC fibers resulted in EPSP trains recorded in SpS neurons of WT (A) and *reeler* mutant mice (B). Temporal summation of EPSPs was measured before (control condition TTX + 4-AP, dark traces) and after additional bath application of ZD7288 (Hblock condition TTX + 4-AP + ZD7288, light traces). The effect of blocking HCN channels on temporal summation of EPSPs was hypothesized to be smaller in *reeler* SpS neurons due to a reduced HCN channel expression.

Reliable excitation of SpS neuron dendrites was achieved by optogenetic stimulation of ChR2-expressing TC fibers (10 pulses of 1 ms at 40 Hz) while simultaneously recording from SpS neurons kept in current clamp at –70 mV (see **Figure 27**). In order to record only direct monosynaptic thalamic input, recording ACSF contained 0.5 µM TTX and 0.1 mM 4-AP (see Methods). The effect of I_h on temporal summation of EPSPs was evaluated by comparing these recordings before and after pharmacologically blocking HCN channels by additional bath application of 1 µM ZD7288 (Hblock condition, WT n = 15, *reeler* n = 12, see **Figure 28A and B**). In total, 10 iterations were recorded per condition with an interstimulus interval of 10 s, from which the average was used for further analysis. Confirmation of blocking HCN channels was established by measuring the resting membrane potential and input resistance from the voltage responses to current pulses (-50 pA, 1s). Supplementary wash in of ZD7288 resulted in a hyperpolarization of the resting membrane potential of most SpS neurons in WT (Control -72.04 mV ± 3.67, HBlock -75.73 mV ± 3.64; one-tailed paired T-test, t (14) = 2.300, p = 0.040, power = 0.700) and *reeler* mutant mice (Control -74.49 mV ± 5.29, HBlock -75.14 mV ± 6.58; one-tailed paired T-test, t (11) = 0.533, p = 0.302, power = 0.126, see **Figure 28C**). In addition, pharmacological wash in of ZD7288 resulted in a significant increase in input resistance of WT SpS neurons (Control 167.47 MΩ ± 46.33, Hblock 258.61 MΩ ± 66.34; one-tailed paired T-test, t (14) = -5.593, p = <0.001, power = 1.000) and *reeler* SpS neurons (Control 185.84 MΩ ± 36.75, HBlock 265.91 MΩ ± 67.24; one-tailed paired T-test, t (11) = -

5.717, p = <0.001, power = 1.000, see **Figure 28D**). In order to exclude potential variability in trains of EPSP responses caused by cell-to-cell differences in short-term depression, the laser intensity was adjusted prior to each stimulation protocol (before and after wash in of additional ZD7288) to maintain a comparable first response amplitude. For each SpS neuron, the laser intensity was adjusted to set the first EPSP response amplitude at approximately 10 mV prior to recording the Control train stimulation, the laser power adjustment was repeated prior to recording the HBlock train stimulation. As a consequence, the first response amplitude was stable and did not change between the two conditions in WT SpS neurons (Control 10.23 mV ± 1.47, HBlock 9.50 mV ± 1.19; two-tailed paired T-test, t (14) = 1.539, p = 0.146, power = 0.300) and *reeler* SpS neurons (Control 10.36 mV ± 1.97, Hblock 9.72 mV ± 1.58; two-tailed paired T-test, t (11) = 1.050, p = 0.316, power = 0.161, see **Figure 28E**). The laser power used to maintain this steady first response amplitude is shown in **Figure 28F**.

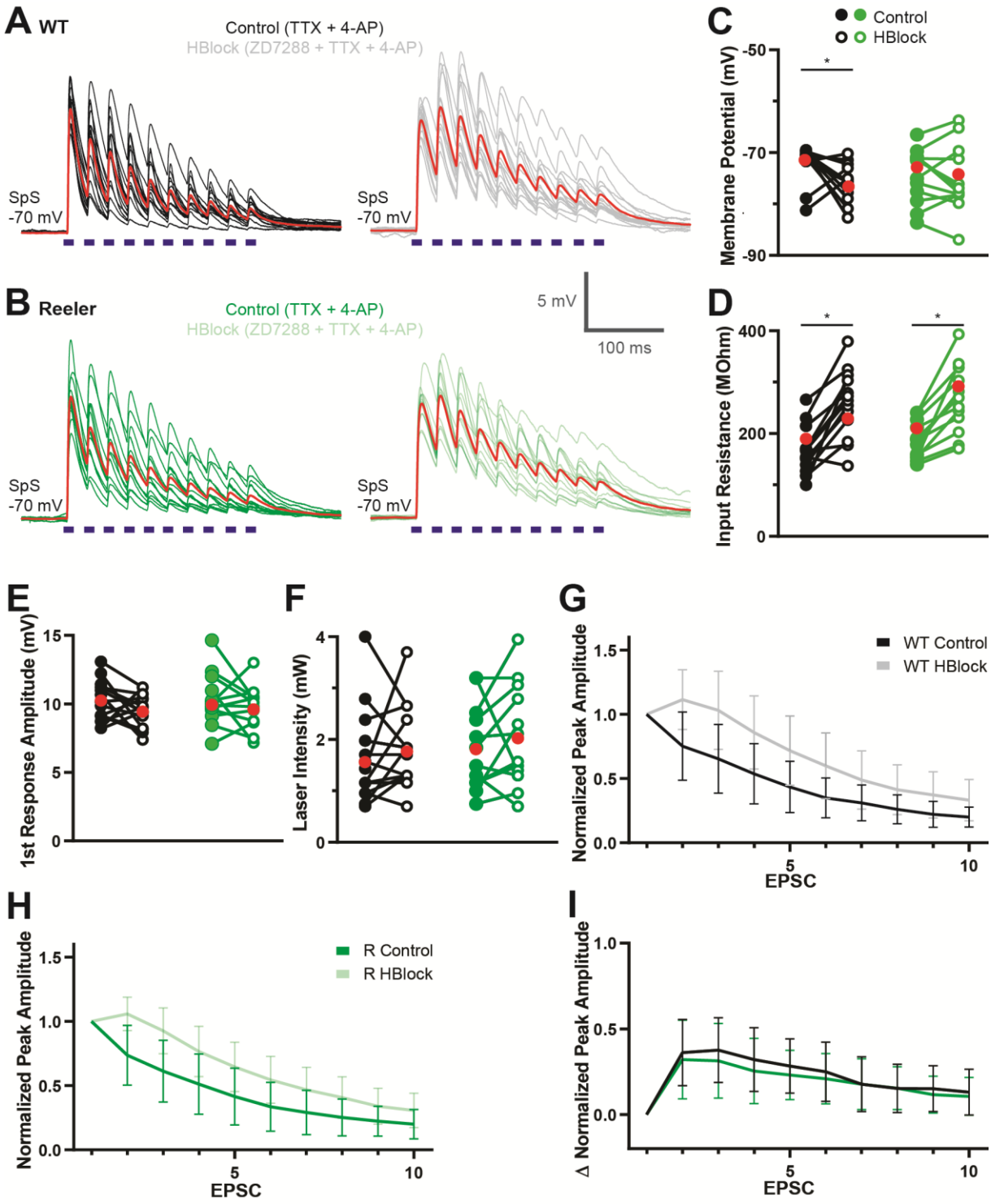

Figure 28: Effect of I_h on temporal summation of EPSPs in SpS neurons.

A) EPSP trains generated by optogenetic stimulation of ChR2-expressing TC fibers at 40 Hz (blue stripes, 10 pulses of 1 ms) recorded in SpS neurons of WT mice (*n* = 15). EPSP train averages per SpS neuron are shown, with the grand average per condition and per genotype in red. Dark traces represent control condition (TTX + 4-AP), light traces represent HBlock condition (TTX + 4-AP + ZD7288). **B)** EPSP trains recorded in control and HBlock condition in *reeler* SpS neurons (*n* = 12). **C)** Wash in of additional ZD7288 was confirmed by a hyperpolarization of the membrane potential observed in most WT SpS neurons (Control -72.04 mV ± 3.67, HBlock -75.73 mV ± 3.64; one-tailed paired T-test, t (14)

= 2.300, p = 0.040, power = 0.700) and *reeler* SpS neurons (Control -74.49 mV ± 5.29, HBlock -75.14 mV ± 6.58; one-tailed paired T-test, t (11) = 0.533, p = 0.302, power = 0.126). Red indicates the average value for each condition. **D)** Wash in of additional ZD7288 caused significant increase in input resistance of WT SpS neurons (Control 167.47 MΩ ± 46.33, Hblock 258.61 MΩ ± 66.34; one-tailed paired T-test, t (14) = -5.593, p = <0.001, power = 1.000) and *reeler* SpS neurons (Control 185.84 MΩ ± 36.75, HBlock 265.91 MΩ ± 67.24; one-tailed paired T-test, t (11) = -5.717, p = <0.001, power = 1.000). **E-F)** To allow for comparison of temporal summation, the first response amplitude was set at 10 mV by adjusting the laser intensity accordingly before and after washing in additional ZD7288. **G-H)** Normalized peak amplitude averages with standard deviation for control and HBlock condition from WT (**G**) and *reeler* mutant mice (**H)**. Blocking I_h had an effect on temporal summation in both genotypes. **I)** The Δ Normalized peak amplitude showed no difference in the effect of I_h on temporal summation of EPSPs between WT and *reeler* mutant mice.

Next, the strength of temporal summation was calculated and compared between the Control and HBlock condition, for both genotypes (WT n = 15, *reeler* n = 12). More specifically, temporal summation was analyzed by measuring the peak amplitude of each EPSP response from each recorded train (an example is shown in **Figure 29**, left). The peak amplitude was defined by the voltage difference between the EPSP peak and the baseline membrane potential. Using this analysis on trains recorded before and after blocking HCN channels, the effect of I_h on temporal summation was determined in WT and *reeler* mutant mice. Not only in WT mice, but also in *reeler* mutant mice, a significantly stronger temporal summation of EPSPs was observed after blocking HCN channels (three-way-ANOVA, F (1, 200) = 24.719, p = <0.001). More specifically, the significantly stronger temporal summation upon blocking HCN channels was limited to the first part of the train, from the second through the fourth EPSP (post-hoc Holm-Sidak, p = <0.001). The average normalized peak amplitudes of EPSPs are illustrated in **Figure 28G** (for WT SpS neurons) and **Figure 28H** (for *reeler* SpS neurons). No difference was observed between WT SpS neurons and *reeler* SpS neurons (three-way ANOVA, F (1, 200) = 0.866, p = 0.353). In addition, no difference was found in the temporal summation between WT and *reeler* mutant mice in either of the conditions (three-way ANOVA, F (1, 200) = 0.019, p = 0.890). These results indicate that blocking HCN channels had a similar effect on SpS neurons in WT mice as it had in *reeler* mutant mice (see **Figure 28G and H**). The effect of I_h on temporal summation was directly compared between genotypes, by calculating the normalized Δ peak amplitude (see **Figure 28I**). The normalized Δ peak amplitude was defined as the difference in normalized peak amplitudes of control and HBlock condition, see **Figure 29**, right. Although the increase in temporal summation upon HCN channel blockade was smaller in *reeler* SpS neurons, the difference did not reach statistical significance (see **Figure 28I**).

In summary, blocking HCN channels resulted in an increased temporal summation in WT SpS neurons. The effect of I_h was limited to the beginning of the EPSP train, suggesting that HCN channels became deactivated afterwards. Likewise, the blockade of HCN channels resulted in an increased temporal summation of *reeler* SpS neurons, indicating the presence of I_h. However, on average the increase in temporal summation was found to be smaller in *reeler* SpS neurons, suggesting a potential decrease of I_h compared to WT SpS neurons. Nevertheless, the optogenetic approach and pharmacological blockade of HCN channels provided an indirect insight to I_h in the dendrites of SpS neurons. When using optogenetic stimulation of TC fibers it is unknown exactly how many synapses become activated upon laser stimulation, the distribution of these TC synapses onto SpS neurons and potential differences in the synaptic targeting of TC fibers onto SpS neurons in WT versus *reeler* mutant mice. Taken together, this approach might lack the sensitivity required to detect minor differences in I_h. As a result of inconclusive outcomes, a different approach was performed to test whether I_h is indeed affected in *reeler* SpS neurons.

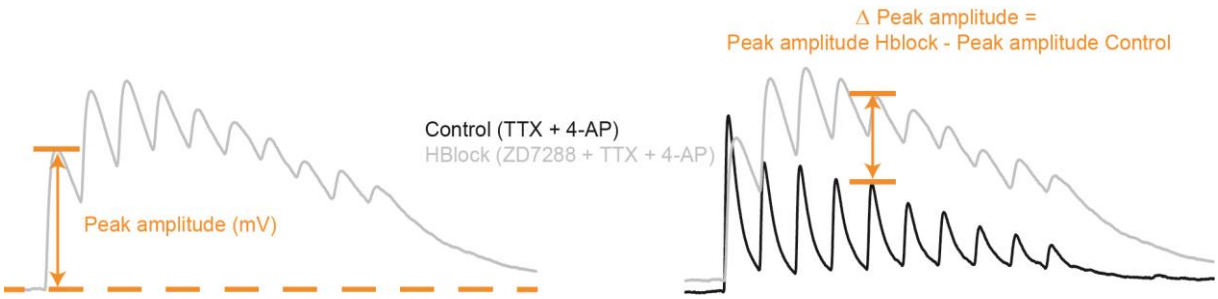

Figure 29: Quantification of the temporal summation of EPSPs.

Left, peak amplitude was calculated as the difference between EPSP peak amplitude (mV) and baseline (mV) (for every optical stimulus in the train). Right, the difference in temporal summation of EPSPs between control and HBlock condition was calculated by the Δ peak amplitude (also for every optical stimulus in the train). The difference in temporal summation of EPSPs was determined by subtracting the EPSP peak amplitude of the control condition from the EPSP peak amplitude of the HBlock, for each EPSP response in the train.

An HCN channel modulator restores connection probability in *reeler* mutant mice

Subsequently, it was investigated whether pharmacologically manipulating I_h during paired recordings between FS interneurons and SpS neurons could affect the connection probability and strength. Initial paired recordings between FS interneurons and SpS neurons with potassium-based IC solution showed a significantly reduced connection probability in *reeler*

mutant mice compared to WT mice (see **Figure 15**). To investigate whether the apparent reduced connectivity was caused by a reduction of I_h in *reeler* SpS neurons, paired recordings between FS interneurons and SpS neurons were performed as described in the Methods section, however now in presence of FK506. By inhibiting calcineurin, a strong modulator of HCN1 channels, FK506 indirectly enhances the activity of HCN1 channels resulting in an increased I_h (Dumont, 2012; Evans et al., 2013; Jung et al., 2010). If indeed *reeler* SpS neurons have reduced HCN channel expression, then pharmacologically increasing I_h in *reeler* SpS neurons should restore the connection probability between FS interneurons and SpS neurons by making inhibitory currents recordable at somatic sites. To investigate this possibility, 300 µm thick thalamocortical slices were incubated in recording ACSF containing 25 µM FK506 (for 60 min at RT) prior to paired recordings. To test whether pharmacologically increasing I_h restores connection probability, I tested for connections between the FS interneurons and SpS neurons in presence of FK506 (see Methods). To be able to accurately interpret connectivity results, the effect of FK506 on basic electrophysiological properties of SpS neurons and FS interneurons was first studied.

The effect of FK506 on various passive and active electrophysiological properties of SpS neurons and FS interneurons in the WT and *reeler* S1BF were investigated (see **Table 3 and 4**). For each recorded cell, an averaged voltage response to a 1 s hyperpolarizing current injection (-50 pA) at V_{rest} was used to determine passive properties. From the voltage responses recorded at rheobase, single action potential parameters were studied. The effect of enhancing HCN channel activity on SpS neuron electrophysiological parameters is summarized in **Table 3**. In presence of FK506, WT SpS neurons showed a lower sag index and *reeler* SpS neurons presented a depolarized V_{rest} compared to the standard condition (without FK506). Increasing HCN channel activity resulted in a reduced the sag index in WT SpS neurons (Standard Mdn 3.15%, FK506 Mdn 1.76 %; Mann-Whitney rank sum test, U = 726.50, p = 0.010). This observation is in conflict with the concept of an increasing I_h resulting in a stronger sag index. However, a sag index lower or equal to 5 % can be disregarded due to it being too small to be accurately calculated. In presence of FK506, *reeler* SpS neurons were found significantly more depolarized compared to the standard condition (V_{rest}: Standard Mdn -73.45 mV, FK506 Mdn -70.00 mV; Mann-Whitney rank sum test, U = 193.00, p = 0.017). A similar, yet not significant depolarization in V_{rest} was observed in WT SpS neurons (V_{rest} mean ± SEM: Standard -72.27 mV ± 0.31, FK506 -70.80 mV ± 1.00, two-tailed T-test, t (132) = -1.745, p = 0.083, power =

0.410). All other examined passive and active SpS neuron parameters were unaffected by incubation with FK506.

Table 3: Effect of FK506 on SpS neuron characteristics.

Data is presented as mean ± SEM	**WT SpS neuron**			***Reeler* SpS neuron**		
	Standard *n = 114*	**FK506** *n = 20*	*p*	**Standard** *n = 52*	**FK506** *n = 13*	*p*
V_{rest} (mV)	-72.27 ± 0.31	-70.80 ± 1.00	*0.083*	-72.70 ± 0.54	-69.15 ± 1.32	***0.017****
Input resistance (MOhm)	133.02 ± 4.27	149.32 ± 16.60	*0.444*	143.20 ± 7.53	143.16 ± 11.35	*0.574*
Tau fit (ms)	8.88 ± 0.31	9.77 ± 0.73	*0.195*	8.37 ± 0.47	9.17 ± 0.86	*0.228*
Sag index (%)	3.89 ± 0.38	1.99 ± 0.38	***0.010****	3.26 ± 0.35	3.48 ± 0.89	*0.993*
Rheobase (pA)	165.10 ± 8.00	138.66 ± 13.58	*0.335*	137.67 ± 7.79	141.22 ± 18.69	*0.760*
Firing threshold (mV)	-32.32 ± 0.61	-32.32 ± 1.07	*0.412*	-31.77 ± 0.64	-31.22 ± 1.44	*0.705*
AP amplitude (mV)	62.79 ± 0.77	60.68 ± 1.70	*0.291*	63.39 ± 1.05	59.36 ± 3.50	*0.35*
AP width (ms)	0.66 ± 0.01	0.68 ± 0.02	*0.507*	0.64 ± 0.01	0.70 ± 0.03	*0.053*

The effect of FK506 on basic electrophysiological properties of FS interneurons in the WT and *reeler* S1BF is presented in **Table 4**. In presence of FK506, *reeler* FS interneurons showed a significantly reduced input resistance (mean ± SEM; 106.74 MΩ ± 8.04) compared to the standard condition (mean ± SEM; 75.63 MΩ ± 6.74; two-tailed T-test, t (30) = 2.554, p = 0.016, power = 0.696). Similar to the observations in SpS neurons, the sag index of FS interneurons in both genotypes decreased as a result of brain slice incubation with FK506. Again in this case, the sag index in both standard and FK506 condition were too small to be measured precisely, therefore the result can be neglected. Compared to the standard condition, FK506 significantly increased the rheobase current for *reeler* FS interneurons (mean ± SEM; standard 270.66 pA ± 32.11, FK506 388.91 pA ± 38.25; two-tailed T-test, t (24) = -2.376, p = 0.026, power = 0.625). Other parameters tested in WT and *reeler* FS interneurons were not affected by the presence of FK506.

Table 4: Effect of FK506 on FS interneuron characteristics.

Data is presented as mean ± SEM	**WT FS interneuron**			***Reeler* FS interneuron**		
	Standard *n = 23*	**FK506** *n = 18*	*p*	**Standard** *n = 21*	**FK506** *n = 11*	*p*
V_{rest} (mV)	-63.86 ± 0.76	-63.00 ± 1.00	*0.268*	-65.07 ± 0.70	-65.55 ± 1.61	*0.945*
Input resistance (MOhm)	92.69 ± 7.64	87.09 ± 6.98	*0.813*	106.74 ± 8.04	75.63 ± 6.74	***0.016****
Tau fit (ms)	4.82 ± 0.33	5.34 ± 0.38	*0.234*	5.33 ± 0.46	5.08 ± 0.25	*0.968*
Sag index (%)	5.60 ± 0.79	3.36 ± 0.46	***0.000****	4.82 ± 0.74	4.27 ± 0.83	***0.004****
Rheobase (pA)	306.77 ± 31.61	387.25 ± 39.23	*0.115*	270.66 ± 32.11	388.91 ± 38.25	***0.026****
Firing threshold (mV)	-35.74 ± 2.05	-31.96 ± 1.47	*0.272*	-34.19 ± 1.71	-31.11 ± 2.20	*0.273*
AP amplitude (mV)	37.38 ± 2.43	36.35 ± 2.10	*0.470*	38.72 ± 2.72	32.79 ± 2.48	*0.133*
AP width (ms)	0.25 ± 0.01	0.25 ± 0.01	*0.755*	0.26 ± 0.01	0.25 ± 0.01	*0.413*

Next, the effect of increasing I_h on the connection probability between FS interneurons and SpS neurons was studied. Increasing I_h revealed a high connection probability between FS interneuron to SpS neuron in *reeler* mutant mice similar to WT mice (see **Figure 30**). Out of 22 pairs tested in WT mice, 14 showed an inhibitory connection (63.7 %, combining bidirectionally connected and unidirectionally connected pairs from FS interneuron to SpS neuron). In *reeler* mutant mice, 8 out of 11 pairs exhibited an inhibitory connection (72.8 %, combining bidirectionally connected and unidirectionally connected pairs from FS interneuron to SpS neuron). These outcomes are in favour of the hypothesis that enhancing I_h restores connection probability from FS interneuron to SpS neuron in *reeler* mutant mice to similar values as observed in WT mice (Chi-square, X^2 (3) = 2.571, p = 0.463, power = 0.238, see **Figure 30**).

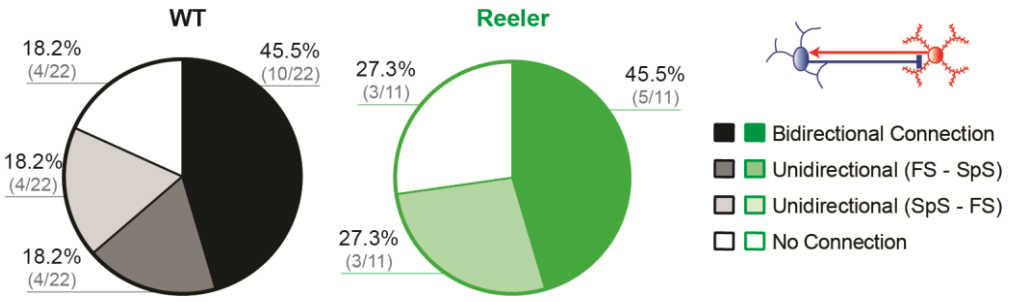

Figure 30: Connectivity between FS interneurons and SpS neurons in presence of FK506.

Pharmacologically increasing I_h, with FK506 incubation, resulted in a high connection probability between FS interneurons and SpS neurons in *reeler* mutant mice (green) and WT mice (black). In these pie charts, tested connections were divided into four categories: bidirectionally connected, unidirectionally connected from FS interneuron to SpS neuron, unidirectionally connected from SpS neuron to FS interneuron and unconnected.

Next, the effect of I_h on the reliability and strength of the inhibitory connection from FS interneurons to SpS neurons was determined by analysing IPSCs. In addition, the role of I_h on connection reliability and strength was further evaluated by blocking HCN channels using additional 1 µM ZD7288 in the recording ACSF. Postsynaptic current responses were recorded first in presence of FK506 and were then recorded again after pharmacological bath application of additional ZD7288. It was anticipated that blocking HCN channels would lead to a decreased inhibitory connection reliability and strength as a result of reduced I_h and diminished driving force for GABA-A receptor mediator currents. The IPSCs recorded in presence of FK506, were recorded again after wash in of additional ZD7288 (WT $n = 7$, *reeler* $n = 4$, see **Figure 31**). The averaged IPSCs per connection and the grand average IPSC per condition and per genotype are shown in **Figure 31A**.

Reliability of each connection, before and after additional wash in of ZD7288, was determined by calculating the synaptic failure rate. The synaptic failure rate increased upon blocking HCN channels in 2 out of 7 connections in WT mice (FK506 0.77 % ± 2.77, FK506 + ZD7288 5.24 % ± 10.16, Chi-square, X^2 (1) = 1.546, $p = 0.214$, power 0.237) and in 3 out of 4 connections in *reeler* mutant mice (FK506 9.29 % ± 18.80, FK506 + ZD7288 42.65 % ± 39.07, Chi-square, X^2 (1) = 28.300, $p = <0.001$, power 1.000, see **Figure 31B**). In line with the hypothesis, these results have demonstrated that enhancing HCN channel activity revealed reliable inhibitory connections in *reeler* mutant mice. Upon blocking HCN channels with additional bath application of ZD7288, the same connection became less reliable as demonstrated by the increased synaptic failure rate. Subsequently, the effect of I_h on the IPSC waveform was analysed in order to investigate the effect of I_h on the strength of the IPSC response. The results demonstrate that the time-to-peak of IPSCs between the FK506 and the FK506 + ZD7288 condition did not significantly differ in WT mice (FK506 1.87 ms ± 0.58, FK506 + ZD7288 2.38 ms ± 0.74; two-tailed paired T-test, t (6) = -2.430, $p = 0.051$, power = 0.531) and *reeler* mutant mice (FK506 1.77 ms ± 0.65, FK506 + ZD7288 1.72 ms ± 0.53; two-tailed paired T-test, t (3) = 0.141, $p = 0.896$, power = 0.051, see **Figure 31C**). Also, no difference was found in the time-to-peak of IPSCs between the two genotypes. Moreover, the IPSC amplitude recorded in the two different conditions in WT (FK506 32.19 pA ± 30.14, FK506 + ZD7288 29.09 pA ± 34.03; two-tailed paired T-test, t (6) = 0.842, $p = 0.216$, power = 0.110) and in *reeler* mutant mice (FK506 18.334 pA ± 12.14, FK506 + ZD7288 16.50 pA ± 19.62; two-tailed paired T-test, t (3) = 0.361, $p = 0.742$, power = 0.058, see **Figure 31D**) was similar. In addition,

the IPSC decay was also found to be comparable between conditions and genotypes (WT FK506 5.23 ms ± 1.42, FK506 + ZD7288 6.60 ms ± 3.47; two-tailed paired T-test, t (6) = -1.168, p = 0.287, power = 0.168; *reeler* FK506 4.24 ms ± 0.61, FK506 + ZD7288 4.20 ms ± 3.62; two-tailed paired T-test, t (3) = 0.029, p = 0.979, power = 0.050, see **Figure 31E**). Taken together, these preliminary results demonstrated the effect of I_h on the inhibitory connection probability, connection reliability and connection strength in WT and *reeler* SpS neurons. In line with the hypothesis, the initially reliable inhibitory connection recorded during enhanced HCN channel activity became less reliable upon blocking HCN channels. Whereas a decrease in I_h results in less reliable inhibitory connections, it had no effect on the IPSC waveform. This preliminary dataset supports the hypothesis of a reduced I_h in *reeler* SpS neurons causing an insufficient driving force for inhibitory inputs as observed in the initial paired recordings.

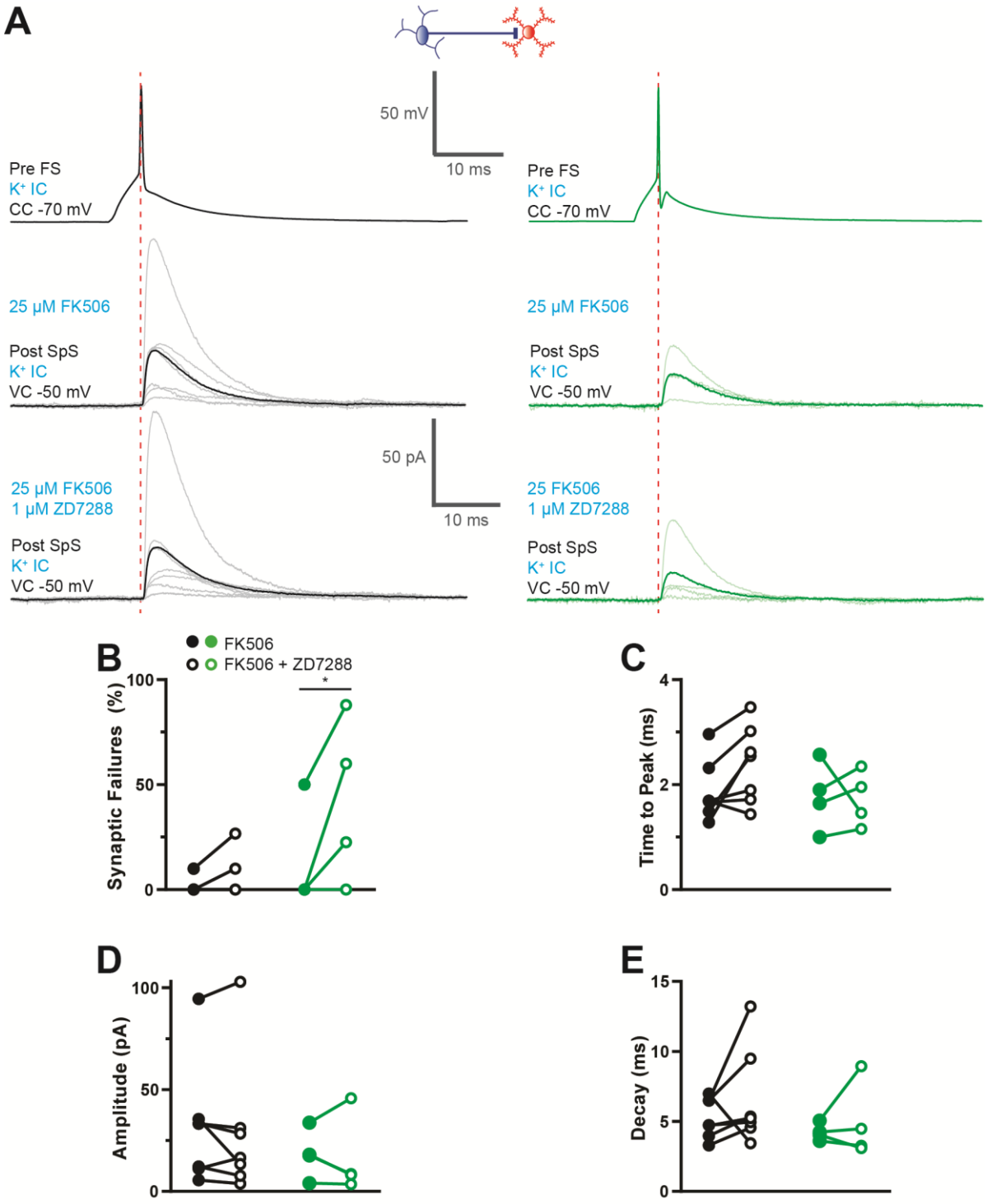

Figure 31: Effect of blocking HCN channels on IPSC reliability and strength.

A) IPSCs recorded in SpS neurons (kept in VC at -50 mV) with potassium-based IC solution after incubation with FK506, and after additional bath application of ZD7288 (WT black *n* = 7, *reeler* green *n* = 4). Light traces represent averaged IPSCs per connection per condition, dark traces represent grand average per genotype per condition. **B)** Synaptic failure rate per connection, in presence of FK506 (closed circle) and after washing in ZD7288 (open circle). A significant increase of synaptic failure rate after additional wash in of ZD7288 was observed in *reeler* (WT: FK506 0.77 % ± 2.77, FK506 + ZD7288 5.24 % ± 10.16, Chi-square, X^2 (1) = 1.546, *p* = 0.214, power 0.237; *reeler*: FK506 9.29 % ± 18.80, FK506 + ZD7288 42.65 % ± 39.07, Chi-square, X^2 (1) = 28.300, *p* = <0.001, power 1.000). **C)**

Time-to-peak of IPSCs recorded in WT and *reeler* mutant mice was not affected by blocking HCN channels. Neither was IPSC amplitude and decay (**D-E).**

Next, the effect of I_h on the excitatory connection from SpS neuron to FS interneuron was analysed. The enhanced HCN channel activity increased the probability to find an excitatory connection between SpS neuron and FS interneuron in both genotypes, see **Figure 30**. The total excitatory connection probability was calculated by combining the percentage of bidirectionally connected pairs and unidirectionally connected pairs from SpS neuron to FS interneuron. Excitatory connections were detected in 14 out of 22 pairs in WT mice (63.7 %) and in 5 out of 11 pairs in *reeler* mutant mice (45.5 %, Chi-square, X^2 (3) = 2.571, p = 0.463, power = 0.238). In summary, enhancing HCN channel activity led to increased connection probability from SpS neuron to FS interneuron in the *reeler* mutant mouse.

The averaged EPSC recorded per connection for each condition and genotype are shown in **Figure 32A**. The connection from SpS neuron to FS interneuron was found highly reliable (synaptic failure rate: WT n = 5, 0.00 % ± 0.00; *reeler* n = 3, 0.00 % ± 0.00) and was unaffected by blocking HCN channels with additional ZD7288 (see **Figure 32B**). Next, the effect of enhancing and blocking HCN channels on the EPSC waveform was determined by measuring the time-to-peak, amplitude and decay. The time-to-peak of EPSCs was not affected by blocking HCN channels (WT: FK506 Mdn 0.68 ms, FK506 + ZD7288 Mdn 0.79 ms; *reeler* FK506 0.63 ms ± 0.01, FK506 + ZD7288 0.66 ms ±0.08, see **Figure 32C**). Washing in of additional ZD7288 did not affect the EPSC amplitude in WT (FK506 50.56 pA ± 24.25; FK506 + ZD7288 -46.18 pA ± 24.27) and *reeler* mutant mice (FK506 Mdn -97.26 pA; FK506 + ZD7288 Mdn -65.88 pA, see **Figure 32D**). In contrast, the EPSC decay was affected by blockage of HCN channels in WT mice (FK506 1.48 ms ± 0.46, FK506 + ZD7288 1.93 ms ± 0.47; two-tailed paired T-test, t (4) = -3.300, p = 0.030, power = 0.698, see **Figure 32E**). The EPSC decay in the *reeler* mutant mouse was not affected by blockage of HCN channels (FK506 2.12 ms ± 0.61, FK506 + ZD7288 2.39 ms ± 0.64; two-tailed paired T-test, t (2) = -0.566, p = 0.628, power = 0.065, see **Figure 32E**). These results demonstrated that the excitatory connection reliability and strength were unaffected by blocking HCN channels.

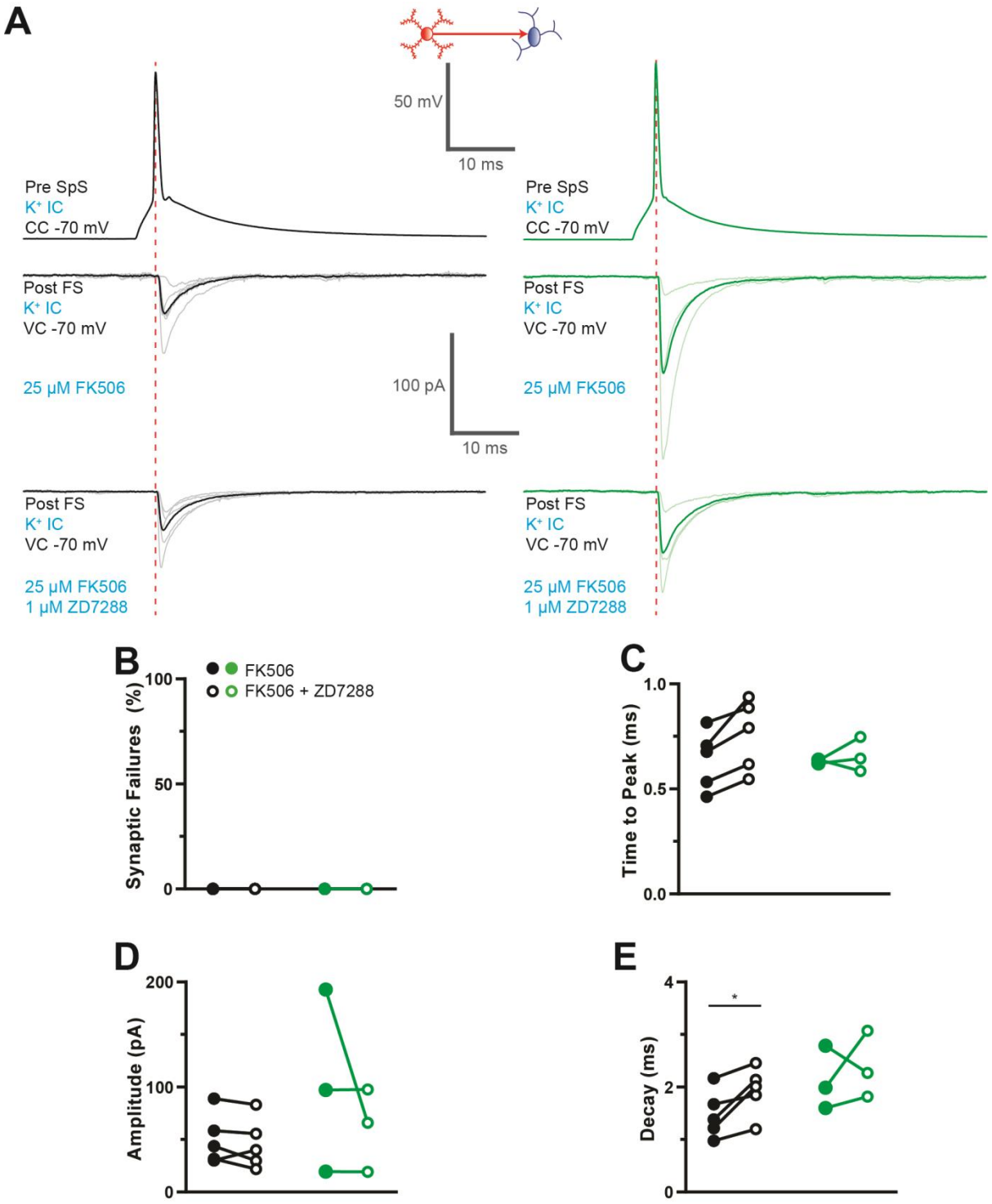

Figure 32: No effect of blocking HCN channels on EPSC reliability and strength.

A) EPSCs recorded in FS interneurons (kept in VC at -70 mV) after incubation with FK506, in order to increase I_h, and after additional bath application of ZD7288 (WT black *n* = 5, *reeler* green *n* = 3). Light traces represent averaged EPSCs per connection per condition, dark traces represent grand average per genotype per condition. **B)** Synaptic failure rate per excitatory connection, in presence of FK506 (closed circle) and after washing in ZD7288 (open circle). **C)** Time-to-peak of EPSCs recorded in WT and *reeler* mutant mice was not affected by blocking HCN channels. Neither was the IPSC amplitude (**D**). **E)** In WT mice, the EPSC decay was found significantly increased following washing in of additional

ZD7288 (FK506 1.48 ms ± 0.46, FK506 + ZD7288 1.93 ms ± 0.47; two-tailed paired T-test, t (4) = -3.300, p = 0.030, power = 0.698).

Overall, these results indicate that the crucial role of I_h in the integration and propagation of inhibitory and excitatory inputs is affected in the *reeler* mutant mouse. More specifically, the reduced HCN-channel mediated depolarization in *reeler* SpS neurons leads to an insufficient driving force for GABAergic transmission. This mechanism was confirmed by the reliable connections recorded between FS interneuron and SpS neuron in the *reeler* S1BF in presence of FK506. The subsequent blockade of HCN channels in the exact same connections led to an increase in synaptic failures, suggesting a deficient driving force for IPSCs. Through a different mechanism, I_h influences excitatory connections in the *reeler* S1BF. By increasing the HCN channel activity, the excitatory connection probability and reliability increased from SpS neuron to FS interneuron in the *reeler* mutant mouse. This could be explained by the HCN channel-mediated depolarization of the membrane potential of SpS neurons, as shown by a more depolarized V_{rest} in presence of FK506 (see **Table 3**). This mechanism also results in more depolarized presynaptic terminals of the SpS neuron, bringing them closer to the threshold for Ca^{2+} entry. Therefore, a reduced I_h in the *reeler* cortex explains the reduced excitatory connection probability observed between SpS neurons and FS interneurons. Taken together, these preliminary findings offer a clarification of the observed changes in neuronal connectivity: a reduced HCN channel expression in the *reeler* S1BF causes reduced inhibitory and excitatory signal transmission.

Discussion

The cortex of *reeler* mutant mice is characterized by a severe disarrangement of neurons culminating in the lack of proper cortical layering. In S1BF, each layer is composed of specific types of neurons and a distinct connectivity pattern. These layer-specific properties endow each layer with the ability to perform an individual task in the processing of sensory information. What happens to single neuron properties and neuronal connections in the absence of this layered organization? Previous studies described a weakened thalamic input onto SpS neurons of the *reeler* S1BF, whereas an overall greater network excitability was found upon optogenetic stimulation of TC fibers (Guy, 2015; Guy et al., 2017). These seemingly contradicting findings, also replicated in this study (see **Figure 7 and 33**), provided the foundation for the present work: which mechanism is responsible for compensating the weakened thalamic input in the *reeler* cortex? Two such mechanisms were investigated in the present work (see **Figure 3 and 33**). The first hypothesized cortical mechanism states that the recurrent excitatory excitation between SpS neurons may be stronger in the *reeler* mutant mouse. The second hypothesized cortical mechanism postulated a weakened FS interneuron mediated inhibition in the *reeler* S1BF compared to WT. The connections between SpS neurons and the connections between FS interneurons and SpS neurons were examined with paired recordings. Prior to studying these neuronal connections, I assessed whether single cell properties are affected in the *reeler* S1BF, as potential changes could interfere with the understanding of neuronal connection properties between the two genotypes. To this end, several passive and active electrophysiological parameters of SpS neurons and FS interneurons were compared between WT and *reeler* mice (see **Figure 9 and 11**). No differences in electrophysiological characteristics were found. Moreover, the various morphological parameters concerning the dendritic arborisation of SpS neurons and FS interneurons were found to be similar in WT and *reeler* mice (see **Figure 10 and 12**). The first hypothesized compensatory mechanism stated a stronger recurrent excitatory excitation between SpS neurons in the *reeler* cortex to compensate the weakened incoming thalamic input. The paired recordings between SpS neurons, however,

indicated a similar connection probability, connection reliability and connection strength in the tested WT and *reeler* connections (see **Figure 12, 13 and 33**), thereby invalidating the hypothesis of an enhanced recurrent excitatory excitation in the *reeler* S1BF. The paired recordings between FS interneurons and SpS neurons tested the second hypothesis proposing a weakened FS interneuron mediated feedforward/feedback inhibition in the *reeler* cortex. The initial paired recordings using a potassium-based IC solution showed a drastically reduced connectivity in the *reeler* cortex, compared to the WT cortex (see **Figure 15 – 17**). Remarkably, a normal connection probability, connection reliability and connection strength were uncovered when repeating the paired recordings between FS interneurons and SpS neurons with a cesium-based IC solution (see **Figure 18, 19 and 33**). These findings disproved the hypothesis of a weakened inhibition in the *reeler* cortex. The contradictory findings between potassium-based IC solution and cesium-based IC solution recordings were hypothesized to be caused by a more distally shifted inhibitory innervation pattern of *reeler* SpS neurons. However, morphological recontructions and Syt-2 immunolabeling demonstrated that inhibitory putative contacts targetted the soma, proximal dendrites and distal dendrites of both WT and *reeler* SpS neurons (see **Figure 21 – 25**). Hence, the contradictory paired recording findings could not be explained by a drastically altered inhibitory innervation pattern in *reeler* SpS neurons. Heretofore, the data suggests that inhibitory synapse location and functioning is likely not affected in the *reeler* mutant mouse. Next, it was assessed whether the dendritic integration of inhibitory inputs could be affected in *reeler* SpS neurons, as it could explain the discrepancy observed in the paired recording results. Specifically, it was investigated whether *reeler* SpS neurons have a reduced I_h compared to WT SpS neurons. As the I_h-mediated dendritic depolarization is required to generate a driving force for inhibitory inputs, a reduction or lack of I_h in *reeler* SpS neurons could explain the nonappearance of inhibitory inputs in the intitial paired recordings. The effect of I_h on temporal summation of EPSPs was compared in WT and *reeler* SpS neurons by performing optogenetic train stimulation of thalamic fibers and pharmacological blockage of HCN channels. Even though the nonsignificant findings hinted at a potential decrease of I_h in *reeler* SpS neurons, the optogenetic approach probably lacked the sensitivity required to detect minor differences in I_h (see **Figure 28**). As a consequence, the reduced I_h hypothesis was tested again with a different approach. Paired recordings between FS interneurons and SpS neurons with standard potassium-based IC solution were repeated, but this time in presence of the drug FK506 in order to enhance HCN channel activity. Strikingly, the presence of FK506 increased the connection probability, connection reliability and connection strength in both WT and *reeler* connections to comparable levels (see **Figure**

30 – 32). Furthermore, pharmacological blockade of HCN channels made the very same inhibitory connections less reliable. These findings are suggestive of a reduced HCN channel expression in the *reeler* S1BF resulting in a reduced inhibitory and excitatory signal transmission between SpS neurons and FS interneurons (see **Figure 33**). All together, these experiments have provided insight in the effect of a disorganized S1BF on the properties of individual neurons, the establishment of the thalamorecipient microcircuits, and the functionality of the thalamorecipient microcircuit.

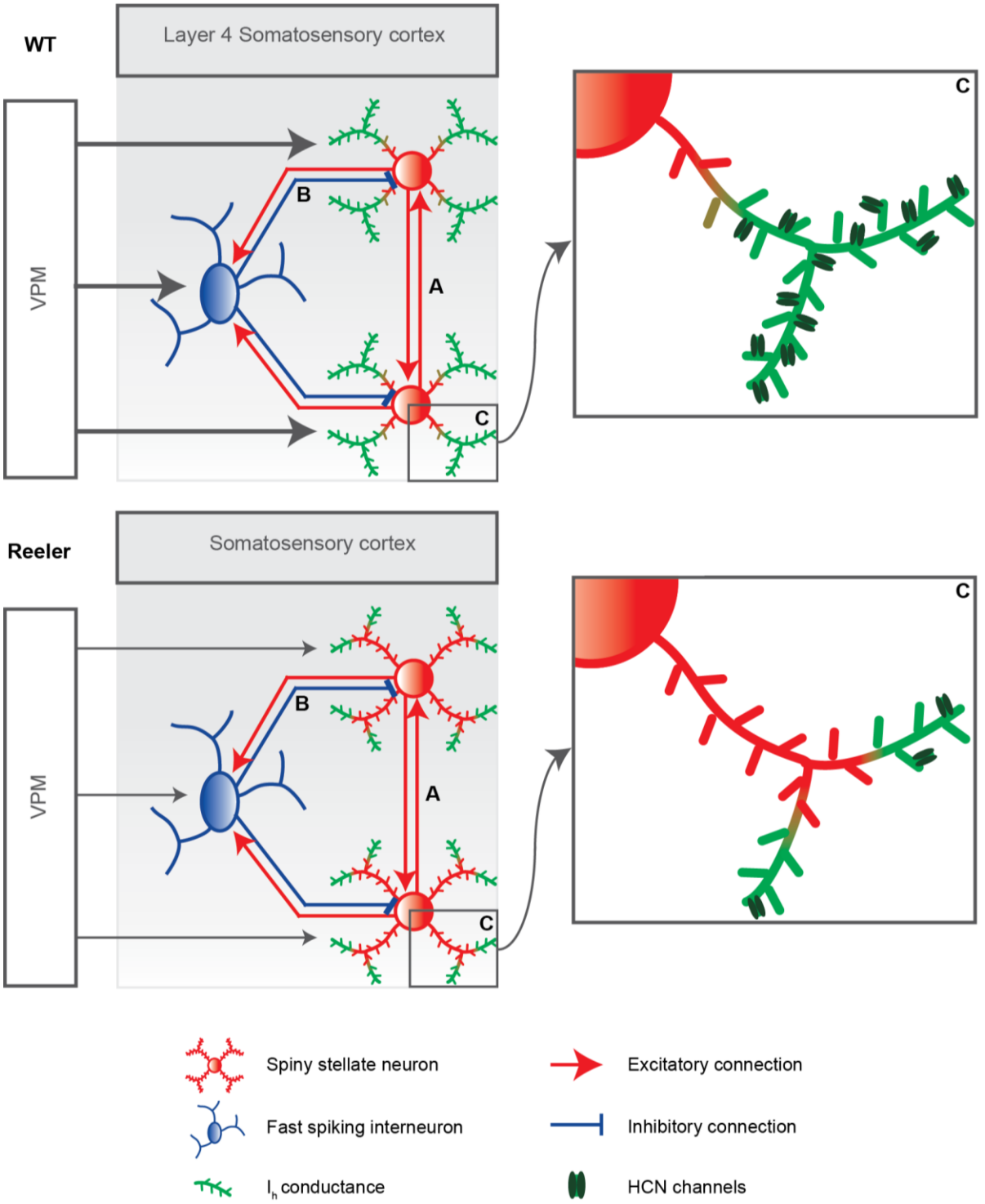

Figure 33: Schematic of investigated connections and mechanisms in the thalamorecipient circuit.

Thalamorecipient circuit in the WT (top) and *reeler* somatosensory cortex (bottom). Three potential compensatory mechanisms for the weakened thalamic input in the *reeler* cortex were investigated (A, B and C). Hypothesis A (enhanced recurrent excitation between SpS neurons in the *reeler* S1BF) was proven false by a similar connection probability and strength between SpS neurons in WT and *reeler* as measured by paired recordings. Hypothesis B (weakened inhibition mediated by *reeler* FS interneurons) was contradicted by comparable connection probability and strength between SpS neurons and FS interneurons in WT versus *reeler* mice, as shown by the paired recordings using a

cesium-based IC. The discrepancy in connection probability between paired recordings using potassium and cesium-based IC could not be explained by an altered innervation pattern of SpS neurons. This led to the investigation of the dendritic integration of inhibitory inputs in *reeler* SpS neurons, hypothesis C (reduced I_h conductance, mediated by HCN channels, in *reeler* SpS neurons causes insufficient driving force for dendritic inhibitory inputs to reach the soma). The increase in connection probability using paired recordings in presence of FK506 revealed that I_h could indeed be affected in *reeler* S1BF resulting in a reduced driving force for dendritic inhibitory iputs.

Properties of SpS neurons and FS interneurons are unaffected by reelin deficiency

The individual tasks of cortical layers in the processing of sensory information is carried out by layer-specific subsets of neuron types, each of which exhibit distinct structural and physiological features. Therefore, absence of proper cortical layering could result in altered cellular properties. For example, L5 pyramidal neurons in the *reeler* S1BF show impaired development of the apical dendrite which could cause altered electrophysiological properties (unpublished data from our laboratory). The present study evaluated whether morphological and electrophysiological properties of SpS neurons and FS interneurons were affected by reelin deficiency. SpS neurons can be morphologically characterized by their dendritic trees being limited to an individual barrel. In line with previous studies, this work suggested that dendrites of SpS neurons are confined to barrel-equivalents in the *reeler* S1BF (see **Figure 8A and B**, Guy et al., 2017; Wagener et al., 2016). In addition to a similar location within the barrel or barrel-equivalent, analysis of biocytin-filled SpS neurons indicated that the complexity of the dendritic arborisation was also not drastically different between WT and *reeler* mice (see **Figure 8**). On a physiological level, SpS neurons of the WT and *reeler* S1BF were found similar (see **Figure 9**). All together, these results indicate that morphological and electrophysiological properties of SpS neurons are not affected in *reeler* mutant mice.

In the postnatal brain, reelin is predominantly expressed in inhibitory interneurons, including the FS PV-expressing interneurons (Pohlkamp et al., 2014). It could therefore be expected that properties of FS interneurons are affected in the *reeler* mutant mouse. Nevertheless, the *reeler* cortex contains a similar density of PV-expressing interneurons compared to the WT cortex, also in the barrel equivalents. (Boyle et al., 2011; Wagener et al., 2016). Morphologically, no

major differences were detected in terms of dendritic arborisation of FS interneurons in the barrel and barrel-equivalent (see **Figure 10**). Furthermore, the various passive and active physiological properties studied showed no difference between WT and *reeler* mice (see **Figure 11**). Taken together, a lack of proper layering in the *reeler* S1BF did not affect physiological properties, such as V_{rest}, input resistance, and firing pattern, of SpS neurons and FS interneurons. Preliminary results in this study demonstrated no drastic alterations in the morphology of SpS neurons and FS interneurons in the *reeler* mutant mouse. The absence of cortical layering does not seem to have a major effect on properties of SpS neurons and FS interneurons.

Improper lamination does not affect the establishment of thalamorecipient microcircuits

The thalamic VPm nucleus is known to project to S1BF, specifically to L4 and the border of L5/6 (Bernardo & Woolsey, 1987; Lu & Lin, 1993). Within L4, a large proportion of the thalamic input is received by both SpS neurons and FS interneurons (Agmon & Connors, 1992; Bagnall et al., 2011; Cruikshank et al., 2007, 2010; Staiger et al., 2009; Swadlow, 1989; Swadlow, 1995). These neurons are known to be interconnected as well (Koelbl et al., 2015). This thalamorecipient circuit is layer-specific and might therefore be affected in the disorganized *reeler* cortex and cause impaired development of neuronal connectivity.

In this study, previous findings regarding ChR2-evoked thalamic responses in SpS neurons were replicated (see **Figure 7**). By performing ChR2-injections in the VPm, it was evidently shown that thalamocortical axons target the barrel equivalents in the *reeler* S1BF (see **Figure 6**). In addition, it was found that these thalamocortical synapses directly innervate SpS neurons and that these synapses were properly functioning (see **Figure 7**). In both WT and *reeler* SpS neurons, ChR2-evoked multicomponent responses consisted of both excitatory and inhibitory inputs indicating the presence and contribution of FS interneurons in the thalamorecipient network (see **Figure 7**). This observation suggests that, similar to observations in the WT S1BF, *reeler* FS interneurons are directly innervated by thalamocortical fibers and/or are bidirectionally connected with local SpS neurons. In summary, thalamocortical axons

originating from the VPm successfully target L4-fated SpS neurons in the *reeler* S1BF. Moreover, the IPSPs included in the ChR2-evoked compound responses indicate the direct involvement of FS interneurons in the thalamorecipient microcircuit.

Using the paired recordings, it was confirmed that connections between SpS neurons exist in the *reeler* S1BF (see **Figure 12**). Moreover, the connectivity rate and connection strength of SpS neurons was found similar between genotype (see **Figure 12 and 13**). From the few EPSCs recorded per genotype, the waveform did not show obvious differences either. These findings indicate that within barrel-equivalents SpS neurons are interconnected with a similar connectivity rate and connection strength as observed in the barrels of the WT S1BF. Next, it was examined whether FS interneurons and SpS neurons in *reeler* mutant mice are connected as known in WT mice. Using a cesium-based IC solution, an equal connectivity rate was found in paired recordings of WT and *reeler* FS interneurons and SpS neurons (see **Figure 18**). Furthermore, the IPSC waveform was also similar in both genotypes (see **Figure 19**). These findings suggest that, similar to the WT cortex, FS interneurons and SpS neurons are connected to each other in the *reeler* S1BF. This inhibitory connection explains the IPSPs observed in the ChR2-evoked multicomponent responses. In addition to the paired recording results, the connection between FS interneuron and SpS neuron in the *reeler* S1BF was also proven by the detection of putative contacts in post-hoc reconstructions of biocytin filled neurons and by the immunolabeling with Syt-2 which is a marker for presynaptic terminals of FS interneurons (see **Figure 21 – 25**). These various approaches all suggest that SpS neurons and FS interneurons in *reeler* are connected, much like it is the case in the WT S1BF.

In summary, these findings contradict the idea that cortical lamination has a crucial role in the establishment of proper neural networks (Hafner et al., 2020; Kowalski et al., 2010). In the *reeler* S1BF, thalamocortical axons mainly target the barrel-equivalents and SpS neurons and FS interneurons are found properly interconnected (see **Figure 33**) (Guy et al., 2017; Kowalski et al., 2010; Wagener et al., 2016). Therefore, the loss of cortical layers does not affect the establishment of neuronal connections.

Lack of proper cortical layering results in functional imbalances in the thalamorecipient microcircuit

The present study demonstrated that the connections observed in the WT S1BF also exist in the *reeler* S1BF (see **Figure 33**). Whereas structurally, all connections are present for the processing of sensory information, I observed various functional alterations in the *reeler* neuron network.

For example, the larger, ChR2-evoked compound responses recorded in SpS neurons indicate an overall greater network activity in the *reeler* S1BF (see **Figure 7**). Interestingly, pharmacological isolation of the pure thalamic contribution showed that VPm input onto *reeler* SpS neurons is weakened (see **Figure 7**). These results formed a replication of prior studies (Guy, 2015; Guy et al., 2017). The contradictory observation of a weakened thalamic input onto a hyperexcitable cortical network led me to investigate various mechanisms that could compensate the weakened thalamic input (as summarized in **Figure 3**). The first hypothesized mechanism was that SpS neurons, among themselves, amplify the weakened thalamic input. However, the connection probability, reliability and strength, as measured with paired recordings between SpS neurons, did not show any significant differences as a result of improper cortical layering (**Figure 12 - 14**). The second hypothesis examined in this study tested, if the feedforward and/or feedback inhibition was affected in the *reeler* S1BF. This was accomplished by performing paired recordings between FS interneurons and SpS neurons. Strikingly, a severe reduction in connectivity rate between FS interneurons and SpS neurons in the *reeler* S1BF was measured, using potassium-based IC solution (see **Figure 15**). This is a particularly interesting finding, as the neural reconstructions and the Syt-2 immunolabeling provided evidence that these connections are structurally present in the *reeler* S1BF (see **Figure 21 - 25**). Furthermore, the paired recordings between FS interneuron and SpS neuron using a cesium-based IC solution, demonstrated that the connection functions properly (see **Figure 18 - 20**). This discrepancy led me to examine whether the I_h in *reeler* SpS neurons could be reduced (see **Figure 33**). The I_h-mediated depolarization is required to establish a sufficient driving force for inhibitory inputs. Therefore, a decreased I_h would hinder the propagation of inhibitory inputs resulting in an absence of detectable connections. As for the excitatory connectivity from SpS neuron to FS interneuron, I_h-mediated depolarization also ensures

depolarization of the excitatory presynaptic terminals to a membrane potential closer to the threshold for Ca^{2+} entry. Consequently, a reduction in I_h would results in a more hyperpolarized presynaptic terminal which might explain the absence of measureable excitatory connections. One way to measure I_h is by calculating the sag index. However, no differences in the sag index was observed in SpS neurons and FS interneurons between WT and *reeler* mutant mice (see **Figure 9**). Although, the lack of a measureable sag index does not necessarily imply absence of I_h as reported in literature (Aponte et al., 2006; Medinilla et al., 2013). The combination and timing of multiple parameters, such as the membrane time constant and the activation time of specific HCN channel subtypes, determine whether a sag index becomes visible. Furthermore, the sag index is measured at the soma, which does not give me an indication of the I_h intensity in the distal dendrites of SpS neurons where HCN channels are assumed to be expressed. A reduced I_h in the distal dendrites of SpS neurons, could therefore explain why some of the inhibitory connections were undetected. It should be noted, that a reduction of distal dendritic HCN channel expression in *reeler* SpS neurons does not explain the undetected inhibitory connections at the soma and proximal dendrites where I_h does not play a role. Nevertheless, the two different approached performed in the present study propose I_h intensity is indeed reduced in *reeler* SpS neurons. First, I examined I_h intensity in SpS neurons by measuring the temporal summation of EPSPs before and after pharmacologically blocking HCN channels (Magee, 1998, 1999). The optogenetically evoked train stimulation activated all TC fibers in direct contact with the recorded SpS neuron, which causes cell to cell variability. Additionally, variability between WT and *reeler* mutant mice could be caused by a potentially different targeting pattern of TC synapses onto SpS neurons. Up to the present time, the amount and distribution of TC synapses targeting SpS neurons in the WT and *reeler* cortex has not been evaluated. These uncertainties need to be taken into account when interpreting the resulting ChR2-evoked train responses. However, in line with the hypothesis, blocking HCN channels had a smaller, yet not significant, effect on the temporal summation of EPSPs in *reeler* SpS neurons as compared to WT SpS neurons. This finding is suggestive of a decreased I_h in *reeler* SpS neurons (see **Figure 33**).

These indicative outcomes became more apparent upon repeating the paired recordings between FS interneurons and SpS neurons during pharmacologically increasing I_h by use of FK506. FK506 is known to enhance HCN channel activity by inhibitory calcineurin, a modulator of HCN channels. Therefore, application of FK506 leads to enhanced HCN channel

activity and thus increased I_h intensity. Remarkably, the preliminary results of enhancing HCN channel activity, demonstrated a high inhibitory and excitatory connection probability between FS interneurons and SpS neurons in the WT and *reeler* S1BF, as compared to the initial paired recordings without FK506 (standard condition) (see **Figure 15 and 30**). Increasing the intensity of I_h conductance resulted in an inhibitory connection probability of 45.5 % (5 out of 11 pairs) in *reeler* mutant mice, a vast increase in comparison to the connectivity observed in the standard recordings (3.7 %, 1 out of 27 pairs) (see **Figure 15 and 30**). These findings indicate that *reeler* SpS neurons have a reduced dendritic I_h leading to an insufficient driving force for propagations of inhibitory inputs and this defect can be rescued by pharmacologically enhancing HCN channel activity. In WT mice, an increased inhibitory connection probability was discovered compared to the standard recordings (standard 47.1 %, 9 out of 17 pairs; FK506 63.7 %, 14 out of 22 pairs), suggesting that enhancing I_h reveals a subset of weaker and more distally located inhibitory inputs that under standard conditions are left undetected (see **Figure 15 and 30**). A similar increasing effect of FK506 on the excitatory connectivity rate in the *reeler* S1BF was observed (standard 3.7 %, 1 out of 27 pairs; FK506 72.8 %, 8 out of 11 pairs; see **Figure 15 and 30**). Under the standard condition in WT mice, an excitatory connection from SpS neuron to FS interneuron was detected in 9 out of 17 pairs (53.6 %), which was slightly lower compared to the FK506 condition (63.7 %, 14 out of 22 pairs; see **Figure 15 and 30**). The increased HCN channel activity leads to a depolarization of the SpS neuron membrane potential (see **Table 3**). Moreover, depolarization of presynaptic terminals of SpS neurons brings the membrane potential closer to the threshold for Ca^{2+} entry and subsequent vesicle release, clarifying the increase in excitatory connectivity rate in presence of FK506. Consistent with the hypothesis, enhancing HCN channel activity with FK506 increased the reliability of inhibitory connections and the IPSC amplitude in both WT and *reeler* mutant mice as a result of increased driving force for propagation of inhibitory inputs (see **Figure 31**). Blockade of HCN channels made the exact same inhibitory connections less reliable as shown by an increased synaptic failure rate, indicating a decrease of driving force for GABAergic transmission (see **Figure 16 and 31**). In one specific inhibitory connection recorded in the *reeler* S1BF, a 50 % synaptic failure rate was measured in presence of FK506 and upon blocking HCN channels this rate increased up to 88 %. In all paired recordings, a connection was defined by a synaptic failure rate lower than 90 %. The strong increase synaptic failure rate upon blocking HCN channels, indicate that a reduced I_h could explain for the lack of inhibitory connections observed in the initial standard paired recordings in the *reeler* S1BF. In both WT and *reeler* mutant mice, presence of FK506 resulted in more reliable excitatory

connections from SpS neuron to FS interneuron. This could be explained by the HCN channel mediated depolarization of presynaptic terminals closer to the Ca^{2+} threshold. This mechanism is supported by the depolarized membrane potential of WT and *reeler* SpS neurons observed in presence of FK506, as shown in **Table 3**. These findings support the hypothesis that a reduced I_h in *reeler* SpS neurons could hamper the inhibitory and excitatory inputs. Additional experiments are required in order to confirm that I_h is indeed affected in *reeler* SpS neurons.

The present work has provided multiple indirect insights in the potentially reduced I_h in *reeler* SpS neurons. Hence, future experiments could measure differences in dendritic I_h more directly by performing dendritic recordings. By performing dual recordings of SpS neuron soma and distal dendrite simultaneously, the propagation of postsynaptic potentials could be studied in WT and *reeler* mutant mice. It might also be possible to perform paired recordings of SpS neurons and FS interneuron, while also recording from the SpS neuron dendrite to more closely monitor the integration and propagation of IPSPs in the WT and *reeler* S1BF.

To be able to observe I_h differences more clearly, future studies could focus on a type of neuron within the S1BF cortex that is known to express HCN channels more abundantly. In comparison to SpS neurons, pyramidal neurons in L5 of S1BF show a high HCN channel expression along their dendrites (Berger et al., 2001). Similar to SpS neurons, L5 pyramidal neurons are known to receive thalamic input and are being controlled by FS interneurons. Various electrophysiological parameters could be measured to determine whether I_h is reduced in L5 pyramidal neurons. For example, calculating the voltage sag and rebound in response to hyperpolarizing current injections, provide an indication of I_h intensity (Halliwell & Adams, 1982; Maccaferri et al., 1993; Mayer & Westbrook, 1983; McCormick & Huguenard, 1992). If I_h is indeed reduced, then the sag index and rebound depolarization in *reeler* L5 pyramidal neurons is expected to be smaller compared to the WT control. Another approach to evaluate I_h is to establish an impedance amplitude profile (ZAP) of WT and *reeler* L5 pyramidal neurons using chirp current injection (Combe & Gasparini, 2021; Hutcheon & Yarom, 2000). The ability of I_h to counteract slow alterations of the membrane potential presents neurons with a high-pass frequency filter in response to ZAP currents. This can be revealed by a dampening of voltage amplitude at lower frequencies. A reduction in I_h intensity, as anticipated in *reeler* excitatory neurons, would therefore be revealed by an increase in voltage responses at lower

frequencies compared to WT excitatory neurons. So as to further evaluate the contribution of I_h to the sag index, rebound depolarization and ZAP of WT and *reeler* L5 pyramidal neurons, these parameters could be recorded before and after blockade of HCN channels with ZD7288.

In addition to these electrophysiological approaches, HCN channel expression could be examined using various other methods. A general overview of the expression of HCN channels in the WT and *reeler* S1BF could be obtained by immunolabeling of HCN channels (Kupferman et al., 2014; Lörincz et al., 2002). Another potential method to gain insight in HCN channel expression in specific neurons within the WT and *reeler* S1BF, would be to perform single cell reverse transcription polymerase chain reaction (RT PCR). This approach allows for quantifying cell type specific HCN channel expression of SpS neurons and L5 pyramidal neurons and compare between genotypes. It is then anticipated that the results demonstrate a reduced HCN channel expression in all tested neurons of the *reeler* S1BF, in comparison to the neurons in the WT S1BF.

Implications for the *reeler* mutant mouse

The present study discovered an impaired GABAergic transmission between FS interneurons and SpS neurons in the *reeler* S1BF. Abnormal inhibitory signalling causes hyperexcitability in the cortical network, as the excitatory SpS neurons are no longer precisely controlled by the powerful inhibition provided by FS interneurons. In addition, this work revealed a potentially reduced HCN channel expression in the *reeler* S1BF. Therefore, it is likely that also the *reeler* L5 pyramidal neurons express a reduced dendritic I_h intensity. The decreased HCN channel expression on L5 pyramidal neurons would also give rise to hyperexcitability of these neurons and in turn a hyperexcitable cortical network. Hyperexcitability of neurons is a characteristic feature of epileptogenesis. In addition, reduced HCN channel expression has been linked to hyperexcitability and epileptogenesis (Brennan et al., 2016; Huang et al., 2009; Jung et al., 2010; Lewis & Chetkovich, 2011; Noam et al., 2011; Santoro et al., 2010). Also, cortical malformations have been associated with epileptic seizure generations (Albertson et al., 2017; Bozzi et al., 2012). Accordingly, it could be hypothesized that *reeler* mutant mice have an increased susceptibility to generate epileptic seizures. To examine whether *reeler* mutant mice are indeed more susceptible to epileptic seizures, various experimental approaches could be

considered. For example, electrophysiological recordings in brain slices could measure the frequency of spontaneous EPSCs. In the presumably hyperexcitable *reeler* cortex, spontaneous EPSC frequency is anticipated to be higher, compared to the WT cortex, as a result of increased firing of excitatory neurons. In addition, future studies could perform *in vivo* electroencephalogram experiments to investigate whether *reeler* mutant mice suffer from spontaneous seizure generations in the cortex. Alternatively, it could be examined whether *reeler* mutant mice are at a greater risk to generate seizures upon seizure induction by kainic acid. These future studies could potentially establish the *reeler* mutant mouse as a new model to study epilepsy.

Conclusion

This project investigated the effect of improper layering on the thalamorecipient microcircuit in the neo cortex that has a key role in the processing of sensory information. Within the *reeler* S1BF, thalamocortical axons manage to target and innervate L4-fated neurons, such as SpS neurons. Via feedforward and feedback inhibition, SpS neurons excitability is controlled by FS interneurons. This study demonstrated that incorrect lamination of S1BF does not grossly affect connectivity between neurons. However, the connections between neurons showed various signs of imbalances between excitation and inhibition. The present study demonstrated that the lack of cortical organization does not majorly affect the morphological and electrophysiological profile of SpS neurons and FS interneurons. On a network level, it was found that the direct thalamic input onto *reeler* SpS neurons was found to be weakened, whereas the overall network excitability was greater. In addition, a lack of integration and propagation of GABAergic inhibitory inputs in *reeler* SpS neurons was demonstrated, which is likely caused by a reduced expression of HCN channels. The greater network activity, hindered GABAergic transmission, and reduced HCN channel expression, cause hyperexcitability in the *reeler* cortical network. Hyperexcitability is the hallmark of the neurological disorder, epilepsy. Therefore, additional experiments are required to proof that *reeler* mutant mice are more susceptible for for seizure generations. Such experiments could establish a novel animal model for the study of epilepsy: the *reeler* mutant mouse.

Abstract

In the severely disorganized *reeler* primary somatosensory cortex, thalamocortical axons manage to target layer 4-fated neurons. Although the *reeler* somatosensory cortex maintains proper activation in response to sensory input, the main thalamic input, from the ventral posteromedial (VPm) nucleus onto layer 4-fated spiny stellates (SpS), was found to be weakened compared to wild-type. These findings suggest that an intracortical mechanism compensates the weakened thalamic input to the *reeler* cortex. In this study, putative compensatory mechanisms were examined by following two dedicated hypotheses. The first hypothesis tested for enhanced recurrent excitation between SpS neurons. The second hypothesis proposed a reduced GABAergic transmission between SpS neurons and fast spiking (FS) interneurons. In order to study layer 4 in the disorganized *reeler* cortex, the Scnn1a-tdTomato-Reeler mouse line was used, where layer 4-excitatory neurons express cre-dependent tdTomato. *In vitro* paired whole-cell voltage clamp recordings of FS interneurons and SpS neurons allowed for assessing connection probability, reliability and strength in *reeler* versus WT mice. Prior to testing these hypotheses, previous findings of the lab that were fundamental to this study were replicated. Using optogenetic stimulation of thalamocortical axons in layer 4, thalamic input was measured in SpS neurons. Like the aforementioned results, it was concluded that *reeler* SpS neurons receive a weakened direct thalamic input, whereas the overall network excitation was increased. Before examining the connections between SpS neurons and FS interneurons, it was experimentally verified that the morphological and electrophysiological properties of SpS neurons and FS interneurons were not affected by improper lamination in the *reeler* cortex. Whole-cell patch clamp recordings between pairs of SpS neurons demonstrated overall comparable connection parameters in WT and *reeler* mutant mice, hence it is unlikely that enhanced recurrent excitation rescued the weakened thalamic input. Subsequently, it was tested whether a decreased GABAergic transmission compensated for the weakened thalamic input. In the *reeler* S1BF, a drastic decrease in connection probability and strength was found between FS interneurons and SpS neurons when using

standard potassium-based intracellular solution. Remarkably, repeating these recordings with cesium-based intracellular solution in *reeler* revealed aWT-level connectivity rate and connection strength. Neuronal reconstructions of recorded neurons and immunolabeling for synaptotagmin-2, marking presynaptic boutons of FS, parvalbumin-expressing interneurons, showed that inhibitory synapses targeting *reeler* and WT SpS neurons have a similar somatodendritic distribution. These results suggest a proper connection probability, connection strength and synapse location between SpS neurons and FS interneurons in the *reeler* S1BF. This led me to examine the dendritic integration of inhibitory postsynaptic potentials (IPSPs) in *reeler* SpS neurons. Dendritic excitability is regulated by the hyperpolarization-activated current (I_h), an inward current mediated by hyperpolarization-activated cyclic nucleotide-gated (HCN) channels. I_h-mediated depolarization ensures a sufficient driving force for the propagation of dendritic inhibitory inputs. In addition, HCN channel activity has an excitatory effect where I_h depolarizes the membrane potential of the presynaptic terminal, bringing it closer to the threshold for Ca^{2+} entry. Thus, a reduced HCN channel expression in *reeler* SpS neurons was hypothesized to impair proper inhibitory and excitatory signal integration. First, the role of I_h on temporal summation of EPSPs in WT and *reeler* SpS neurons was studied, before and after pharmacological blockade of HCN channels. The slightly smaller effect of HCN channel blockade on the temporal summation of EPSPs in *reeler* SpS neurons, compared to WT, indicate a potentially reduced I_h intensity. In a different approach, paired recordings were performed between FS interneurons and SpS neurons in the presence of FK506 in order to increase HCN channel activity. Enhancing HCN channel activity restored connection probability and strength between *reeler* SpS neurons and FS interneurons. Further confirming a role for I_h, pharmacological blockade of HCN channels made inhibitory connection less reliable. These results suggest a reduced I_h in the *reeler* S1BF, resulting in reduced inhibitory and excitatory signaling. Taken together, the increased network activity, compromised GABAergic transmission, and decreased HCN channel expression, cause hyperexcitability in the *reeler* S1BF. These same features are known to cause epileptogenesis, hence the *reeler* mutant mouse presents to be potential model for epilepsy studies.

Bibliography

Agmon & Connors (1992). Correlation between intrinsic firing patterns and thalamocortical synaptic responses of neurons in mouse barrel cortex. *The Journal of Neuroscience : The Official Journal of the Society for Neuroscience*, *12*(1), 319–329. https://doi.org/10.1523/JNEUROSCI.12-01-00319.1992

Agmon & Connors (1991). Thalamocortical responses of mouse somatosensory (barrel) cortex in vitro. *Neuroscience*, *41*(2–3), 365–379. https://doi.org/10.1016/0306-4522(91)90333-J

Ahlssar, Sosnik & Haldarilu (2000). Transformation from temporal to rate coding in a somatosensory thalamocortical pathway. *Nature*, *406*(6793), 302–306. https://doi.org/10.1038/35018568

Albertson, Bohannon & Hablitz (2017). HCN channel modulation of synaptic integration in GABAergic interneurons in malformed rat Neocortex. *Frontiers in Cellular Neuroscience*, *11*(April), 1–13. https://doi.org/10.3389/fncel.2017.00109

Aponte, Lien, Reisinger & Jonas (2006). Hyperpolarization-activated cation channels in fast-spiking interneurons of rat hippocampus. *Journal of Physiology*, *574*(1), 229–243. https://doi.org/10.1113/jphysiol.2005.104042

Ascoli, Alonso-Nanclares, Anderson, Barrionuevo, Benavides-Piccione, Burkhalter, Buzsáki, Cauli, Defelipe, Fairén, Feldmeyer, Fishell, Fregnac, Freund, Gardner, Gardner, Goldberg, Helmstaedter, Hestrin … Yuste (2008). Petilla terminology: Nomenclature of features of GABAergic interneurons of the cerebral cortex. *Nature Reviews. Neuroscience*, *9*(7), 557–568. https://doi.org/10.1038/nrn2402

Atherton, Kitano, Baufreton, Fan, Wokosin, Tkatch, Shigemoto, Surmeier & Bevan (2010). Selective participation of somatodendritic HCN channels in inhibitory but not excitatory synaptic integration in neurons of the subthalamic nucleus. *Journal of Neuroscience*, *30*(47), 16025–16040. https://doi.org/10.1523/JNEUROSCI.3898-10.2010

Bagnall, Hull, Bushong, Ellisman & Scanziani (2011). Multiple Clusters of Release Sites Formed by Individual Thalamic Afferents onto Cortical Interneurons Ensure Reliable Transmission. *Neuron*, *71*(1), 180–194. https://doi.org/10.1016/j.neuron.2011.05.032

Belford & Killackey (1979). Vibrissae representation in subcortical trigeminal centers of the neonatal rat. *Journal of Comparative Neurology*, *183*(2), 305–321. https://doi.org/10.1002/cne.901830207

Benshalom & White (1986). Quantification of thalamocortical synapses with spiny stellate neurons in layer IV of mouse somatosensory cortex. *Journal of Comparative Neurology*, *253*(3), 303–314. https://doi.org/10.1002/cne.902530303

Berger, Larkum & Lüscher (2001). High Ih channel density in the distal apical dendrite of layer V pyramidal cells increases bidirectional attenuation of EPSPs. *Journal of Neurophysiology*, *85*(2), 855–868. https://doi.org/10.1152/jn.2001.85.2.855

Bernardo & Woolsey (1987). Axonal trajectories between mouse somatosensory thalamus and cortex. *Journal of Comparative Neurology*, *258*(4), 542–564. https://doi.org/10.1002/cne.902580406

Biel, Wahl-Schott, Michalakis & Zong (2009). Hyperpolarization-activated cation channels: From genes to function. *Physiological Reviews*, *89*(3), 847–885. https://doi.org/10.1152/physrev.00029.2008

Boyle, Bernard, Thompson, Ng, Boe, Mortrud, Hawrylycz, Jones, Hevner & Lein (2011). Cell-type-specific consequences of reelin deficiency in the mouse neocortex, hippocampus, and amygdala. *Journal of Comparative Neurology*, *519*(11), 2061–2089. https://doi.org/10.1002/cne.22655

Bozzi, Casarosa & Caleo (2012). Epilepsy as a neurodevelopmental disorder. *Frontiers in Psychiatry*, *3*(MAR), 1–14. https://doi.org/10.3389/fpsyt.2012.00019

Brecht (2007). Barrel cortex and whisker-mediated behaviors. *Current Opinion in Neurobiology*, *17*(4), 408–416. https://doi.org/10.1016/j.conb.2007.07.008

Brecht & Sakmann (2002). Dynamic representation of whisker deflection by synaptic potentials in spiny stellate and pyramidal cells in the barrels and septa of layer 4 rat somatosensory cortex. *Journal of Physiology*, *543*(1), 49–70. https://doi.org/10.1113/jphysiol.2002.018465

Brennan, Baram & Poolos (2016). Hyperpolarization-Activated Cyclic Nucleotide- Gated (HCN) Channels in Epilepsy. *Cold Spring Harb Perspect Med*, *6*, 1–12.

Buhl, Halasy & Somogyi (1994). Diverse sources of hippocampal unitary inhibitory postsynaptic potentials and the number of synaptic release sites. *Nature*, *368*(6474), 823–828. https://doi.org/10.1038/368823a0

Caviness (1988). The reeler malformation. Implications for neocortical histogenesis. *Cerebral Cortex*, *7*, 59–89.

Caviness (1976). Patterns of cell and fiber distribution in the neocortex of the reeler mutant mouse. *Journal of Comparative Neurology*, *170*(4), 435–447. https://doi.org/10.1002/cne.901700404

Caviness (1982). Neocortical histogenesis in normal and reeler mice: A developmental study based upon [3H]thymidine autoradiography. *Developmental Brain Research*, *4*(3), 293–302. https://doi.org/10.1016/0165-3806(82)90141-9

Combe & Gasparini (2021). Ih from synapses to networks: HCN channel functions and modulation in neurons. *Progress in Biophysics and Molecular Biology*.

https://doi.org/10.1016/j.pbiomolbio.2021.06.002

Cragg (1975). Absence of barrels and disorganization of thalamic afferent distribution in the sensory cortex of reeler mice. *Experimental Neurology*, *49*(3), 858–862. https://doi.org/10.1016/0014-4886(75)90065-5

Cruikshank & Connors (2007). Synaptic basis for intense thalamocortical activation of feedforward inhibitory cells in neocortex. *Nature Neuroscience*, *10*(4), 462–468. https://doi.org/10.1038/nn1861

Cruikshank, Urabe, Nurmikko & Connors (2010). Pathway-Specific Feedforward Circuits between Thalamus and Neocortex Revealed by Selective Optical Stimulation of Axons. *Neuron*, *65*(2), 230–245. https://doi.org/10.1016/j.neuron.2009.12.025

D'Arcangelo, Miao, Chen, Soares, Morgan & Curran (1995). A protein related to extracellular matrix proteins deleted in the mouse mutant reeler. *Nature*, *374*, 719–723. https://doi.org/10.1038/374719a0

De Marco García, Karayannis & Fishell (2011). Neuronal activity is required for the development of specific cortical interneuron subtypes. *Nature*, *472*(7343), 351–355. https://doi.org/10.1038/nature09865

DeFelipe & Fariñas (1992). The pyramidal neuron of the cerebral cortex: Morphological and chemical characteristics of the synaptic inputs. *Progress in Neurobiology*, *39*(6), 563–607. https://doi.org/10.1016/0301-0082(92)90015-7

Diamond, Armstrong-James, Budway & Ebner (1992). Somatic sensory responses in the rostral sector of the posterior group (POm) and in the ventral posterior medial nucleus (VPM) of the rat thalamus: Dependence on the barrel field cortex. *Journal of Comparative Neurology*, *319*(1), 66–84. https://doi.org/10.1002/cne.903190108

Diamond, Von Heimendahl, Knutsen, Kleinfeld & Ahissar (2008). "Where" and "what" in the whisker sensorimotor system. *Nature Reviews Neuroscience*, *9*(8), 601–612. https://doi.org/10.1038/nrn2411

Dumont (2012). FK506, An Immunosuppressant Targeting Calcineurin Function. *Current Medicinal Chemistry*, *7*(7), 731–748. https://doi.org/10.2174/0929867003374723

Evans, Sammons, Lebron, Dumitrescu, Watkins, Uebele, Renger & Grubb (2013). Calcineurin signaling mediates activity-dependent relocation of the axon initial segment. *J Neurosci*, *33*(16), 6950–6963. https://doi.org/10.1523/jneurosci.0277-13.2013

Falconer (1951). Two new mutants, Trembler and Reeler, with neurological actions in the house mouse (Mus Musculus L). *Journal of Genetics*, *50*(2), 192–205.

Feldmeyer (2005). Monosynaptic Connections between Pairs of Spiny Stellate Cells in Layer 4 and Pyramidal Cells in Layer 5A Indicate That Lemniscal and Paralemniscal Afferent Pathways Converge in the Infragranular Somatosensory Cortex. *Journal of Neuroscience*, *25*(13), 3423–3431. https://doi.org/10.1523/JNEUROSCI.5227-04.2005

Feldmeyer, Brecht, Helmchen, Petersen, Poulet, Staiger, Luhmann & Schwarz (2013). Barrel cortex function. *Progress in Neurobiology*, *103*, 3–27.

https://doi.org/10.1016/j.pneurobio.2012.11.002.

Feldmeyer, Egger, Lübke & Sakmann (1999). Reliable synaptic connections between pairs of excitatory layer 4 neurones within a single “barrel” of developing rat somatosensory cortex. *Journal of Physiology*, *521*(1), 169–190. https://doi.org/10.1111/j.1469-7793.1999.00169.

Freund & Katona (2007). Perisomatic Inhibition. *Neuron*, *56*(1), 33–42. https://doi.org/10.1016/j.neuron.2007.09.012

Frotscher (1998). Cajal-Retzius cells, Reelin, and the formation of layers. *Current Opinion in Neurobiology*, *8*(5), 570–575. https://doi.org/10.1016/S0959-4388(98)80082-2

Guy (2015). Dissertation: *Order under the guise of chaos : functional neuroanatomy of the somatosensory barrel cortex of the reeler mutant mouse*.

Guy, Sachkova, Möck, Witte, Wagener & Staiger (2017). Intracortical Network Effects Preserve Thalamocortical Input Efficacy in a Cortex Without Layers. *Cerebral Cortex*, *27*(10), 4851–4866. https://doi.org/10.1093/cercor/bhw281

Guy, Wagener, Möck, Staiger (2015). Persistence of functional sensory maps in the absence of cortical layers in the somsatosensory cortex of reeler mice. *Cerebral Cortex*, *25*(9), 2517–2528. https://doi.org/10.1093/cercor/bhu052

Hafner, Guy, Witte, Truschow, Rüppel, Sirmpilatze, Dadarwal, Boretius & Staiger (2020). Increased Callosal Connectivity in Reeler Mice Revealed by Brain-Wide Input Mapping of VIP Neurons in Barrel Cortex. *Cerebral Cortex*, *31*(3), 1427–1443. https://doi.org/10.1093/cercor/bhaa280

Halliwell & Adams (1982). Voltage-clamp analysis of muscarinic excitation in hippocampal neurons. *Brain Research*, *250*(1), 71–92. https://doi.org/10.1016/0006-8993(82)90954-4

Hammond (2006). Layer Positioning of Late-Born Cortical Interneurons Is Dependent on Reelin But Not p35 Signaling. *Journal of Neuroscience*, *26*(5), 1646–1655. https://doi.org/10.1523/JNEUROSCI.3651-05.2006

Hevner, Daza, Englund, Kohtz & Fink (2004). Postnatal shifts of interneuron position in the neocortex of normal and reeler mice: Evidence for inward radial migration. *Neuroscience*, *124*(3), 605–618. https://doi.org/10.1016/j.neuroscience.2003.11.033

Huang, Walker & Shah (2009). Loss of dendritic HCN1 subunits enhances cortical excitability and epileptogenesis. *Journal of Neuroscience*, *29*(35), 10979–10988. https://doi.org/10.1523/JNEUROSCI.1531-09.2009

Hull, Isaacson & Scanziani (2009). Postsynaptic Mechanisms Govern the Differential Excitation of Cortical Neurons by Thalamic Inputs. *Journal of Neuroscience*, *29*(28), 9127–9136. https://doi.org/10.1523/JNEUROSCI.5971-08.2009

Hutcheon & Yarom (2000). Resonance , oscillation and the intrinsic frequency preferences of neurons. *Trends in Neuroscience*, *23*(5), 216–222.

Jung, Bullis, Lau, Jones, Warner & Poolos (2010). Downregulation of dendritic HCN channel

gating in epilepsy is mediated by altered phosphorylation signaling. *Journal of Neuroscience*, *30*(19), 6678–6688. https://doi.org/10.1523/JNEUROSCI.1290-10.2010

Karagiannis, Gallopin, David, Battaglia, Geoffroy, Rossier, Hillman, Staiger & Cauli (2009). Classification of NPY-Expressing Neocortical Interneurons. *Journal of Neuroscience*, *29*(11), 3642–3659. https://doi.org/10.1523/JNEUROSCI.0058-09.2009

Karube (2004). Axon Branching and Synaptic Bouton Phenotypes in GABAergic Nonpyramidal Cell Subtypes. *Journal of Neuroscience*, *24*(12), 2853–2865. https://doi.org/10.1523/JNEUROSCI.4814-03.2004

Kawaguchi & Kubota (1993). Correlation of physiological subgroupings of nonpyramidal cells with parvalbumin- and calbindinD28k-immunoreactive neurons in layer V of rat frontal cortex. *Journal of Neurophysiology*, *70*(1), 387–396. https://doi.org/10.1152/jn.1993.70.1.387

Koelbl, Helmstaedter, Lubke & Feldmeyer (2015). A barrel-related interneuron in layer 4 of rat somatosensory cortex with a high intrabarrel connectivity. *Cerebral Cortex*, *25*(3), 713–725. https://doi.org/10.1093/cercor/bht263

Kowalski, Geuting, Paul, Dieni, Laurens, Zhao, Drakew, Haas, Frotscher & Vida (2010). Proper layering is important for precisely timed activation of hippocampal mossy cells. *Cerebral Cortex*, *20*(9), 2043–2054. https://doi.org/10.1093/cercor/bhp267

Kubota, Hatada, Kondo, Karube & Kawaguchi (2007). Neocortical Inhibitory Terminals Innervate Dendritic Spines Targeted by Thalamocortical Afferents. *Journal of Neuroscience*, *27*(5), 1139–1150. https://doi.org/10.1523/JNEUROSCI.3846-06.2007

Kubota, Kondo, Nomura, Hatada, Yamaguchi, Mohamed, Karube, Lubke, Kawaguchi, Lübke & Kawaguchi (2015). Functional effects of distinct innervation styles of pyramidal cells by fast spiking cortical interneurons. *ELife*, *4*(July 2015), 1–27. https://doi.org/10.7554/eLife.07919

Kupferman, Basu, Russo, Guevarra, Cheung & Siegelbaum (2014). Reelin Signaling Specifies the Molecular Identity of the Pyramidal Neuron Distal Dendritic Compartment. *Cell*, *158*(6), 1335–1347. https://doi.org/10.1016/j.cell.2014.07.035

Lambert de Rouvroit & Goffinet (1998). *The reeler mouse as a model of brain development*.

Lefort, Tomm, Floyd Sarria & Petersen (2009). The Excitatory Neuronal Network of the C2 Barrel Column in Mouse Primary Somatosensory Cortex. *Neuron*, *61*(2), 301–316. https://doi.org/10.1016/j.neuron.2008.12.020

Lewis & Chetkovich (2011). HCN channels in behavior and neurological disease: Too hyper or not active enough? *Molecular and Cellular Neuroscience*, *46*(2), 357–367. https://doi.org/10.1016/j.mcn.2010.11.007

Lörincz, Notomi, Tamás, Shigemoto & Nusser (2002). Polarized and compartment-dependent distribution of HCN1 in pyramidal cell dendrites. *Nature Neuroscience*, *5*(11), 1185–1193. https://doi.org/10.1038/nn962

Lu & Lin (1993). Thalamic afferents of the rat barrel cortex: A light-and electron-

microscopic study using phaseolus vulgaris leucoagglutinin as an anterograde tracer. *Somatosensory & Motor Research*, *10*(1), 1–16. https://doi.org/10.3109/08990229309028819

Lübke, Egger, Sakmann & Feldmeyer (2000). Columnar organization of dendrites and axons of single and synaptically coupled excitatory spiny neurons in layer 4 of the rat barrel cortex. *The Journal of Neuroscience : The Official Journal of the Society for Neuroscience*, *20*(14), 5300–5311. https://doi.org/20/14/5300 [pii]

Lübke & Feldmeyer (2007). Excitatory signal flow and connectivity in a cortical column: Focus on barrel cortex. *Brain Structure and Function*, *212*(1), 3–17. https://doi.org/10.1007/s00429-007-0144-2

Maccaferri, Mangoni, Lazzari & DiFrancesco (1993). Properties of the hyperpolarization-activated current in rat hippocampal CA1 pyramidal cells. *Journal of Neurophysiology*, *69*(6), 2129–2136. https://doi.org/10.1152/jn.1993.69.6.2129

Magee (1998). Dendritic hyperpolarization-activated currents modify the integrative properties of hippocampal CA1 pyramidal neurons. *Journal of Neuroscience*, *18*(19), 7613–7624. https://doi.org/10.1523/jneurosci.18-19-07613.1998

Magee (1999). Dendritic l(h) normalizes temporal summation in hippocampal CA1 neurons. *Nature Neuroscience*, *2*(6), 508–514. https://doi.org/10.1038/9158

Magee (2000). Dendritic integration of excitatory synaptic input. *Nature Reviews Neuroscience*, *1*(3), 181–190. https://doi.org/10.1038/35044552

Mayer & Westbrook (1983). A voltage-clamp analysis of inward (anomalous) rectification in mouse spinal sensory ganglion neurones. *The Journal of Physiology*, *340*(1), 19–45. https://doi.org/10.1113/jphysiol.1983.sp014747

McCormick & Huguenard (1992). A model of the electrophysiological properties of thalamocortical relay neurons. *Journal of Neurophysiology*, *68*(4), 1384–1400. https://doi.org/10.1152/jn.1992.68.4.1384

Medinilla, Johnson & Gasparini (2013). Features of proximal and distal excitatory synaptic inputs to layer V neurons of the rat medial entorhinal cortex. *Journal of Physiology*, *591*(1), 169–183. https://doi.org/10.1113/jphysiol.2012.237172

Meyer, Schwarz, Wimmer, Schmitt, Kerr, Sakmann & Helmstaedter (2011). Inhibitory interneurons in a cortical column form hot zones of inhibition in layers 2 and 5A. *Proceedings of the National Academy of Sciences*, *108*(40), 16807–16812. https://doi.org/10.1073/pnas.1113648108

Mingo-Moreno (2018). Dissertation: *From inside-out to outside-in : cortical lamination development in the Reelin-deficient neocortex*.

Miyoshi, Hjerling-Leffler, Karayannis, Sousa, Butt, Battiste, Johnson, Machold & Fishell (2010). Genetic Fate Mapping Reveals That the Caudal Ganglionic Eminence Produces a Large and Diverse Population of Superficial Cortical Interneurons. *Journal of Neuroscience*, *30*(5), 1582–1594. https://doi.org/10.1523/JNEUROSCI.4515-09.2010

Moosmang, Biel, Hofmann & Ludwig (1999). Differential distribution of four hyperpolarization-activated cation channels in mouse brain. *Biological Chemistry*, *380*(7–8), 975–980. https://doi.org/10.1515/BC.1999.121

Noam, Bernard & Baram (2011). Towards an integrated view of HCN channel role in epilepsy. *Current Opinion in Neurobiology*, *21*(6), 873–879. https://doi.org/10.1016/j.conb.2011.06.013

Notomi & Shigemoto (2004). Immunohistochemical Localization of Ih Channel Subunits, HCN1-4, in the Rat Brain. *Journal of Comparative Neurology*, *471*(3), 241–276. https://doi.org/10.1002/cne.11039

Oberlaender, Ramirez & Bruno (2012). Sensory Experience Restructures Thalamocortical Axons during Adulthood. *Neuron*, *74*(4), 648–655. https://doi.org/10.1016/j.neuron.2012.03.022

Pavlov, Scimemi, Savtchenko, Kullmann & Walker (2011). Ih-mediated depolarization enhances the temporal precision of neuronal integration. *Nature Communications*, *2*(1). https://doi.org/10.1038/ncomms1202

Paxinos & Franklin (2001). The Mouse Brain in stereotaxic Coordinates. In *Academic Press* (second).

Petersen (2002). Short-term dynamics of synaptic transmission within the excitatory neuronal network of rat layer 4 barrel cortex. *Journal of Neurophysiology*, *87*(6), 2904–2914. https://doi.org/10.1152/jn.01020.2001

Petersen & Sakmann (2000). The excitatory neuronal network of rat layer 4 barrel cortex. *The Journal of Neuroscience : The Official Journal of the Society for Neuroscience*, *20*(20), 7579–7586.

Petreanu, Mao, Sternson & Svoboda (2009). The subcellular organization of neocortical excitatory connections. *Nature*, *457*(7233), 1142–1145. https://doi.org/10.1038/nature07709

Pla, Borrell, Flames & Marin (2006). Layer Acquisition by Cortical GABAergic Interneurons Is Independent of Reelin Signaling. *Journal of Neuroscience*, *26*(26), 6924–6934. https://doi.org/10.1523/JNEUROSCI.0245-06.2006

Pohlkamp, Dávid, Cauli, Gallopin, Bouché, Karagiannis, May, Herz, Frotscher, Staiger & Bock (2014). Characterization and distribution of reelin-positive interneuron subtypes in the rat barrel cortex. *Cerebral Cortex*, *24*(11), 3046–3058. https://doi.org/10.1093/cercor/bht161

Porter, Johnson & Agmon (2001). Diverse types of interneurons generate thalamus-evoked feedforward inhibition in the mouse barrel cortex. *The Journal of Neuroscience : The Official Journal of the Society for Neuroscience*, *21*(8), 2699–2710. https://doi.org/21/8/2699 [pii]

Robinson & Siegelbaum (2003). Hyperpolarization-Activated Cation Currents: From Molecules to Physiological Function. *Annual Review of Physiology*, *65*(4), 453–480.

https://doi.org/10.1146/annurev.physiol.65.092101.142734

Santoro, Lee, Englot, Gildersleeve, Piskorowski, Siegelbaum, Winawer & Blumenfeld (2010). Increased seizure severity and seizure-related death in mice lacking HCN1 channels. *Epilepsia*, *51*(8), 1624–1627. https://doi.org/10.1111/j.1528-1167.2010.02554.x

Schubert, Kotter, Zilles, Luhmann & Staiger (2003). Cell Type-Specific Circuits of Cortical Layer IV Spiny Neurons. *J. Neurosci.*, *23*(7), 2961–2970. http://www.jneurosci.org/content/23/7/2961

Shah (2014). Cortical HCN channels: function, trafficking and plasticity. *The Journal of Physiology*, *592*(13), 2711–2719. https://doi.org/10.1113/jphysiol.2013.270058

Shigematsu, Nishi & Fukuda (2018). Gap Junctions Interconnect Different Subtypes of Parvalbumin-Positive Interneurons in Barrels and Septa with Connectivity Unique to Each Subtype. *Cerebral Cortex*, *July*, 1–16. https://doi.org/10.1093/cercor/bhy038

Sommeijer & Levelt (2012). Synaptotagmin-2 is a reliable marker for parvalbumin positive inhibitory boutons in the mouse visual cortex. *PLoS ONE*, *7*(4), 1–12. https://doi.org/10.1371/journal.pone.0035323

Staiger (2015). *Scholarpedia of Touch: S1 laminar specialization*.

Staiger (1996). Distribution of GABAergic elements ppstsynaptic to ventroposteromedial thalamic projections in layer IV of rat barrel cortex. *European Journal of Neuroscience*, *8*(11), 2273–2285. https://doi.org/10.1111/j.1460-9568.1996.tb01191.x

Staiger, Flagmeyer, Schubert, Zilles, Kötter & Luhmann (2004). Functional diversity of layer IV spiny neurons in rat somatosensory cortex: Quantitative morphology of electrophysiologically characterized and biocytin labeled cells. *Cerebral Cortex*, *14*(6), 690–701. https://doi.org/10.1093/cercor/bhh029

Staiger & Petersen (2021). Neuronal circuits in barrel cortex for whisker sensory perception. *Physiological Reviews*, *101*(1), 353–415. https://doi.org/10.1152/physrev.00019.2019

Staiger, Zuschratter, Luhmann & Schubert (2009). Local circuits targeting parvalbumin-containing interneurons in layer IV of rat barrel cortex. *Brain Structure and Function*, *214*(1), 1–13. https://doi.org/10.1007/s00429-009-0225-5

Stratford, Tarczy-Hornoch, Martin, Bannister & Jack (1996). Excitatory synaptic inputs to spiny stellate cells in cat visual cortex. *Nature*, *382*(6588), 258–261. https://doi.org/10.1038/382258a0

Swadlow (1989). Efferent neurons and suspected interneurons in motor cortex of the awake rabbit: Axonal properties, sensory receptive fields, and subthreshold synaptic inputs. *Journal of Neurophysiology*, *71*(2), 437–453. https://doi.org/10.1152/jn.1994.71.2.437

Swadlow (2003). Fast-spike Interneurons and Feedforward Inhibition in Awake Sensory Neocortex. *Cerebral Cortex*, *13*(1), 25–32. https://doi.org/10.1093/cercor/13.1.25

Swadlow (1995). Influence of VPM afferents on putative inhibitory interneurons in S1 of the

awake rabbit: evidence from cross-correlation, microstimulation, and latencies to peripheral sensory stimulation. *Journal of Neurophysiology*, *73*(4), 1584–1599.

Tamas, Buhl, Lorincz & Somogyi (2000). Proximally targetd GABAergic synapses and gap junctions synchronise cortical interneurons. *Nature Neuroscience*, *3*(4), 366–371.

Tarczy-Hornoch, Martin, Stratford & Jack (1999). Intracortical excitation of spiny neurons in layer 4 of cat striate cortex in vitro. *Cerebral Cortex*, *9*(8), 833–843. https://doi.org/10.1093/cercor/9.8.833

Van Der Loos (1976). Barreloids in mouse somatosensory thalamus. *Neuroscience Letters*, *2*(1), 1–6. https://doi.org/10.1016/0304-3940(76)90036-7

Varani, Vecchia, Zucca, Forli & Fellin (2021). Stimulus Feature-Specific Control of Layer 2 / 3 Subthreshold Whisker Responses by Layer 4 in the Mouse Primary Somatosensory Cortex. *Cerebral Cortex*, *00*, 1–18.

Vereczki, Veres, Müller, Nagy, Rácz, Barsy & Hájos (2016). Synaptic Organization of Perisomatic GABAergic Inputs onto the Principal Cells of the Mouse Basolateral Amygdala. *Frontiers in Neuroanatomy*, *10*(March). https://doi.org/10.3389/fnana.2016.00020

Veres, Nagy, Vereczki, Andrási & Hájos (2014). Strategically Positioned Inhibitory Synapses of Axo-axonic Cells Potently Control Principal Neuron Spiking in the Basolateral Amygdala. *The Journal of Neuroscience*, *34*(49), 16194–16206. https://doi.org/10.1523/JNEUROSCI.2232-14.2014

Wagener, Zhao, Haas & Staiger (2010). The Somatosensory Cortex of reeler Mutant Mice Shows Absent Layering But Intact Formation and Behavioral Activation of Columnar Somatotopic Maps. *Journal of Neuroscience*, *30*(46), 15700–15709. https://doi.org/10.1523/JNEUROSCI.3707-10.2010

Wagener, Witte, Guy, Mingo-Moreno, Kügler & Staiger (2016). Thalamocortical Connections Drive Intracortical Activation of Functional Columns in the Mislaminated Reeler Somatosensory Cortex. *Cerebral Cortex*, *26*(2), 820–837. https://doi.org/10.1093/cercor/bhv257

Wang, Tucciarone, Jiang, Yin, Wang, Wang, Jia, Jia, Li, Yang, Xu, Akram, Wang, Zeng, Ascoli, Mitra, Gong, Luo & Huang (2019). Genetic Single Neuron Anatomy Reveals Fine Granularity of Cortical Axo-Axonic Cells. *Cell Reports*, *26*(11), 3145-3159.e5. https://doi.org/10.1016/j.celrep.2019.02.040

Welt & Steindler (1977). Somatosensory cortical barrels and thalamic barreloids in reeler mutant mice. *Neuroscience*, *2*(5), 755–766. https://doi.org/10.1016/0306-4522(77)90029-X

Williams & Stuart (2003). Voltage- and site-dependent control of the somatic impact of dendritic IPSPs. *The Journal of Neuroscience*, *23*(19), 7358–7367. https://doi.org/23/19/7358 [pii]

Wimmer, Bruno, De Kock, Kuner & Sakmann (2010). Dimensions of a projection column

and architecture of VPM and POm axons in rat vibrissal cortex. *Cerebral Cortex, 20*(10), 2265–2276. https://doi.org/10.1093/cercor/bhq068

Woolsey & Van der Loos (1970). The structural organization of layer IV in the somatosensory region (S I) of mouse cerebral cortex. The description of a cortical field composed of discrete cytoarchitectonic units. *Brain Research, 17*(2), 205–242. https://doi.org/10.1016/0006-8993(70)90079-X

Yabut, Renfro, Niu, Swann, Marín & D'Arcangelo (2007). Abnormal laminar position and dendrite development of interneurons in the reeler forebrain. *Brain Research, 1140*(1), 75–83. https://doi.org/10.1016/j.brainres.2005.09.070

Acknowledgements

This thesis would not have been imaginable without the support and contribution of many others.

First of all, I would like to thank my supervisor Prof. Dr. Jochen Staiger for giving me the opportunity to work on this exciting project in his laboratory at the Institute for Neuroanatomy. His wealth of knowledge and eagerness to help and provide feedback, greatly contributed to the progress of this project. Next, I want to express my gratitude to Dr. Julien Guy. Julien has welcomed me to Göttingen, taught me optogenetics and electrophysiology, took care of the mouse lines used in this project and always shared helpful insights and ideas during data discussions. I cannot thank you enough for all your help, patience, guidance, advise, and encouragement throughout the years.

I would like to thank my colleagues who have supported me or contributed to my work in one way or another. I am especially thankful to Dr. Martin Möck. Thank you Martin for the valuable discussions, teaching me about electrophysiology, the Signal configurations and scripts, proofreading this thesis, and helping out with any problem at any time. Next, I would like to thank Patricia Sprysch for performing all immunohistochemistry and genotyping for this project. I am grateful to Pavel Truschow for his imaging assistance and his help in quantifying Syt-2 puncta. Also, I would like to thank Aybeniz Çetin for her feedback on datasets and presentations and her encouragement. Furthermore, I would like to thank Nicolas Zdun, Sabrina Hübner and Johanna Rieke for their help with morphological reconstructions.

I would like to thank my thesis committee members: Prof. Dr. Jochen Staiger, Prof. Dr. Tim Gollisch and Dr Camin Dean for evaluating my thesis and for their valuable feedback and support during the thesis committee meetings.

Special thanks are due to my dear friends Andreia Cepeda, Pauline Ulmke, Valerie Clavet, Sofia Elizarova and Heba Ali. Thank you for proofreading this thesis, your immense support over the last years and the great fun we had. Without your support I would not have gotten this far. Wherever our paths may go, let us always keep in touch!

Last, I would like to thank all of my friends and family for their unconditional love and support. In particular, I would like to thank my parents. Their faith in me and tremendous support, encourages me to achieve any goal. I am really grateful to have you.

Thank you.

Anouk Meeuwissen